UNIVERSITÉ DU LUXEMBOURG

PhD-FSTC-16-2010

Faculté des Sciences, de la Technologie et de la Communication

THÈSE

Soutenue le 10/06/2010 à Luxembourg

En vue de l'obtention du grade académique de

DOCTEUR DE L'UNIVERSITÉ DU LUXEMBOURG

EN PHYSIQUE

par

Carmine Lampitelli
né le 11 mars 1961 à Caserta (Italie)

HYDROLOGICAL EFFECTS ON GRAVITY AT THE STATION OF WALFERDANGE, LUXEMBOURG

Jury de thèse

Dr. Olivier Francis, directeur de thèse
Professeur, Université du Luxembourg

Dr. Susanna Zerbini
Professeur, Université de Bologna

Dr. Massimo Malvetti, président
Professeur, Université du Luxembourg

Dr. Frédéric Nguyen
Professeur, Université de Liège

Dr. Tonie van Dam, président suppléant
Assistant Professeur, Université du Luxembourg

Acknowledgements

The present work has represented for me an important human and professional experience, and I want to express my gratitude to all the persons who allowed me to achieve it.

First, I thank Prof. Olivier Francis, who accepted to be my thesis advisor and assisted me all along the period of research work and the period of manuscript redaction. I am deeply grateful to Prof. Tonie van Dam for the help she provided in improving and revising the work, and for always offering essential assistance. Thanks are due to Prof. Massimo Malvetti, who showed interest for this research and offered constant encouragements.

I am grateful to Prof. Susanna Zerbini and Prof. Frédéric Nguyen, for accepting to read the present work and to be members of the jury of my PhD defense.

I thank Dr. Michel Van Camp, Ing. Gilbert Klein, Mrs. Maren Westkott and Mrs. Laura Kipfstuhl for contributing to determine the transfer function of the Observatory Superconducting Gravimeter CT040.

I want also thank Pr. Norman Teferle, Dr. Jan Wuite and Dr. Christian Rothleiner for their assistance and encouragements.

Index

Introduction

The time and space variability of the gravity acceleration g can be related to several causes. Among them, we can mention the ocean loading and Earth tides due to the luni-solar attraction, the polar motion, the atmospheric air pressure changes and the surface and subsurface water storage variations due to meteorological events.

If the tidal and polar motion effects can be deterministically modeled with high accuracy, the hydrological effects on gravity are generally more difficult to describe. These effects are characterized by a significant irregularity at different space and time scales, due to the limited predictability of meteorological events like precipitation.

Besides, the response of local gravity to local changes in water storage is significantly site dependent. Techniques and schemes for mitigating the signal in gravity data at one location are usually not entirely applicable to another location. Consequently, it is difficult to attempt a description of the hydrological effects on gravity with models having a general applicability.

Nevertheless, because of the remarkable precision achieved with the modern instruments (the precision of superconducting gravimeters ranges from 10^{-11} g for periods comprised between a few hours and a few days to 10^{-9} g for yearly periods), the effect of water storage variations on gravity has become an important issue for improving the investigation of gravity measurements. Specifically, local water storage variations within 10 km of a station alter the local mass field and thus can significantly affect gravity observations [*Van Camp et al*, 2006]. Various authors have analyzed the effects of parameters such as local precipitation, soil moisture and groundwater storage on gravity observations [e.g. *Meurers et al., 2007*; *Hokkanen et al., 2005*]. Other authors [*van Dam et al., 2001; Crossley et al., 2005; Hinderer et al., 2006; Lambert and Beaumont, 1977*] have investigated the consequences of longer wavelength (several 100 km) water storage components on the gravity signal. At these wavelengths, the displacement of the Earth's surface due to the excess mass is also important.

In this study, we look at the physical relationship between water storage variations driven by local precipitation events and local gravity changes at Walferdange, in the Grand Duchy of Luxembourg. A synthesis of the different approaches that can be found in recent literature is proposed. Then, a new and simple scheme is provided to remove the effects of precipitation events in the gravity observations

For the gravity observations, we use the data collected by the superconducting gravimeter CT040 (SG) located in the Walferdange Underground Laboratory for Geodynamics (WULG), which provides high resolution relative gravity measurements from December 2003.

In Chapter 1, some basic notions of hydrology are presented. Attention is particularly pointed on the description of the hydrological recharge and discharge processes and on the general laws describing the dynamics of the subsurface flows. Then, the hypotheses

leading to a Tank Model representation are described. In order to underline the dependence of the model parameters on hydrological parameters, such as porosity and hydraulic conductivity, as indicated by *Van Camp et al*. [2006], the steps leading to the fundamental model equations are detailed. This is achieved by combining the mass continuity equation and Darcy's law [*Fetter,* 2001; *Roche,* 1963], which describes the flow of a fluid through a porous medium.

In Chapter 2, the attention is focused on the calculation of the hydrological effects on the gravity field. The modeled gravity variations are estimated using an admittance factor between the gravity change and the precipitation height. This is done with the use of a Digital Elevation Model (DEM), based on the decomposition of the area above the gravimeter in a discrete number of prismatic elements (the precipitation height corresponding to the element thickness). The gravity effect on the SG is calculated using Newton's law of universal attraction. The determination of the admittance between the gravity change and the precipitation height allows us to write the Tank Model in terms of gravity variations. A further hypothesis is developed, regarding the seasonal variability of a model parameter, which represents the gravity recovery rate after a rainfall and its physical significance is discussed. A second model is then introduced: the Double Exponential Model, which, contrarily to the Tank Model, allows for the description of both the hydrological recharge and discharge phases.

In Chapter 3, the modalities of acquisition of the input data (precipitation time series) and the observed gravity data are described. The determination of the transfer function of the superconducting gravimeter, essential in order to qualify the instrument, is also carried out. Then, the tank model outputs for a set of empirically evaluated parameters are presented and discussed. The modeled gravity time series is compared to the observed gravity time series. Finally, a second comparison is undertaken between the Tank Model outputs and the outputs provided by the more sophisticated Double Exponential Model, showing that the tank model offers an accurate enough description of the hydrological gravity variations in Walferdange.

In Chapter 4, a statistical analysis is presented to determine the correlation between the gravity signal variations registered by the SG and the water level of the nearby flowing Alzette River. The idea is that the gravity variation due to the precipitation should appear before the change in river level. Contrarily to the simple precipitation data, the gravity observation should also contain information on the degree of soil saturation, which depends on processes having a seasonal variability, as evapotranspiration, and on hydrogeological parameters like hydraulic conductivity. Understanding the relationship and temporal dependence between the observed precipitation and the gravity changes might improve the capacity to predict of extreme events like flooding. The mean time delay between the maximum variation of the gravity signal and the Alzette water level is estimated as a function of a set of sampled showers. Finally, the correlation between the gravity variation and water level change is calculated and discussed.

Chapter 1

Chapter 1: Elements of Hydrology

1.1 Introduction

In order to define models relating observed water storage variations with observed changes in gravity, we introduce here some of the concepts regarding hydrological processes and the water cycle. The transfer of water between the primary reservoirs in the water cycle can be broken up into four main components:

- the movement of water from the atmosphere to the ground, i.e., precipitation, in its various forms;
- the movement of water above ground and underground, i.e., processes such as runoff, surface and subsurface flows, infiltration, snowmelt (runoff related to the melting snow) etc;
- the movement of water from ground to air, i.e., evaporation, evapotranspiration, and sublimation;
- and the movement of atmospheric water, represented by the advection (movement of water in its different states through the atmosphere).

In this thesis we pay particular attention to the analysis of the processes related to the movement of water beneath the Earth's surface.

The amount of groundwater storage is determined by comparing hydrological recharge and hydrological discharge. The first process represents the groundwater storage increase due to the infiltration of part of the precipitation. The second process represents the groundwater storage decrease due to the efflux from the soil-saturated layers.

The timescale of these processes is governed by different factors, including the local topography, evapotranspiration rates, type and quantity of vegetation and the soil composition.

The influence of the soil composition is described by defining an important parameter: the hydraulic conductivity, K. This parameter quantifies the capacity of fluids to move through porous media. It depends on both the medium and on the fluid characteristics.

The models, which describe groundwater flow through porous media are based on a combination of the mass continuity equations and Darcy's law, which relates the flow to the hydraulic head via the hydraulic conductivity.

One of the simplest groundwater flow models is the tank model, which describes the efflux of the fluid contained in a tank through a porous plug. For our applications, the fluid entering the tank is due to precipitation. This simple model allows us to provide a straightforward description of water-storage variations due to the local precipitation events in Walferdange.

In the basic tank model, the hydraulic conductivity is a constant. But we will show that this parameter is actually subject to significant seasonal fluctuations. In order to define reliable models, the seasonal variability of this parameter should be considered.

The influence of the seasonal variability of the evapotranspiration rates on the recharge and discharge processes will also be investigated.

1.2 Precipitation

Precipitation is defined as any product of the condensation of atmospheric water vapor that is pulled down by gravity and deposited on the Earth's surface. This includes water in either the liquid (rain) and/or solid (snow, hail) state. When warm and saturated air currents ascend, they are subject to thermo dynamical processes including adiabatic or isobaric cooling, and condense to form clouds, which are themselves made of microscopic water drops. Saturation is a necessary condition for condensation, but the process also requires the presence of condensation nuclei, upon which the formation of actual water drops can begin. These nuclei can appear through dynamical processes, or they can simply be atmospheric aerosols, i.e., solid particles suspended in the air. Their dimensions can range between 0,0001μm and more than 2μm. They act as catalysists for the drop formation. If the weight of the condensed drop reaches a critical value allowing it to overcome the buoyancy of ascending currents, precipitation results. Further, if the condensation occurs at a temperature higher than 0°C and the drop diameter exceeds 3mm, the precipitation occurs in liquid form, otherwise the water molecules crystallize and the precipitation occurs in solid form.

The quantity of precipitated water is expressed in terms of height (usually in mm) of precipitated water and in terms of intensity (height/time). The measurement is mainly realized with two kinds of instruments: the pluviometers, registering the water height on daily time scales, and the pluviographs, registering the water heights on shorter time scales. Nowadays, digital pluviographs have a time resolution on the order of one minute. The precipitations are subject to strong spatial and temporal variability, on different space and time scales. The temporal variability can range from a few minutes to many years. To quantify the yearly variation in precipitation, different indices have been proposed, such as the seasonality index defined by Walsh and Lawler in 1981, which is based on the differences between the monthly heights and a reference configuration representing a uniform distribution of precipitations through the year:

$$I_s = \frac{1}{P_a} \cdot \sum_{m=1}^{12} \left| P_m - \frac{P_a}{12} \right| \tag{1.1}$$

where P_a and P_m represent the yearly and monthly precipitation, respectively. The graphical representation of the precipitation is usually given in form of histograms, expressing the water heights as a function of the reference time interval.

One important component of the present research, is that we make reference to 'shower' events. One shower [*Musy and Higy ,2003*] can be defined as an ensemble of precipitation events related to the same meteorological perturbation. The exact definition of a shower requires the introduction of the continuity parameters Δt_o and Δh_o: two showers are considered distinct if for a time period longer than a defined Δt (a multiple of the basic time interval) the water heights in each basic time interval are inferior to a defined value Δh. One example is given in Figure1.1.

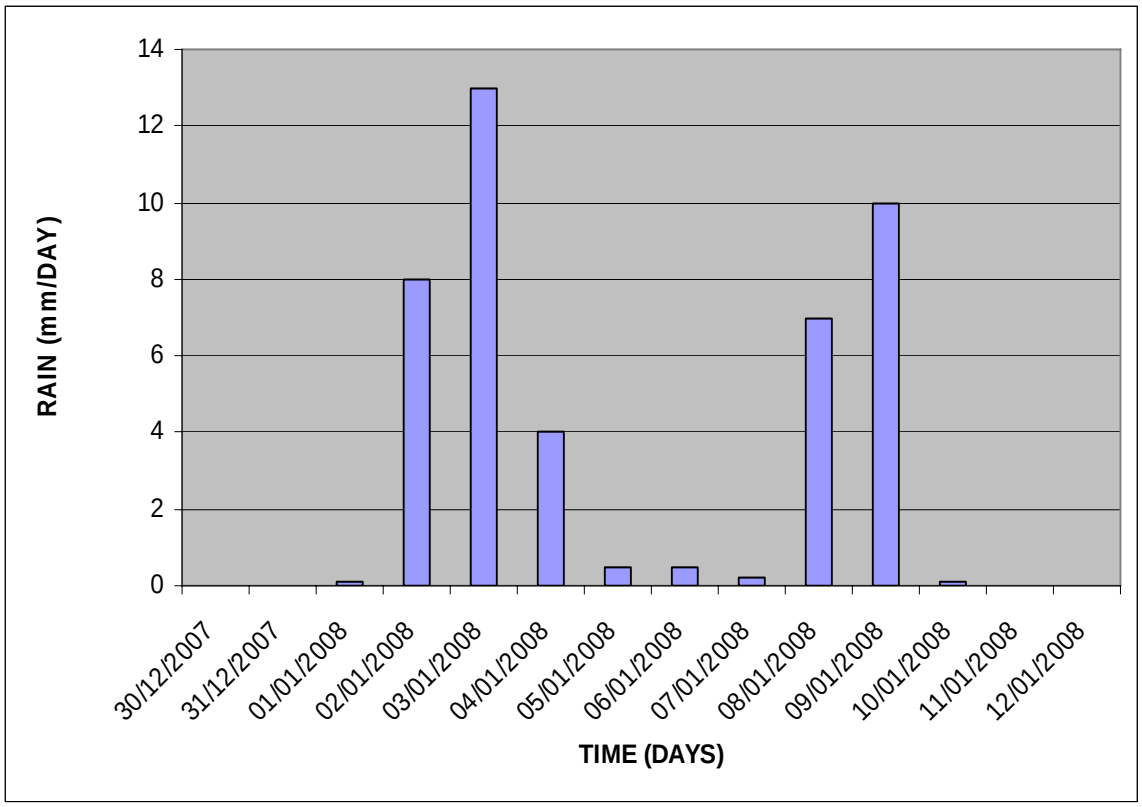

Fig. 1.1: *Illustration of the continuity criteria in the definition of a shower event*

If we assume Δh_o= 1 mm/day and Δt_o= 2 days, we define two shower events: one occurring between 02-01-2008 and 05-01-2008 and the other between 08-01-2008 and 10-01-2008. Conversely, assuming Δh_o= 0.15 mm/day and Δt_o= 2 days, we define one single shower event between 02-01-2008 and the 10-01-2008.

Thus, one shower is essentially characterized by the following parameters:

- The water height (mm) representing the global height of precipitated water during the shower event.
- The duration (time), representing the total duration of the shower event (multiple of the basic time interval unity).
- The mean intensity (mm/time) representing the ratio between the water height and the duration.
- The maximum intensity (mm/time).

Other parameters related to the structure of the shower are more difficult to quantify. The structure of a shower can be defined as the distribution of the precipitation height along the shower duration [*Musy and Higy, 2003*]. As shown in Figure 1.2, which represents the cumulated water fraction (% of total height) as a function of the cumulative time fraction (% of global duration), two showers with the same global height and the same duration can have radically different structures. And this difference has a strong influence on the water flow.

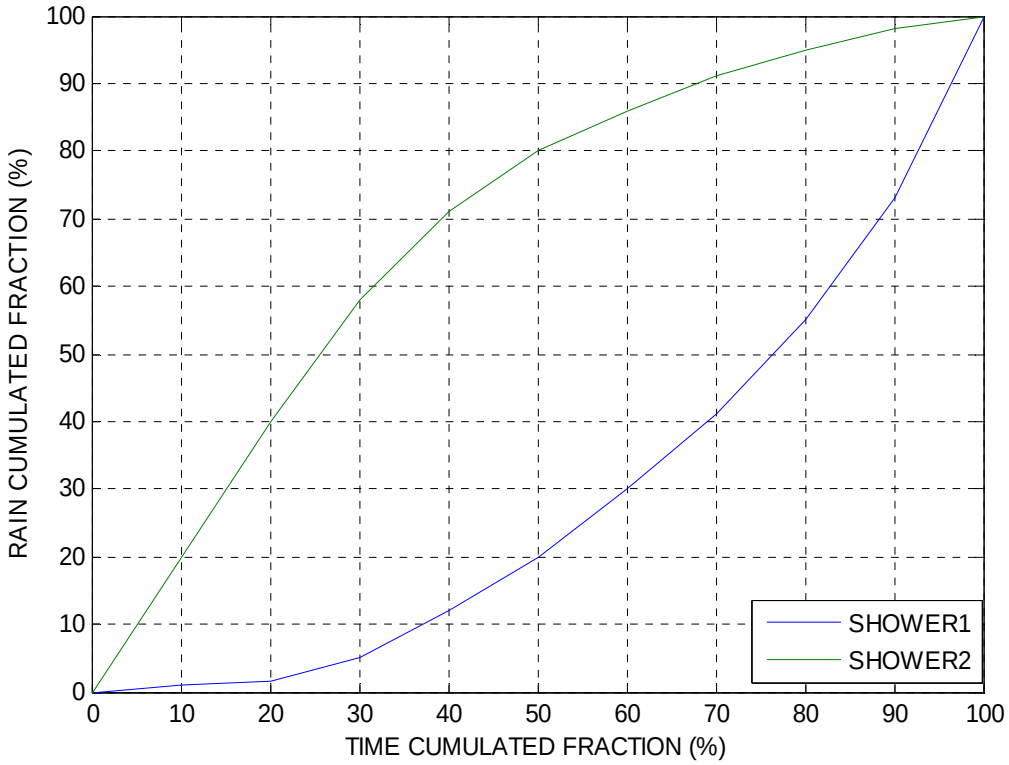

Fig. 1.2*: Structure difference between two showers. For shower 1, the most part of the precipitation occurs in the second phase of the shower. The opposite happens for shower 2.*

1.3 Hydrological recharge and discharge processes

The essential purpose of this section is to examine hydrological processes related to water storage variations. In the zone of subsurface water [*Milly and Schmakin, 2002*], the water table represents the interface between the saturated zone (below) and the unsaturated zone (above). The volume contained in the saturated zone represents the groundwater reservoir**.** When precipitation occurs, part of the fallen volume of water is retained by the vegetation canopy and other human artifacts, another part is subject to direct surface runoff or other subsurface flow, and one part infiltrates through the unsaturated zone to increase the groundwater reservoir. This represents the recharge process, which results in an increase of the water storage. After precipitation and recharge, the groundwater level will decrease through different mechanisms, including evaporation, evapotranspiration or efflux via percolation from the saturated zone, to reach flows which lead to the major drainage basin. This discharge process results in the reduction of the water storage. Before the analysis of the dynamical aspects of the groundwater transport, it is important to attempt a more detailed examination of the subsurface water distribution.

As indicated above, the primary subdivision of the subsurface water is between the unsaturated zone and the saturated zone. This demarcation is defined by an important hydro-geological parameter, porosity. The materials, which make up the soil are not

compacted, but contain empty spaces in their solid matrix. For a given volume of material V_t, the non-dimensional parameter porosity is defined as the ratio between the volume V_v of the empty spaces (pores) and the total volume V_t.

$$n = \frac{V_v}{V_t} \tag{1.2}$$

The porosity can also expressed in percentage PI=n·100, and is also indicated as total porosity because V_t represents the total volume that can potentially filled with water.

With respect to the potential of groundwater flow, a more significant parameter is the effective porosity. Actually, not all the empty volume can be subject to groundwater flow: the fluid can move only if the pores are connected. In addition, part of the water is attached to the granules of the solid matrix through surface tension, and can consequently not be subject to movement. The effective porosity takes into account only the void volume where the flow can actually occur. Thus, the effective porosity is defined as:

$$n_e = \frac{V_e}{V_t} \tag{1.3}$$

where n_e represents the effective porosity and V_e represents the part of the void volume where the stored water can be put into motion under the action of gravity and pressure.

The medium's porosity depends on the granulometry. The porosity is generally higher when the granules composing the solid matrix have similar dimensions.

The arrangement of the granules also plays an important role (Figure 1.3). If we hypothesize that the granules have a spherical form their arrangement in a cubic space leads to a theoretical porosity of 0.48. On the other hand, a rhomboid arrangement leads to a porosity of only 0.26.

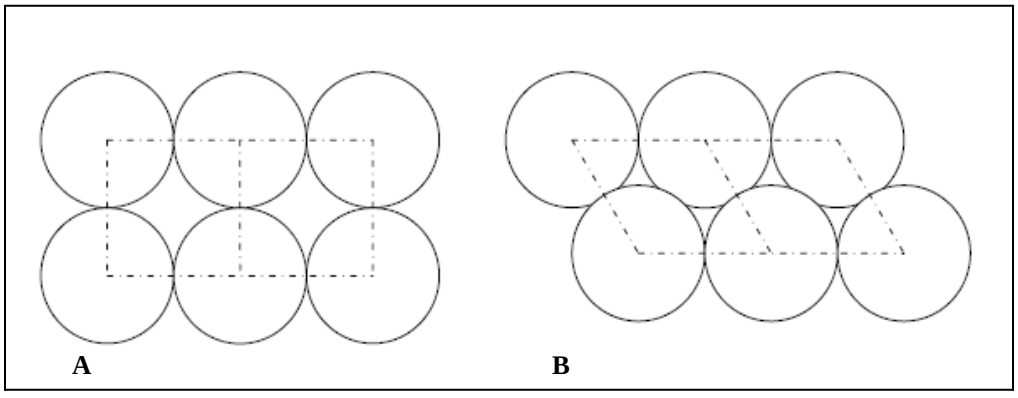

Fig. 1.3: *With a cubic space arrangement of the spherical granules (A), the theoretical porosity is 0.48. With a rhomboid arrangement (B), the theoretical porosity is reduced to 0.26.*

Because of lithostatic pressure, the porosity decreases with depth. Deeper layers tend to be more compacted than upper sedimentary layers. This observation is often described

using the Athy equation (1930), which expresses the porosity as a function of the depth below the surface:

$$n(z) = n_0 \cdot e^{-\beta \cdot z} \tag{1.4}$$

where n_0 represents the surface porosity, z the depth and β is known as the compaction coefficient (1/length).

The saturation index is defined as the ratio between the volume of water V_w and the volume of the empty spaces:

$$S_i = \frac{V_w}{V_v} \tag{1.5}$$

If Si=1, corresponds to a situation where the water completely fills the empty spaces, the material is *saturated*. On this basis, we give the following definitions [*U.S. Geological Survey Professional Paper, Washington*]:

- An aquifer is a geological layer containing water in its pores and having Si=1, meaning that it is saturated (some authors use the term of aquifer even in the case of non saturation). In the aquifer, we have two phases: the solid phase of the matrix and the liquid phase of the water contained in the pores of the matrix.
- An aquiclude is a completely impermeable geological layer, thus totally impeaching any water transfer.
- A confined aquifer is an aquifer located between two aquicludes, thus presenting no free surfaces. The pressure in a captive aquifer can be higher than the atmospheric pressure.
- A free aquifer is an aquifer presenting one upper free surface, thus confined only by one inferior impermeable layer. The upper free surface is called the water table. The volume of water contained in the aquifer is the groundwater reservoir. We must underline that some authors use the term water table as synonymous for the aquifer itself (incorrectly). The pressure at the level of the water table, also defined as piezometric level, corresponds to the atmospheric pressure. The pressure under the water table is greater than the atmospheric pressure.

The water table represents the interface between the saturated and unsaturated zone. In the unsaturated zone above the water table, we have three phases. In addition to the solid (matrix) and liquid (water) phases, there is also gas made up of the air present in the incompletely filled pore spaces. The unsaturated zone can be further subdivided into three zones:

- The upper layer represents the root zone. Het he water is present in the form of soil moisture. In particular, the soil is not saturated in this zone, but the saturation index can be subject to strong spatial and temporal variability. This zone is subject to evapotranspiration, whose intensity varies throughout the year because of changes in the seasonal thermodynamic and hydrological conditions.
- The second layer represents the intermediate zone. Here, the volume of water is not sufficient to fill the empty spaces, and the matrix is unsaturated (S_i<1). The

water movement under the effect of the gravitational attraction is essentially represented by vertical percolation [*Dupuit, 1863*].

- The third layer, immediately above the water table, represents the capillary fringe. In this zone, capillarity processes induce the raise of water from the saturated zone through the small channels made up of a succession of pore spaces. The pores are completely filled, but water movement is not only driven by gravity, and the water is held under tension.

In Figure 1.4 we schematically represent the zones of water penetration in the case of a free aquifer, with the presence of only one underlying impermeable layer.

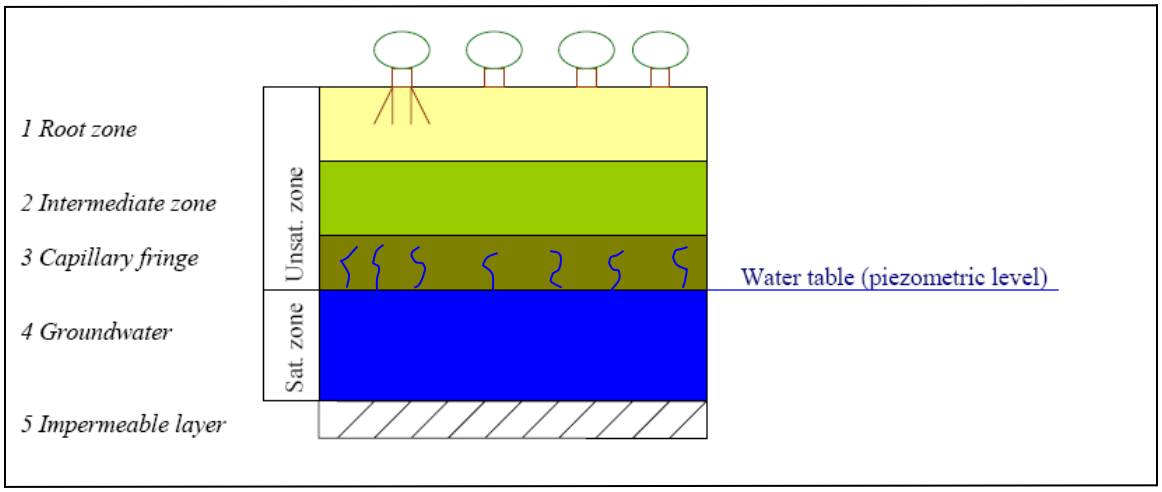

Fig. 1.4*: Subdivision of the zone of water penetration. The water table represents the interface between the saturated and the unsaturated zone. The unsaturated zone can be subdivided into the root zone, the intermediate zone and the capillary fringe.*

The total height of water resulting from a precipitation event can be expressed as the sum of three components:

$$P = P_n + R_s + F \qquad (1.6)$$

where P represents the total height, P_n is defined as the net rain (that can be identified with the surface runoff), R_s represents the surface retention (sum of evapotranspiration and interception components) and F represents the part of precipitated water that infiltrates into the soil (*Ambroise, 1988*).

The ability of a soil to allow water infiltration is defined by the infiltration capacity (length/time). In fact, infiltration capacity is often difficult to quantify, because it depends on a significant number of variables [*Bois, 2000; Laborde, 2000*]. It depends obviously on the soil characteristics, but it is also dependent on the degree of soil saturation. Thus, it is subject to variability during the precipitation event. The infiltration capacity is maximal at the beginning of a precipitation event, in the condition of maximal dryness of the soil, but as soil moisture increases during a precipitation event, it decreases because of the reduction in soil permeability [*Caquot, 1941*]. Finally, the infiltration capacity stabilizes at some constant lower limit. If the limit is less than the precipitation rate

(length/time), part of the precipitated water will not be absorbed by the soil at all and will instead be subject to direct surface runoff.

We must point out that infiltration capacity has also a seasonal variability. Because of evapotranspiration processes depend on soil and air temperature, the initial conditions of soil dryness are subject to variation throughout the year. In Figure 1.5 we display the qualitative trends of infiltration capacity with respect to the duration of a precipitation event for a cold and a warm month.

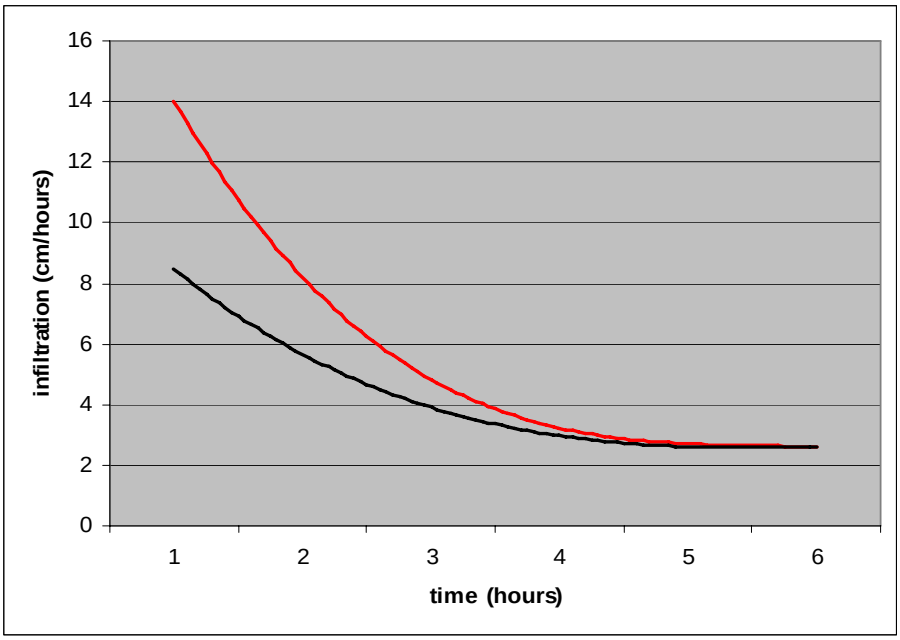

Fig. 1.5*: Infiltration capacity as a function of the precipitation duration for a cold (black) month and for a warm (red) month. The initial infiltration capacity is lower in a cold month because of the greater initial quantity of soil moisture in the soil.*

The infiltrated water, as indicated above, is essentially subjected to vertical percolation through the unsaturated zone to reach the saturated zone under the water table. In the configuration of an unconfined aquifer, the water movement in the saturated zone can be essentially described as a horizontal filtration through a solid porous matrix. This process can be analyzed with the use of the Darcy's law.

1.4 Navier-Stokes Equations, Bernoulli's law and hydraulic head

A fluid can be considered a continuous medium. Thus, its movement can be described with the use of the Navier-Stokes equations (*Ledoux, 2003; Todd, 1959; Landau, 1971).* The Navier-Stokes equations are non–linear differential equations, based on the mass balance, linear momentum balance and energy balance of the fluid [*Forchheimer, 1940*].

These equations provide an Eulerian specification of the fluid properties. The different fluid parameters, such as velocity and density, are evaluated as a function of fixed positions (x,y,z) and of time t. Consequently, a field of these parameters is specified.

The equation describing the mass balance of a fluid is expressed in Cartesian Coordinates by:

$$\frac{\partial \rho}{\partial t} + \vec{\nabla} \cdot (\rho \cdot \vec{v}) = 0 \tag{1.7}$$

where ρ represents the fluid density ($kg \cdot m^{-3}$ in S.I units), and $\vec{v}$ the Eulerian velocity. The equation describing the linear momentum balance of a fluid is expressed in Cartesian coordinates by:

$$\frac{\partial (\rho \cdot \vec{v})}{\partial t} + \vec{\nabla} \cdot (\rho \cdot \vec{v} \otimes \vec{v}) = -\vec{\nabla} p + \vec{\nabla} \cdot \vec{\vec{\tau}} + \rho \vec{f} \tag{1.8}$$

where p represents the fluid pressure (Pascal in SI units), $\vec{\vec{\tau}}$ represents the tensor of viscous constraints (force/surface area) and $\vec{f}$ represents the resultant of the mass forces in the fluid ($N \cdot Kg^{-1}$ in SI units).

The symbol $\otimes$ represents the tensor product. For the given vectors $\vec{v}\,(v_x,v_y,v_z)$ and $\vec{u}\,(u_x,u_y,u_z)$, defined in Cartesian coordinates, the tensor product is expressed by:

$$\vec{u} \otimes \vec{v} = \begin{pmatrix} u_x v_x & u_x v_y & u_x v_z \\ u_y v_x & u_y v_y & u_y v_z \\ u_z v_x & u_z v_y & u_z v_z \end{pmatrix} \tag{1.9}$$

The equation describing the energy balance of a fluid is expressed in Cartesian coordinates by:

$$\frac{\partial (\rho \cdot E)}{\partial t} + \vec{\nabla} \cdot [(\rho \cdot e + p) \cdot \vec{v}] = \vec{\nabla} \cdot (\vec{\vec{\tau}} \cdot \vec{v}) + \rho \cdot \vec{f} \cdot \vec{v} - \vec{\nabla} \cdot \vec{q} + r \tag{1.10}$$

where E represents the total energy per mass unit, and $\vec{q}$ represents the heat flux due to thermical conduction ($J \cdot s^{-2} \cdot m^{-2}$ in SI units).

In the case of the steady flow of non viscous fluids, the Navier-Stokes equations can be reduced to a simplified set of equations known as the Euler Equations. The mass balance is expressed by:

$$\frac{\partial \rho}{\partial t} + \vec{\nabla} \cdot (\rho \cdot \vec{v}) = 0 \tag{1.11}$$

The simplified linear momentum balance is expressed by:

$$\frac{\partial (\rho \cdot \vec{v})}{\partial t} + \vec{\nabla} \cdot (\rho \cdot \vec{v} \otimes \vec{v}) + \vec{\nabla} p = 0 \tag{1.12}$$

The simplified energy balance is expressed by:

$$\frac{\partial(\rho \cdot E)}{\partial t} + \vec{\nabla} \cdot [(\rho \cdot e + p) \cdot \vec{v}] = 0 \tag{1.13}$$

The integration of the Euler equations on a line of flow results in the Bernoulli equation.

The mechanical energy possessed by a fluid can be expressed as the addition of three components [*Fetter, 2001*]:

- The kinetic energy represents the component, which depends on the fluid state of motion, and is expressed by the half of the product of the mass and the square of the velocity

$$E_c = \frac{1}{2} \cdot m \cdot v^2 \tag{1.14}$$

  where E_c represents the kinetic energy, m the mass and v the velocity.
- The potential energy represents the component, which depends on the position of the mass in the gravity field, evaluated with respect to a reference level. It expresses the potential work that the mass can accomplish because of its position: if a mass m is lifted in the gravity field of a distance z, it acquires a potential energy corresponding to the work necessary to lift the mass:

$$E_p = m \cdot g \cdot z \tag{1.15}$$

  where E_p represents the potential energy, m the mass and z the height with respect to a reference level. The product m·g is the gravity force.
- The fluid-pressure energy represents the potential energy related to the pressure exerted on the fluid mass from other surrounding fluid mass. If A is the cross-sectional area perpendicular to the flux, F=P·A represents the force on A, and the work of moving in the x direction perpendicular to A is W=P·A·x.

$$E_{pr} = p \cdot V \tag{1.16}$$

  where E_{pr} represents the pressure energy, p the pressure (force/surface) and V the volume.

In the case of steady flow of a non viscous and incompressible fluid, the sum of the three components remains constant on a single smooth line of flow:

$$\frac{1}{2} \cdot m \cdot v^2 + m \cdot g \cdot z + p \cdot V = c \tag{1.17}$$

where c is a constant.

As previously indicated, Equation 1.19 represents a particular form of the *Navier-Stokes* equations, i.e. the case of non-viscous fluids, and is known as Bernoulli's law. We

remark that the value of the constant can be different for different lines of flow. If ρ is the fluid density, m= ρ·V is the mass of the considered fluid volume. Dividing equation 1.19 by the product ρ·V·g it is possible to express Bernoulli's law in terms of energy per unit weight, which corresponds to the dimension of a length:

$$\frac{v^2}{2 \cdot g} + z + \frac{p}{\rho \cdot g} = h \qquad (1.18)$$

In equation 1.18, h represents the total hydraulic head, that is, the sum of the kinetic head, the potential or elevation head and the pressure head.

In the problems related to groundwater fluxes, the kinetic component is usually significantly smaller than the elevation and pressure components [*Fetter, 2001; Dessargues, 1995*], and can consequently be considered as negligible. Equation 1.20 then becomes:

$$z + \frac{p}{\rho \cdot g} = h \qquad (1.19)$$

Equation 1.21 shows that for groundwater fluxes the total hydraulic head is the sum of the elevation head (from a defined reference level) and the pressure head (Figure 1.6). In the case of a non moving fluid, $P=\rho \cdot g \cdot h_p$, where h_p is the height of the water column.

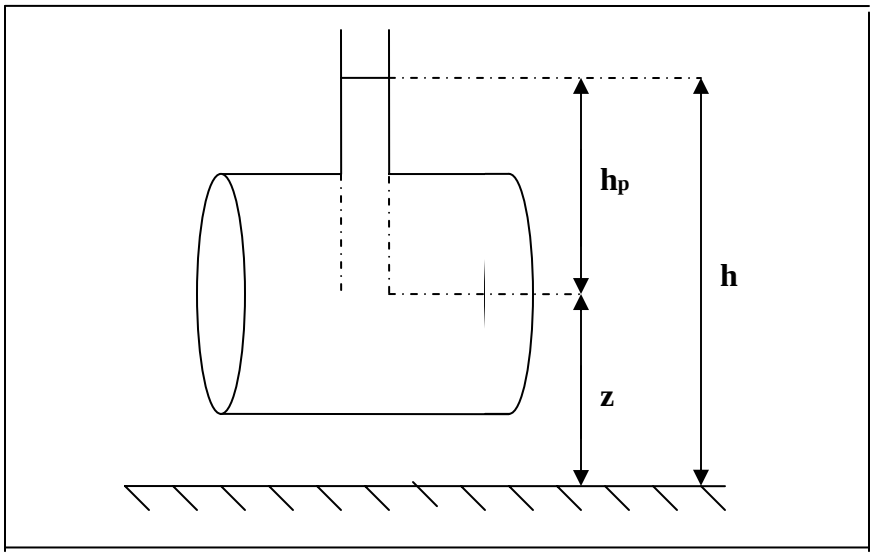

Fig. 1.6: *The total hydrological head for groundwater flow is the sum of elevation head z and pressure head* $h_p = p \cdot \rho^{-1} \cdot g^{-1}$.

Equation 1.21 can be also written in terms of force potential, by multiplying with the gravity acceleration g:

$$g \cdot z + \frac{p}{\rho} = \Phi \qquad (1.20)$$

Thus, force potential Φ is the product of the total hydraulic head and the acceleration of gravity, and has the dimensions of energy per unit mass. Posing $P=\rho \cdot g \cdot h_p$, we have:

$$\Phi = g \cdot (z + h_p) = g \cdot h \tag{1.21}$$

1.5 Darcy's law and hydraulic conductivity

The French engineer Henry Darcy in 1856 attempted to determine the laws of the water flow through sand [*Darcy, 1856*]. To this purpose, he developed the experimental device schematized in Figure 1.7.

The device's cylindrical body is subdivided into two chambers by an iron grid at level B. The upper chamber is partially filled with sand for a depth L. The pressure at the levels A and B is adjustable. The water flow Q is measured for different combinations of of the pressures set at A and B. Darcy observed that the specific flow q (flow for unity of surface) is directly proportional to the hydraulic (or piezometric) head difference, Δh, and inversely proportional to L. The relation can be expressed in the form:

$$\frac{Q}{S} = -K \cdot \frac{\Delta h}{L} \tag{1.22}$$

where Q is the water flow (volume/time), Δh the hydraulic head difference (length), S and L are the surface and length of the cylindrical sand filled volume respectively, and K is defined as the hydraulic conductivity (length/time). Setting q=Q/S as the specific flow (flow for unity of surface), and writing equation [1] in differential form, we obtain:

$$q = -K \cdot \frac{dh}{dL} \tag{1.23}$$

In the case of a three-dimensional flux through an isotropic mean, [2] can be written along the directions x,y and z, obtaining [*Scheidegger, 1963*]:

$$\begin{cases} q_x = -K \cdot \dfrac{\partial h}{\partial x} \\ q_y = -K \cdot \dfrac{\partial h}{\partial y} \\ q_z = -K \cdot \dfrac{\partial h}{\partial z} \end{cases} \tag{1.24}$$

in vector form:

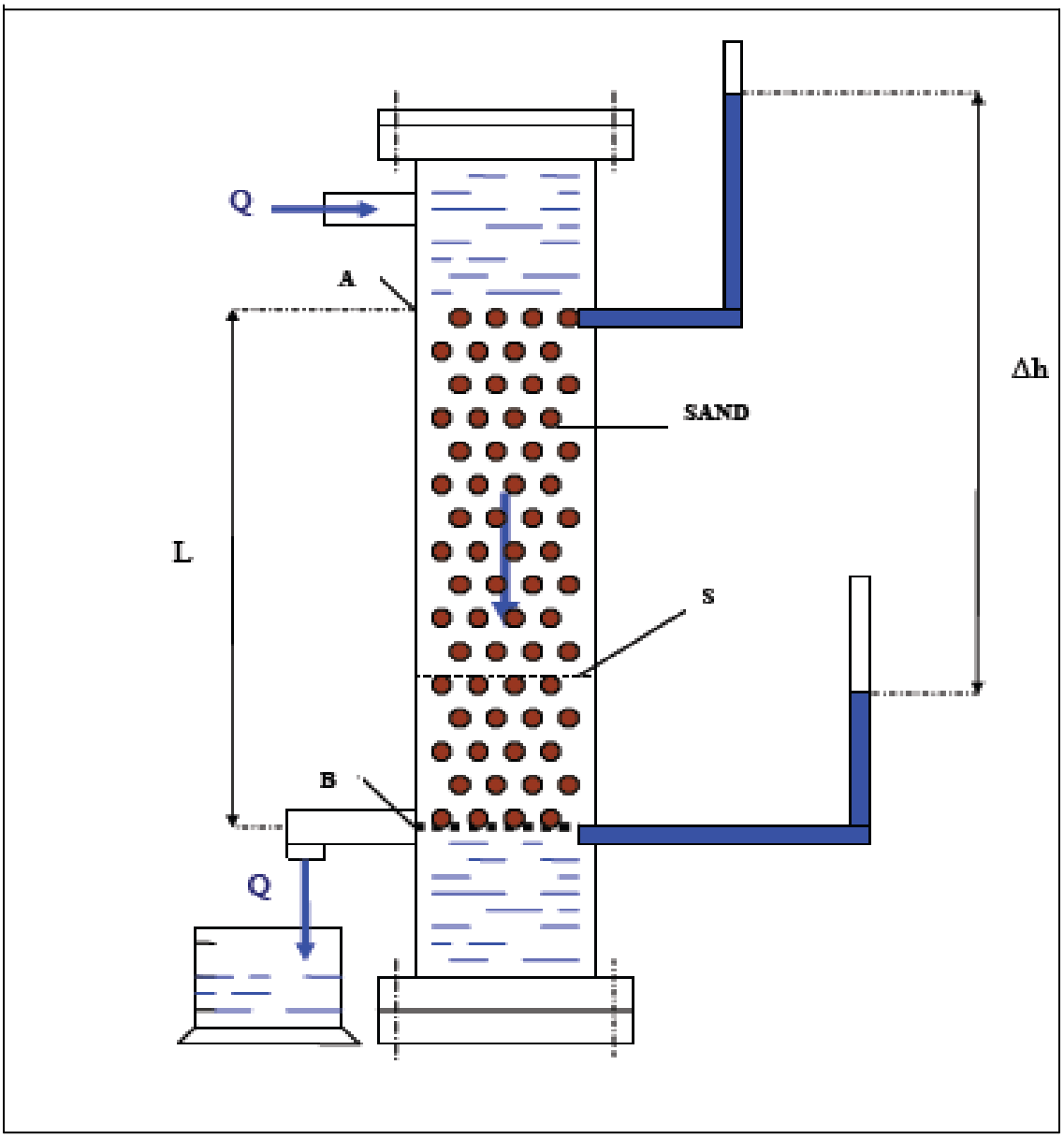

Fig. 1.7*: Darcy's experimental device: a cylindrical column is subdivided into two chambers by the grid B. The upper chamber is filled with sand to a depth L. Q is the water flow and ΔH the hydraulic charge variation in the sand filled zone.*

$$\vec{q} = -K \cdot \vec{\nabla} h \tag{1.25}$$

where

$$\vec{\nabla} h = \frac{\partial h}{\partial x} \cdot \vec{i} + \frac{\partial h}{\partial y} \cdot \vec{j} + \frac{\partial h}{\partial z} \cdot \vec{k} \tag{1.26}$$

represents the hydraulic gradient [*Lefebvre, 2006; Lindquist, 1935*]. The hydraulic conductivity K can be expressed in the following form:

$$K = k \cdot \frac{g}{\nu} \tag{1.27}$$

where k is defined as permeability of the porous medium [*Bear, 1972; Morland, 1978*] and has the dimensions of surface area, g is the gravitational acceleration and ν is the kinematic viscosity of the fluid (surface area/time). We can observe that the term k depends only on the characteristics of the solid matrix, while the term g/ν depends only on the fluid characteristics. Besides, the kinematic viscosity ν has a dependence on the fluid temperature, which represents an important constraint for the evaluation of the time variability of K. Different expressions have been proposed for the permeability k.Kozeny-Carman (1937) have proposed the following:

$$k = C_0 \cdot \frac{n^3}{(1-n^2) \cdot M_s^2} \tag{1.28}$$

where n is the solid matrix porosity, M_s is the surface of the solid matrix per unit volume and C_o is a non-dimensional coefficient. Another empirical expression of the permeability is given by:

$$k = \frac{1}{\beta} \cdot \left[\frac{1-n^2}{n^3.} \cdot \left(\frac{\alpha}{100} \cdot \sum_m \frac{P_m}{d_m} \right)^2 \right]^{-1} \tag{1.29}$$

where β represents the compaction coefficient, α is the granule form factor, P_m representing the percentage (in weight) of the sand between contiguous meshes of the bolter having average diameter d_m.

In Table 1.1 we provide characteristic permeability values ranges ($cm \cdot s^{-1}$) for some common types of soil.

Medium	**Permeability ($cm \cdot s^{-1}$)**
Clean gravel	1 to 10^2 (high permeability)
Clean sand	10^{-3} to -1 (medium permeability)
Fine sand or sand mixed with clay	10^{-7} to 10^{-3} (low permeability)
Clay	10^{-9} to 10^{-7} (very low permeability)

Tab. 1.1: *Characteristic permeability values ranges ($cm \cdot s^{-1}$) for some common media constituting the soil.*

In the case of anisotropy of the porous medium Darcy's law has to be written in the form:

$$\begin{cases} q_x = -K_{xx} \cdot \dfrac{\partial h}{\partial x} - K_{xy} \cdot \dfrac{\partial h}{\partial y} - K_{xz} \cdot \dfrac{\partial h}{\partial z} \\ q_y = -K_{yx} \cdot \dfrac{\partial h}{\partial x} - K_{yy} \cdot \dfrac{\partial h}{\partial y} - K_{yz} \cdot \dfrac{\partial h}{\partial z} \\ q_z = -K_{zx} \cdot \dfrac{\partial h}{\partial x} - K_{zy} \cdot \dfrac{\partial h}{\partial y} - K_{zz} \cdot \dfrac{\partial h}{\partial z} \end{cases} \tag{1.30}$$

or in a more compact form:

$$\vec{q} = -\vec{\vec{K}} \cdot \vec{\nabla} h \tag{1.31}$$

where $\vec{\vec{K}}$ represents the tensor of hydraulic conductivity and is expressed by:

$$\vec{\vec{K}} = \begin{bmatrix} K_{11} & K_{12} & K_{13} \\ K_{21} & K_{22} & K_{23} \\ K_{31} & K_{32} & K_{33} \end{bmatrix} \tag{1.32}$$

We assume that $\vec{\vec{K}}$ is a symmetric tensor, so that $K_{ij} = K_{ji}$. It is always possible to reduce $\vec{\vec{K}}$ to a diagonal form, choosing as the reference system the three orthogonal axes representing the principal axes of anisotropy.

1.6 Hydraulic conductivity in the unsaturated zone

In the unsaturated zone (soil moisture zone), the water content in the soil is the ratio of the water volume contained in a defined sample volume and the total sample volume. Another often used parameter is the volumetric moisture content, expressed by:

$$\theta = \frac{W_w - W_d}{V} \tag{1.33}$$

where θ is the volumetric moisture content, V the sample volume, W_w the weight of the wet sample and W_d the weight of the sample dried at a temperature of 105 °C. The degree of soil moisture content depends on parameters such as precipitation and evapotranspiration [*de Marsilu, 1981*]. In the case in which the moisture content reaches a value for which the force of gravity attracting the water mass down is equal to the

surface tension attracting the water mass upwards, there is no more water infiltration. The corresponding moisture content is defined as the field capacity of the soil.

Consequently, in the case of an unconfined aquifer, the infiltration process in the unsaturated zone depends not only on gravity [*Freeze, 1971*] but also on the soil moisture content. This can be expressed through the expression of the total potential [*Fetter, 2001*] in the unsaturated zone as the sum of elevation potential and the soil moisture potential:

$$\Phi = Z + \varphi(\theta) \tag{1.34}$$

where Φ represents the total potential (acceleration multiplied by a length), Z the elevation potential and φ, which depends on θ, the soil moisture potential. We observe that the curve of φ as a function of θ is different for increasing or decreasing values of θ.

The most important aspect which we underline is that Darcy's law can be applied both in the saturated and unsaturated zone, but with the essential difference that in the unsaturated zone the hydraulic conductivity K is a function of the volumetric moisture content θ, which continually changes with the different infiltration waves related to the precipitation. Another aspect is also dependent on the structure of the precipitation event, and the consequent succession of the infiltration waves. If a precipitation event saturates the soil superficial layer, the unsaturated zone below, which is made up of a solid, the liquid and a gas phases, can be subject to an overpressure (Figure 1.8).

Because of these aspects, the description of the flow in the unsaturated zone is often difficult, i.e. the flow equations are often nonlinear. For strongly simplified configurations, we have the possibility of calculating equivalent coefficients, thus reducing the problem to the casse of saturated flow (see the following section).

1.7 Equivalent hydraulic conductivity in the case of stratified geologic layers

In the case of non-homogenous and anisotropic aquifers, defining the hydraulic conductivity tensor as a function of space is generally difficult [*Reynolds and Elrick, 1991]*. Only for some simple geometries is it possible to calculate equivalent coefficients of hydraulic conductivity.

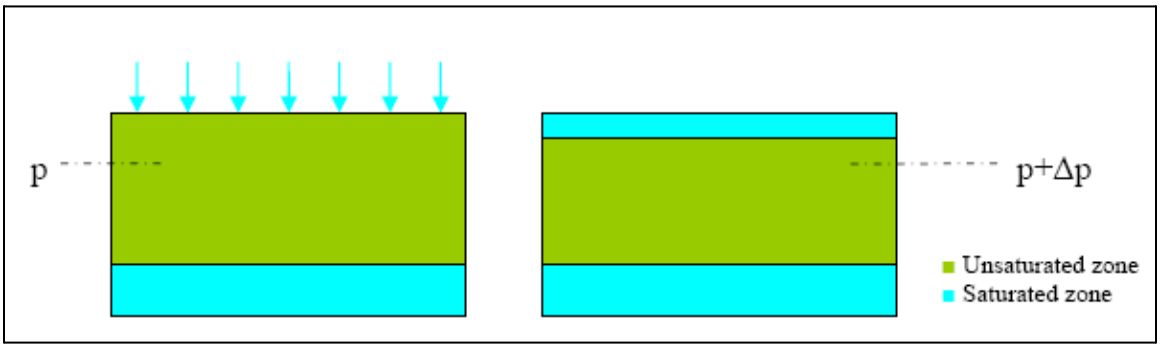

Fig. 1.8: *A precipitation saturating the superficial soil layer can produce an overpressure in the unsaturated three-phasic layer.*

The simplest model of a non-homogenous aquifer can be represented as the superposition of different horizontal geological layers with different values of K.

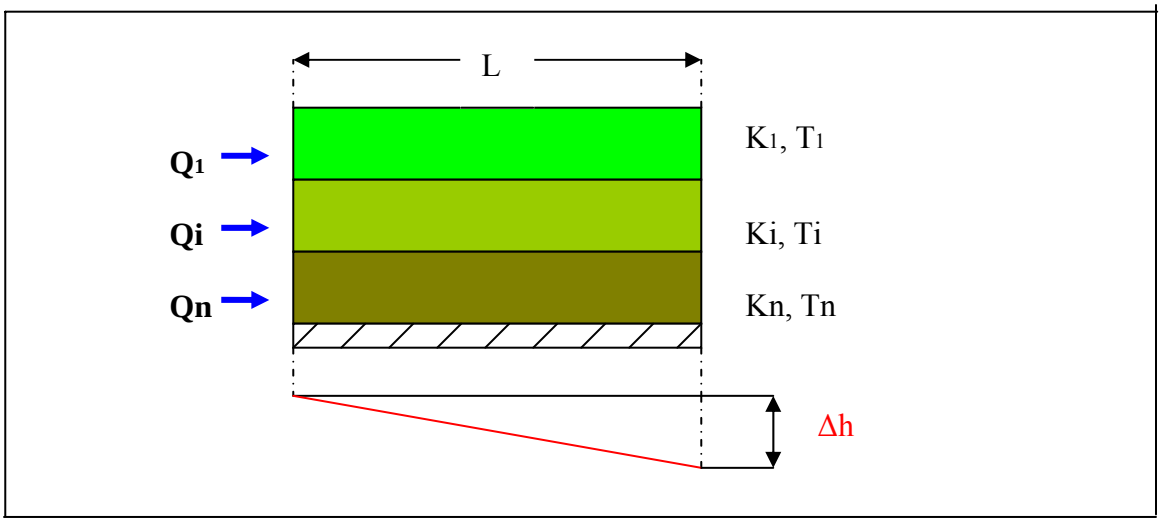

Fig. 1.9: *Parallel flux. Q_i represents the flux through the layer i, K_i the hydraulic conductivity of layer i, Ti the thickness of layer i, ΔH the piezometric head variation along the distance L.*

We assume that each layer is homogeneity and isotropic, so that each layer is characterized by a single value of K. It is possible to calculate the equivalent hydraulic conductivity for two basic situations:

- Horizontal flow in a superposition of different geological layers (parallel configuration)
- Vertical flow in a superposition of different geological layers (series configuration)

The parallel configuration is displayed in Figure 1.9. In this configuration, the total flow is expressed as the sum of the fluxes in the different parallel horizontal layers:

$$Q = \sum_{i=1}^{N} Q_i \tag{1.35}$$

Where Q_i the horizontal flow through the layer identified by i and N the total number of layers. Defining S as the surface area of the layer, $T = \sum_{i=1}^{N} T_i$ as the global thickness, and expressing the flux via Darcy's Law, we obtain:

$$Q_i = B \cdot K_i \cdot T_i \cdot \frac{\Delta h}{L} \tag{1.36}$$

$$\text{thus} \qquad Q = B \cdot \frac{\Delta h}{L} \cdot K_{eqP} \cdot T = B \cdot \frac{\Delta h}{L} \cdot \sum_{i=1}^{N} K_i \cdot T_i \quad => \quad K_{eqP} = \frac{1}{T} \cdot \sum_{i=1}^{N} K_i \cdot T_i \tag{1.37}$$

where K_{eqP} is the equivalent hydraulic conductivity for horizontal flux through horizontally superposed layers. The series configuration is displayed in Figure 1.10.

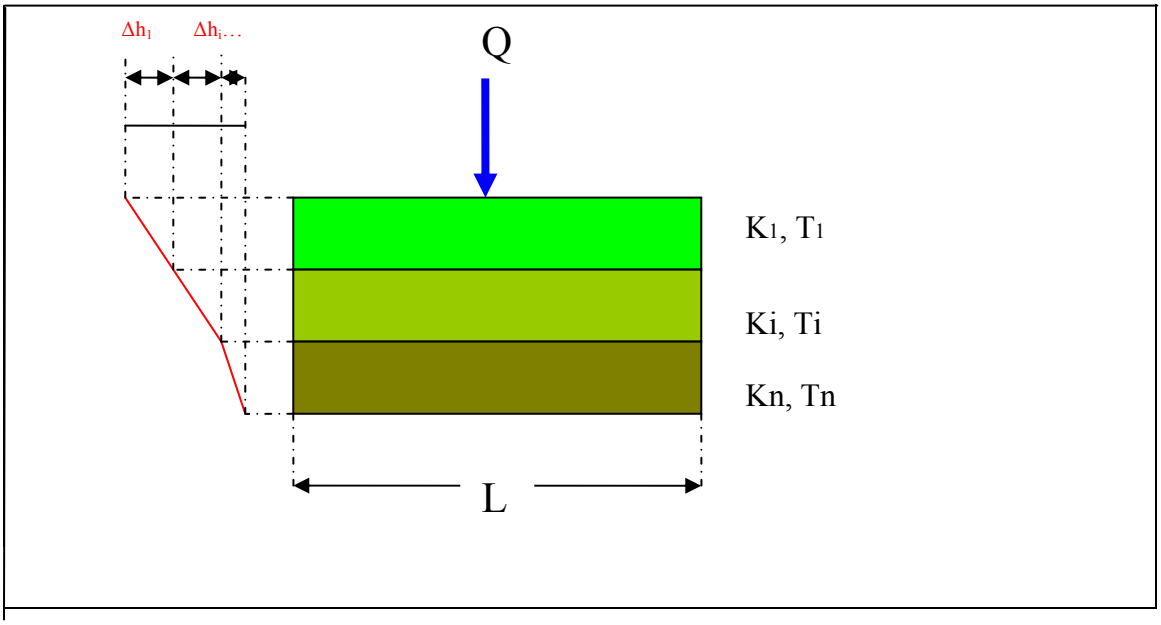

Fig. 1.10: *Series flux. Q represents the flux, K_i the hydraulic conductivity of layer i, T_i the thickness of layer i, ΔH_i the piezometric head variation along the layer i.*

In this configuration, the same flux Q passes through the different layers, and the global piezometric head variation is expressed as the sum of the piezometric head variation in the different layers.

$$\Delta h = \sum_{i=1}^{N} \Delta h_i \tag{1.38}$$

where ΔH_i the piezometric head variation along the layer identified by i and N the total number of layers. Defining S as the surface area of the layer, $T = \sum_{i=1}^{N} T_i$ as the global thickness, and expressing the flow in the layer i through the Darcy's law, we obtain:

$$\Delta h_i = \frac{Q \cdot T_i}{K_i \cdot L \cdot S} \tag{1.39}$$

$$\Delta h = \frac{Q}{S \cdot L} \cdot \sum_{i=1}^{N} \frac{T_i}{K_i} = \frac{Q}{S \cdot L} \cdot \frac{K_{eqS}}{T} \quad => \quad \frac{T}{K_{eqS}} = \sum_{i=1}^{N} \frac{T_i}{K_i} \tag{1.40}$$

where K_{eqS} is the equivalent hydraulic conductivity for vertical flow through horizontally superposed layers

1.8 Seasonal variability of the hydraulic conductivity

As indicated in the Introduction, one of the principal aims of the present research is the implementation of an empirical model relating the local precipitation at the station of Walferdange to the gravity variations registered by the SG located in the WULG. The quality of the model output is strongly dependent on a specific hypothesis: the seasonal variability of one fundamental model parameter, describing the gravity recovery rate after a rainfall event. Now, as it will appear on the model description, we consider that this parameter is correlated to the hydraulic conductivity. Thus, even if our model is empirically parameterized, we consider it useful to make some general considerations about the time variability of the hydraulic conductivity.

As indicated in Section 1.2., the hydraulic conductivity can be expressed as the product of two terms: the first is the permeability k (L^2) that depends only on the properties of the solid matrix, the second is expressed by $\rho \cdot g/\mu = \rho/\nu$ and depends only on the fluid properties, specifically the fluid viscosity. Now, the viscosity is a function of the fluid temperature. Concerning water specifically the dependence of the dynamic viscosity on temperature can be expressed by the following empirical relation: $\eta = \eta_0 \cdot 10^{(B/(T-C))}$ where $\eta_0 = 4.414 Pa \cdot s \cdot 10^{-5}$, B=247.8 K, and c=140 K. In Table 1.2 are displayed the values of the water dynamic viscosity (mPa·s) for some values of the temperature (°C).

Temperature (°C)	Viscosity (mPa·s)
0	1.793
10	1.308
20	1.003
30	0.798
40	0.653

Tab. 1.2*: Values of the dynamic viscosity (mPa·s) for water for different values of temperature (°C).*

Consequently, a seasonal variation of the groundwater temperature determines a corresponding variation of the groundwater viscosity and finally a variation of the hydraulic conductivity. In the frame of the specific issues that we examine, it is important to take into account the fact that the seasonal variation range of the groundwater temperature is a function of the depth below the land surface. *Bertolino [2003]* has carried out an investigation on this subject in the region of central New Mexico beneath the Rio Grande. We show his results in Figure 1.11, displaying maximal and minimal annual temperatures with respect to the depth.

At a depth of 1 m below the surface, the annual temperature range is about 22°C. At a depth of 15 m the range is reduced to about 4°C.

In addition, if we consider the case of non-homogeneity of the hydro geological parameters, we can identify another factor affecting the seasonal variability of hydraulic conductivity. As shown in 3.1., in the case of superposition of geological layers with different values of K, we can calculate equivalent values. Consequently, if the presence

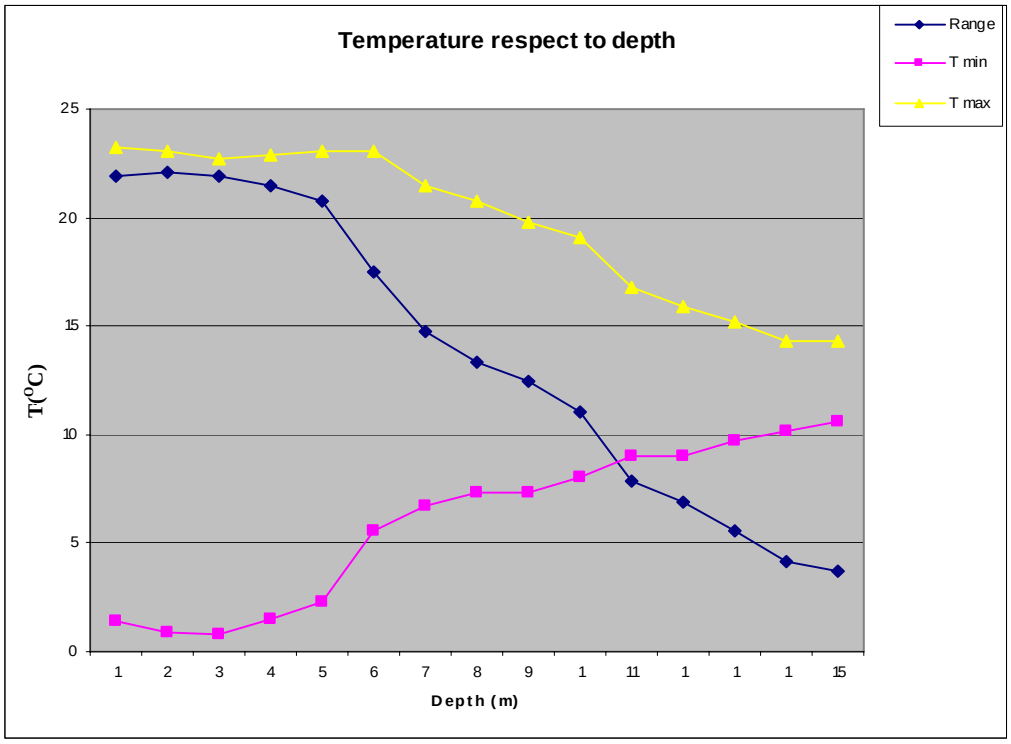

***Fig. 1.11**: Maximal annual temperatures (yellow, °C), minimal annual temperatures (pink, °C) and annual range, difference between annual maximal and minimal temperatures (blue, °C) as a function of depth below the surface in central New Mexico beneath the Rio Grande.*

of water in the different layers is subject to seasonal variations, the equivalent value of the hydraulic conductivity will also be subject to variation. We can consider for instance a simple two layer configuration, $T_1=T_2=T$ being the layer thickness. If water is present only in the underlying layer 2, then $K_{eq}=K_2$. If the water is present in the two layers, we have:

$$K_{eq} = \frac{1}{2 \cdot T} \cdot (T \cdot K_1 + T \cdot K_2) = \frac{K_1 + K_2}{2} \neq K_2 \quad \text{if} \quad K_1 \neq K_2 \tag{1.41}$$

1.9 General equations of the groundwater fluxes for confined aquifers

The classical equations describing the groundwater fluxes are based on a combination of Darcy's law, which describes the flux of fluids through porous means, and mass continuity equations on definite control volumes [*Anderson, 2007; Cooper, 1966; Davis and De Wiest, 1966; Hubbert, 1940; Ledoux, 2003; Polubarinova-Kochina, 1962; Rosenheim and Bennet, 1984*]. Different models can be constructed, depending on the different hydro-geological configurations, which can have an extreme variability. To construct models, which can be implemented it is often necessary to make reference to basic simplified geometries [*Domenico, 1972; Jacob, 1950*].

In the case of unconfined aquifers, with the presence of only an underlying impermeable layer, we can assume that the groundwater movement is essentially due to the effect of gravity. In the case of confined aquifers, where the water-saturated zone is located between two impermeable geologic layers (aquicludes), the water storage variation in the aquifer depends on the pressure variations. We introduce here a new parameter, volumetric storage. Volumetric specific storage is defined as the amount of water released from storage for unit of volume of the aquifer and for unit of change in hydraulic head [*Narashiman and Kanehiro*, 1980; *Bredehoeft and Cooley, 1983*].

$$S_s = \left| \frac{1}{V_a} \cdot \frac{\Delta V_w}{\Delta h} \right| \tag{1.42}$$

where S_s is the specific storage, V_a is the volume of the aquifer from which water is released, V_w is the volume of released water, H the hydraulic or piezometric head. The relation between the change of volume of water V_w stored in a control volume of aquifer V_a and the hydraulic head variation can be expressed in the form:

$$\Delta V_w = -V_a \cdot S_s \cdot \Delta h \tag{1.43}$$

In differential form, the instantaneous variation with reference to the elementary time interval δt is given by the expression:

$$\frac{\partial V_w}{\partial t} = -V_a \cdot S_s \cdot \frac{\partial h}{\partial t} \tag{1.44}$$

We can now calculate a volume balance in a Cartesian frame by considering an elementary control volume dV=dx·dy·dz with sides parallel to the x, y and z axes, respectively (Figure 1.12). We define as q_x, q_y, q_z the specific fluxes (fluxes for unity of surface) through the control volume faces perpendicular to the axes x, y and z respectively. Considering the x direction, the flux at abscissa x is given by:

$$Q_x = q_x \cdot dy \cdot dz \tag{1.45}$$

The flux at abscissa x+dx is given by:

$$Q_{x+dx} = (q_x + \frac{\partial q_x}{\partial x} \cdot dx) \cdot dy \cdot dz \tag{1.46}$$

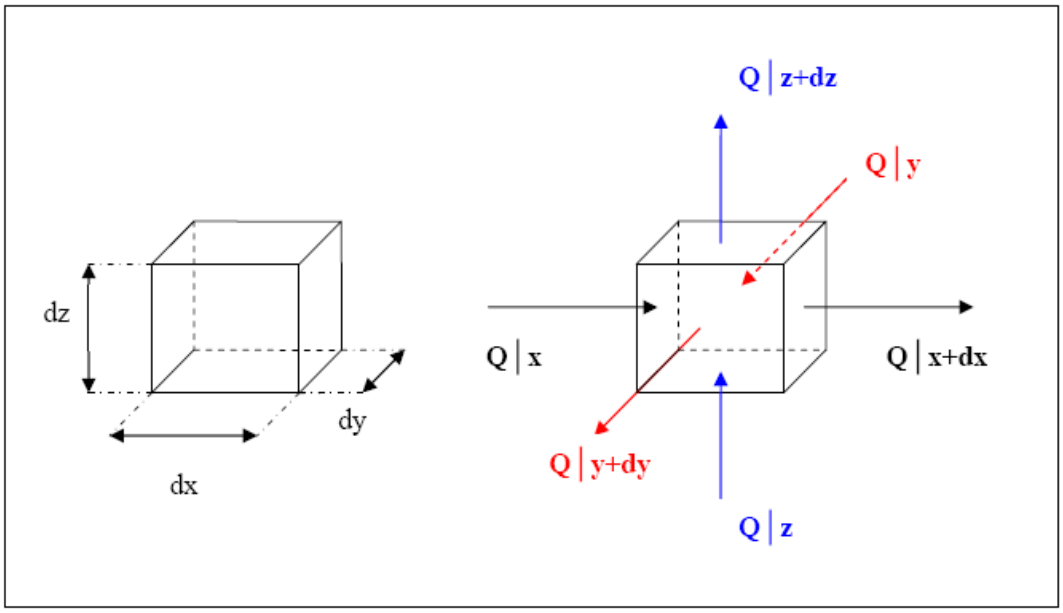

***Fig. 1.12**: Elementary control volume in a Cartesian reference system. The sides dx, dy and dz are aligned along the directions x, y and z respectively.*

The flux variation along x is thus expressed by:

$$Q_x - Q_{x+dx} = (\frac{\partial q_x}{\partial x} \cdot dx) \cdot dy \cdot .dz \qquad (1.47)$$

Writing the similar equations for the directions y and z and summing, we obtain the global flux variation through the control volume dV. With the use of equation 1.47, and introducing a source term G, representing a water volume input or subtraction for unity of volume of the aquifer and unity of time, we can calculate a volume balance with reference to the elementary time δt:

$$\frac{\partial q_x}{\partial x} \cdot dx \cdot dy \cdot dz + \frac{\partial q_y}{\partial y} \cdot dy \cdot dx \cdot dz + \frac{\partial q_z}{\partial z} \cdot dz \cdot dx \cdot dy = -S_s \cdot \frac{\partial h}{\partial t} \cdot dx \cdot dy \cdot dz - G \cdot dx \cdot dy \cdot dz$$

and finally :

$$\frac{\partial q_x}{\partial x} + \frac{\partial q_y}{\partial y} + \frac{\partial q_z}{\partial z} = -S_s \cdot \frac{\partial h}{\partial t} - G \quad \text{or in vector form} \quad S_s \cdot \frac{\partial h}{\partial t} = -\vec{\nabla} \cdot \vec{q} - G \qquad (1.48)$$

where ∇ is the nabla operator and $\vec{\nabla} \cdot \vec{q}$ represents the divergence of the specific flux $\vec{q}$ in Cartesian coordinates. In the case of heterogeneity and isotropy, the hydraulic

conductivity is a scalar (not a tensor) and the flux vector can be expressed in terms of the hydraulic head with the use of Darcy's Law [3]. Equation 1.49 becomes:

$$S_s \cdot \frac{\partial h}{\partial t} = -\nabla^2 h - G \tag{1.49}$$

Dividing Equation 1.49 by the specific storage S_s, defining $\alpha = K/S_s$ as hydraulic diffusivity and posing $Gs = G/Ss$, we finally obtain the general expression for the groundwater equation for homogenous and isotropic confined aquifers:

$$\frac{\partial h}{\partial t} = -\alpha \cdot \nabla^2 h - G_s \tag{1.50}$$

Because of the difficulty of an accurate evaluation of hydro-geological parameters, the previous equation is generally integrated with reference to simplified ground models. For instance, the finite elements model *modflow* makes reference to a simplified quasi-three-dimensional representation. In the empirical approach to our specific problem, we will have to also simplify our geometriy in order to achieve an implementable model.

1.10 Seasonal variability of the evapotranspiration processes

As previously indicated, an important issue for the parameterization of our model is the seasonal variability of some hydrological parameters and processes [*Hupet and Vanclooster, 2005*]. Amongst them, the evapotranspiration processes assumes a significant relevance. Under the global definition of evapotranspiration two different processes are considered:

- Evaporation represents the transition of the water contained in the ground's upper layer (root zone) from the liquid phase (in the soil) to the gas phase (in the atmosphere), due to the input of environmental energy.
- Transpiration represents the transition to the gas phase in the atmosphere of part of the water absorbed by the plant roots in liquid form, through the micro pores present in the plant leaves. The remainder of the absorbed water is used by the plant for photosynthesis.

The evaporation and evapotranspiration have different characteristics. Evaporation is a purely thermo dynamical process due to the environment energy input, represented essentially by the solar electromagnetic radiation. Transpiration, instead, is also based on more complex biological mechanisms. However, particularly in regions of extended vegetal cover, it can be quite difficult to analyze the two processes separately, and they are almost considered as a unique process. Evapotranspiration is normally reported in terms of water height (usually mm) per unit of time. Distinction is made between the potential evapotranspiration (ETp) and real evapotranspiration (ETr):

- Potential evapotranspiration (ETp), also defined as reference evapotranspiration (ETo), represents the maximal amount of water (mm/time) that can be transferred from the liquid phase to the gas phase in the atmosphere from a soil with homogenous vegetal cover, supplied with adequate water and nourishment, under defined climatic conditions. The ETp depends solely on the climatic conditions,

the vegetal cover characteristics being brought to a standard configuration. Thus, the ETp is the parameter that can be used as a term of comparison.

- Real evapotranspiration (ETr) represents the actual amount of water (mm/time) transferred to the gas phase in the atmosphere from a soil with specific conditions of soil coverage under defined climatic conditions.

As indicated above**,** the ETp is determined only by the climatic factors. The principal factors are:

- Solar radiation, providing the principal part of the energy required by the process of phase transition.
- Wind: the wind speed, but also the wind characteristics, such as humidity and temperature of the air mass, can have a significant influence on evapotranspiration. Specifically, hot and dry winds will improve the process.
- Air humidity: the humidity gradient between air and soil is directly proportional to the amount of evapotranspiration.

In addition to the above climatic parameters, ETr is also dependent on other kinds of factors. The most significant are:

- Vegetal cover**:** the kind of vegetation, its degree of development, its distribution and other cultivation characteristics have a direct influence on the evapotranspiration processes.
- Soil moisture**:** obviously, the evapotranspiration processes are subjected to the presence of water. In the absence of water, these processes can not take place.

In order to make a quantitative estimation of evapotranspiration, different empirical models have been proposed. We present some of the simplest and most widespread, underlying the fact that, because of the assumed simplifications, they imply large margins of uncertainty. For the calculation of the ETp, one of the most frequently used methods is based on the empirical equation proposed by *Thorntwhite* in 1948:

$$ETpj = k_j \cdot 16.2 \cdot (\frac{10}{I} \cdot T_j)^a \tag{1.51}$$

Where ETpj represents the potential evapotranspiration (mm/month) at month j, Tj represents the average temperature during month j, k_j represents the radiation coefficient at month j, defined as the ratio between the average diurnal hours during the month and the half of the daily hours (12 hours). Consequently, k_j is a function of the latitude. I is defined as the annual heath index, expressed by:

$$I = \sum_{j=1}^{12} (\frac{T_j}{5})^{1.514} \tag{1.52}$$

and a is a polynomial function of I expressed by:

$$a = 0.49239 + 1.792 \cdot 10^{-2} \cdot I - 7.71 \cdot 10^{-5} \cdot I^2 + 6.75 \cdot 10^{-7} \cdot I^3 \tag{1.53}$$

For the calculation of the ETr, one of the most frequently used methods is based on an empirical equation, proposed by *Turc* in 1954, relating the annual evapotranspiration to the temperature and the precipitation, and expressed by:

$$ETr = \frac{P}{(0.9 + (\frac{P}{L})^2)^{0.5}} \tag{1.54}$$

where ETr represents the annual real evapotranspiration (mm/year), P represents the total yearly amount of precipitation (mm/year), L is defined as the atmosphere evaporation power, expressed by:

$$L = 300 + 25 \cdot T + 0.05 \cdot T^2 \tag{1.55}$$

where $T = \frac{\sum_{j=1}^{12} P_j \cdot T_j}{P}$ is the yearly weighted average temperature, T_j representing the average temperature (°C) at month j and P_j the precipitation height at month j. In the frame of our research, the essential issue is represented by the seasonal variability of the evapotranspiration processes. Our interest is to make reference to the ET_p, which depends only on the climatic conditions, and not on the ET_r that depends also on the typology, state of development and other characteristics of the vegetal cover.

We estimated the monthly potential evapotranspiration in the Grand Duchy of Luxembourg. The calculation of the average monthly amounts of ETp has been made by introducing into the Thornthwhite equation the values of the radiation coefficients k_j referred to the mean latitude of Luxembourg and monthly average temperatures registered in Luxembourg for the last 10 years. The results are displayed in Figure 1.13.

We observe that the estimated ET_p monthly amounts range from a low value of 0.2 mm in January to a maximum value of 116.5 mm in July. This implies that the percentage of precipitated water that actually infiltrates the soil to increase the groundwater storage is subject to seasonal variation. During the warm months, a significantly lower fraction of precipitation contributes to the recharge process than in the warm months. This represents an important issue in regard to the model parameterization.

1.11 Simplified models of groundwater flow: The Tank Model

In Section 1.5 we discussed the behavior of the groundwater fluxes in the general configuration of confined aquifers. The equations describing the processes are obtained by combining mass continuity equations with reference to appropriate control volumes and Darcy's law, which relates the flux of a fluid through a porous medium to the hydraulic gradient *[Newman and Witherspon, 1970*]. The application of the same method to some basic, yet specific, geometries allows us to construct simpler models that, with the assumption of different simplifying hypothesis, can be relatively easily to implement

(in a numerical sense). The Tank Model represents one of the basic reference models we employ.

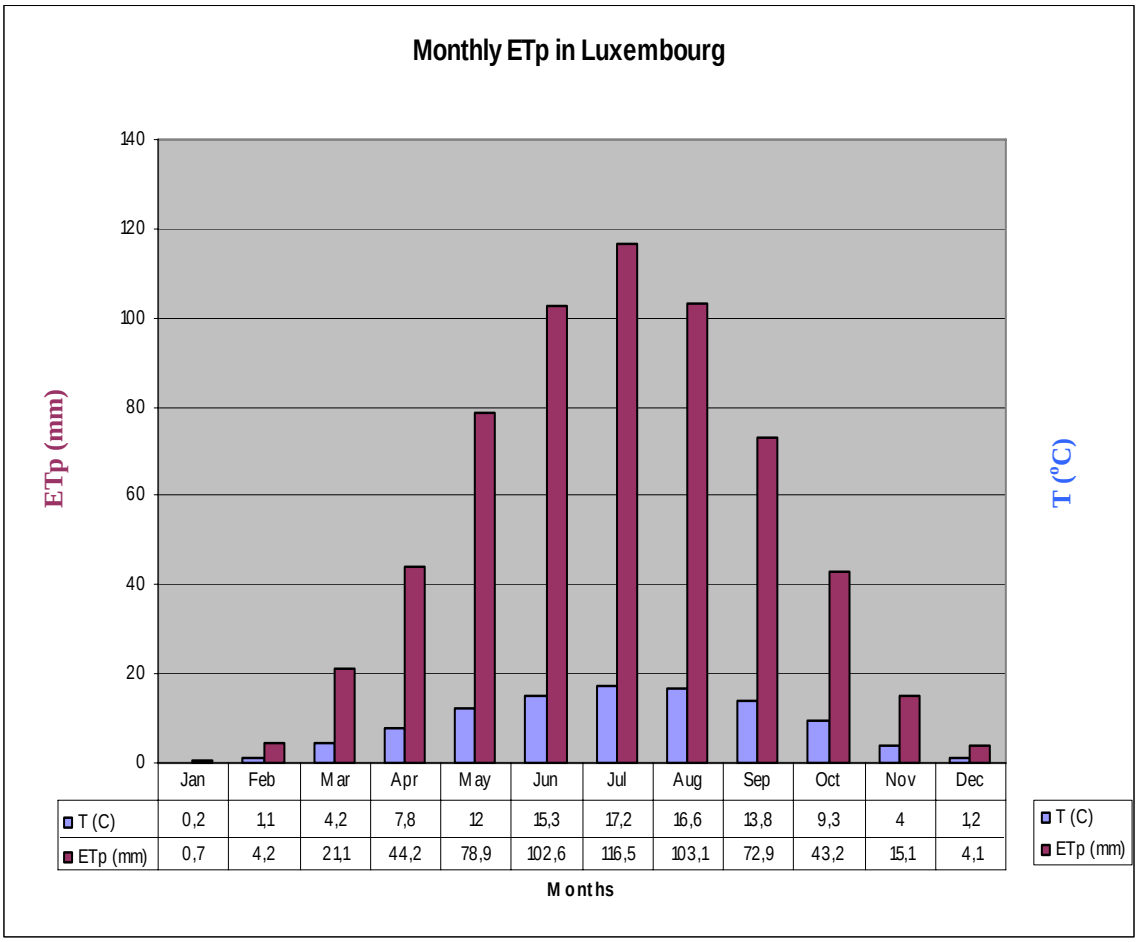

	Jan	Feb	Mar	Apr	May	Jun	Jul	Aug	Sep	Oct	Nov	Dec
T (C)	0,2	1,1	4,2	7,8	12	15,3	17,2	16,6	13,8	9,3	4	1,2
ETp (mm)	0,7	4,2	21,1	44,2	78,9	102,6	116,5	103,1	72,9	43,2	15,1	4,1

Fig. 1.13*: Average registered monthly temperatures (blue, °C) and estimated monthly ETp amounts (violet, mm) in the Grand Duchy of Luxembourg.*

To introduce the Tank Model, we must start by analyzing the water fluxes in the simple hydro-geological configuration represented by an unconfined aquifer, in the presence of a single aquicludes (impermeable geological layer) under one or more permeable layers (constituted by porous mediums). A schematic representation of this configuration is displayed in Figure 1.14.

The essential point to underline here is that, in this configuration, the water movement happens only under the effect of gravity. We must also specify that there is a substantial difference between the dynamical behaviors of the water mass in the unsaturated zone (above the water table) and the saturated zone (below the water table). In the unsaturated zone, there is no continuity in the water mass because the liquid does not completely fill the pores in the solid matrix. Here, the water movement can be essentially described as vertical percolation.

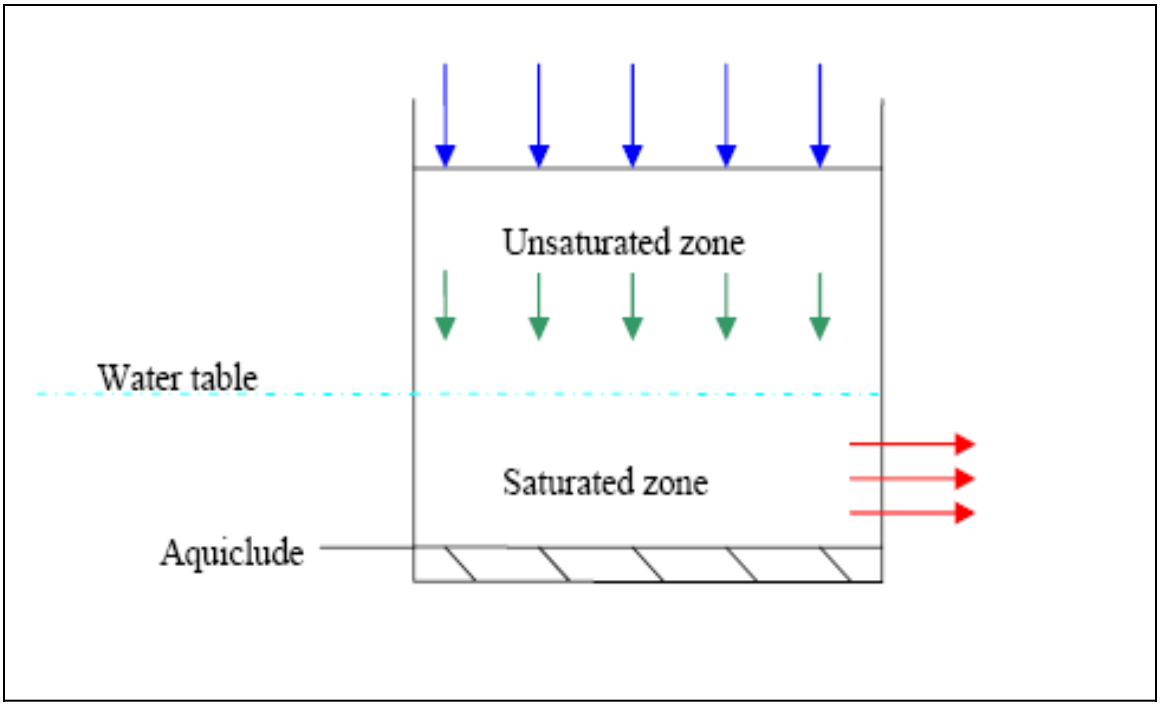

***Fig. 1.14**: Unconfined aquifer, in the presence of a single underlying aquiclude. Precipitation is represented in blue, percolation through unsaturated zone in green and filtration through saturated zone in red.*

In the saturated zone, to the contrary, there is continuity in the water mass, because the liquid fills the pores of the solid matrix completely. Here, the water movement can be essentially described as horizontal filtration through the medium.

The Tank Model (Figure 1.15) is based on a further simplification of this configuration. The discharge process is reduced to the efflux of the water contained in a tank through a porous mean represented by a simple plug [*Roche, 1963*]. Here, the liquid mass is not distributed in the pores of a solid matrix, and the hydraulic head simply corresponds to the water level in the tank. In addition, the model defines a precise direction of the efflux. In this case, Darcy's law can be expressed in the following form:

$$Q = K \cdot \frac{s}{L} \cdot h \qquad (1.56)$$

where Q represents the water flux from the plug (volume/time), s and L represent the section and length of the plug, respectively. Obviously, the geometric parameters are specific to this simplified model. Note that the outgoing flux is related, through Darcy's law, to hydro geological parameters like hydraulic conductivity, which itself is dependent on parameters such as the soil porosity and the fluid viscosity.

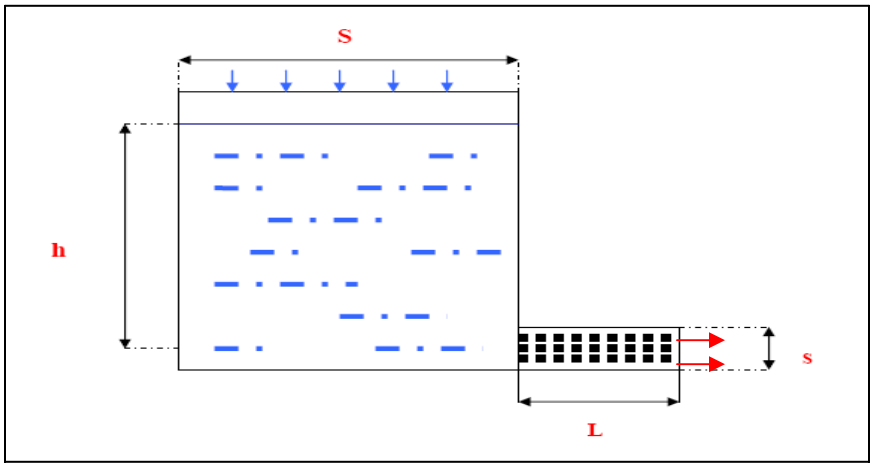

Fig. 1.15: *The tank model: S is the surface area of the tank, h the water level, s and L the section and length of the plug.*

It is now possible to write a mass (or volume, if we assume a constant density) continuity equation, considering precipitation events as the incoming volume of water. We define as rainfall rate, r (length/time), as the precipitation height per unit time. To obtain an analytical expression of the equation, we assume r(t) is a continuous function of time. Actually, precipitation is represented by a discrete set of values referred to discrete time indexes, and the equation has to be solved numerically. The volume balance equation expresses the fact that the liquid volume variation in the tank, with reference to the elementary time interval dt corresponds to the difference between the incoming liquid volume (precipitation) and the outgoing liquid volume (efflux from the plug) with reference to the same time interval dt:

Volume difference = Entering volume – Outgoing volume

$$S \cdot dh(t) = -Q(t) \cdot dt + S \cdot r(t) \cdot dt \tag{1.57}$$

Combining the equation with Darcy's law and defining c (1/time) as the level variation rate:

$$c = \frac{K \cdot s}{S \cdot L} \tag{1.58}$$

We obtain the analytical form of the equation describing the level variation in the tank:

$$\frac{dh(t)}{dt} = -c \cdot h(t) + r(t) \tag{1.59}$$

In absence of precipitation, Equation 1.59 can be analytically integrated leading to an exponential decay expression describing the emptying of a tank through a porous plug as a function of time. We assume the initial conditions that at the instant zero ($t_{o=0}$) the level is h_0.

$$h = h_0 \cdot e^{-c*t} \tag{1.60}$$

It can be easily verified that parameter c has the dimensions of the inverse of a time. The parameter $\tau = 1/c$ is a characteristic time parameter of the tank model, representing the time necessary for the water level to decrease from the initial value h_o to 0.37 h_o. The model of exponential decay is frequently used in hydrology for describing the emptying of ponds, the decrease of soil humidity and other analogous processes.

1.12 Correspondences between the Tank Model and the Antecedent Precipitation Index (API) model

Hydrologists make often use of different indices characterizing the variation of soil moisture as a function of precipitation [*Iffly et al. 2004*]. For this purpose, one of the most frequently used indices is the Antecedent Precipitation Index (API). API is expressed in terms of water height (usually mm) and relates the level of soil humidity to the antecedent precipitation through the expression [*Musy and Higy, 2003*]:

$$API_i = API_{i-1} \cdot K + P_{i-1} \tag{1.61}$$

where API_i represents the Antecedent Precipitation index at time i, API_{i-1} represents the Antecedent Precipitation Index at time i-1 and P_{i-1} represents the precipitation at time i-1. In Section 1.11 we obtained the analytical expression of the Tank Model equation. The actual precipitation time series are a discrete set of values referred to finite time intervals. Consequently, equation 1.60 has to be rewritten as a discrete expression defining the terms of a progression. We obtain the expression:

$$h_{i+1} = (1-b) \cdot h_i + r_i \tag{1.62}$$

where b is now a non dimensional parameter and r_i (length) correspond to r_t (length/time) integrated to the basic unity time intervals. We observe that this last expression is formally identical to 1.62. Even if Equation 1.62 is essentially used to evaluate the soil humidity variation in the upper layer (root zone), information of seasonal variability of parameter K of the API model can prove useful for the estimation of the variability of the parameter (1-c) of the Tank Model. (We will make a more general use of this later.) We must take into consideration that the root zone is the layer principally submitted to the evapotranspiration processes, which we have discussed in Section 1.10.

Rosenthal et al. [1982] have estimated that in Washita Basin (USA), for a superficial layer of 15 cm thickness, the value of K_p ranges from 0.84 in July to 0.99 in December.

The correlation between c and K_p indicates that the local value of c may have a significant seasonal variability.

1.13 Conclusion

In order to obtain simplified models describing the hydrological effects due to gravity, we begin by providing a review of the principal processes related to the water cycle.

We have presented a survey of these different processes, dedicating particular attention to the problem of subsurface water dynamics.

Simplifying, a fraction of the volume of water derived from precipitation events in their different forms (rain, snow, and hail) is subject to infiltration into the soil's porous layers, increasing the groundwater storage. This represents the hydrological recharge process.

The subsequent hydrological discharge process, the reduction of the groundwater storage, is due to different sub-processes, such as the efflux from the groundwater reservoir, or evapotranspiration from the soil superficial layers.

We have shown how most of the models describing groundwater dynamics in porous media are based on the combination of the Navier-Stokes equations (often in simplified form) and Darcy's law.

The Navier-Stokes equations are a system of non-linear partial differential equations describing the dynamics of fluids considered as continuous media. The equations express three fundamental physical principles:

- Mass conservation (continuity equation).
- Consevation of linear momentum, derived from Newton's second principle of dynamics.
- and Energy conservation, derived from the first principle of thermodynamics.

In the particular case of steady flow of non viscous fluids, the Navier-Stokes equations, integrated on a line of flow, lead to Bernoulli's equation.

Darcy's Law presents an empirical description of the flow of fluids through porous media. The law expresses the proportionality between the specific flow (flow for surface unit) through a porous medium and the hydraulic head acting on the fluid. The proportionality coefficient, known as hydraulic conductivity and designated as K, is an essential parameter in the field of the groundwater dynamics.

We have shown how different simplified models for the description of the groundwater flows are based on the combination of mass continuity equations, with reference to defined control volumes, and Darcy's Law.

In this category, the basic Tank Model, in which essential simplifications are required, the problem is reduced to the efflux of the fluid contained in a tank (and not distributed in a porous matrix) through a porous plug. The continuity equation expresses the fact that the difference between the incoming volume of fluid and the outgoing volume of fluid in a reference time interval corresponds to the volume variation in the tank in the same time interval. In this simplified model, the water level in the tank simply corresponds to the hydraulic head. The incoming volume of water is represented by the precipitation, which consequently corresponds to the model input. The outgoing volume of water corresponds to the efflux from the porous plug.

We have adopted the Tank Model as the basis for the description of the effect of the groundwater storage variations on the gravity signal registered at the station of Walferdange.

In the basic Tank Model, the seasonal variability of hydro-geological parameters such as hydraulic conductivity and evapotranspiration rates is not directly taken into account. Nevertheless, we have expressed the hypothesis that this variability represents an important issue and is necessary for the development of reliable and precise models.

We have pointed out how hydraulic conductivity depends both on soil parameters, such as porosity, and on fluid parameters, such as viscosity. Viscosity, in particular, is a function of the fluid temperature, which is subject to seasonal variability. Furthermore, hydraulic conductivity in unsaturated soil layers is a function of the degree of saturation, which varies significantly throughout the year. This implies a variability of the parameter c of the tank model.

Evapotranspiration rates depend both on air and soil temperature, and are consequently also subject to seasonal fluctuations. We have pointed out that this can significantly affect the actual level of the model input.

The seasonal variability of these important hydro-geological parameters will be taken in account in Chapter 3, where the Tank Model is rewritten in terms of gravity changes.

Glossary of Meteorology (2009). "Precipitation". American Meteorological Society. Retrieved 2009-01-02.

Chapter 2

Chapter 2: Hydrological effects on gravity

2.1 Introduction

Environmental mass changes, in particular atmospheric as well as surface and subsurface water mass changes due to the occurrence of meteorological events, can have a significant effect on the gravity signal. These effects are extremely difficult to characterize as they exhibit tremendous variability in their temporal and spatial scales [*Kroner, 2001; Kroner et al., 2001; Llubes et al. 2004; Lambert and Beaumont, 1977; Zerbini et al,. 2010*]. For instance, the processes related to the atmospheric air mass redistribution are mostly characterized by long wavelengths (>500 km) [*van Dam et al.,* 2001*; Crossley et al.,* 2005; *Hinderer et al.,* 2006]. Shorter wavelength effects (<10 km), such as those related to groundwater storage variability arising from local precipitation, can also have a significant effect on the gravity signal [*Meurers et al., 2007*; *Van Camp et al. 2006, Kroner and Jahr,* 2006*; Bower and Courtier,* 1998*; Boy and Hinderer,* 2006*; Kroner, 2001; Takemoto et al. 2002*].

The direct evaluation of the hydrological effects on gravity is only possible when accurate information on groundwater storage changes at different temporal and spatial scales is available. In addition, effective modeling also requires the knowledge of local hydrogeological parameters.

In the absence of this information, only empirical relationships can be built. We will describe the hydrological gravity changes at Walferdange, using the local precipitation time series as input for two simple empirical models:

- The Tank Model, introduced in Chapter 1, which describes only the hydrological discharge phase following a precipitation event. The recharge phase is considered as instantaneous.
- The Double Exponential Model, which describes both the hydrological recharge and discharge phases following a precipitation event.

We will modify both of these basic models in order to describe, 1) the short scale effects due to the local precipitation and 2) the seasonal hydrological gravity fluctuations. We do this by introducing the seasonal variability of the model's parameters (as discussed in Chapter 1). Specifically we characterize the recharge and discharge durations as a function of the time of year. We find that with our empirical parameterization, we are unable to identify the different causes of these seasonal fluctuations.

In order to define the models in terms of gravity variations, we must estimate the admittance between a given precipitation height and the resulting gravity perturbation. This will be achieved with the use of a Digital Elevation Model (DEM) of the area above the gravimeter.

The topography of Walferdange is characterized by significant height gradients. It is therefore unreliable to use values of the admittance obtained with simplified analytical models, such as the Boguer's infinite plate model.

2.2 Newton's Law of Universal Attraction

Surface and subsurface water storage changes can affect the gravity signal through two essential mechanisms:

- The direct Newtonian attraction due to the water mass.
- The displacement of the surface due to the water load. At the periods we investigate here, the Earth, the Earth is considered to be elastic.

Thus, any precipitation event produces a displacement of the surface with as associated mass redistribution.

Newton's law of universal attraction states that the force exerted between two point masses is directly proportional to the product of the masses and inversely proportional to the square of the distance separating the masses. The force is directed along the direction joining the two point masses and is always attractive. In vector form, Newton's law can be expressed in the following way:

$$\vec{F}_{12} = -G \cdot \frac{m_1 \cdot m_2}{r^2} \cdot \hat{r}_{12} \tag{2.1}$$

where $\vec{F}_{12}$ represents the force exerted from mass m_1 on mass m_2, $\hat{r}_{12}$ represents the unit vector in the direction joining the point masses and the proportionality constant, $G=6.7428 \cdot 10^{-11} \pm 0.00067 \cdot 10^{-11}$ N m^2 kg^{-2}, is Newton's universal constant of gravity (*CODATA, 2006*). In addition, we also invoke the law 'that for every action there is an equal and opposite reaction'. Stated mathematically we have:

$$\vec{F}_{21} = -\vec{F}_{12} \tag{2.2}$$

Newton's law can be perfectly applied in the case of point masses, i.e., masses with no volume extension. More generally, the field of applicability of Newton's law can be extended to bodies whose characteristic dimensions are much smaller that the distance separating their centers of mass. In this case, $\hat{r}_{12}$ represents the unit vector in the direction joining the bodies' centers of mass. In the case of extended bodies, an integration must be carried out, by performing a sum of all the elementary forces exerted between all the elementary volume elements in which the bodies are subdivided.

As a consequence of Gauss's theorem, if the bodies have a spherical form, the integration gives the same results as point masses, where the centers of mass of the bodies correspond to the point mass positions [*Telford et al. 1990; Dufour, 2001*].

2.3 Gravity field at earth surface

The gravity field produced by a single point mass is a central and consequently conservative field, having a spherical symmetry. The force lines are directed toward the point mass and equipotential surfaces are concentric spheres centered on the point mass. A consequence of Gauss's theorem is that the gravity field produced by spherical bodies, for the points lying outside the volume but included in the body surface, is the same as if the body's mass were concentrated at its center of mass. Using Newton's law, we can thus

calculate the force exerted by a spherical body having the Earth's mass and the average Earth radius on a mass lying on its surface (Figure 2.1).

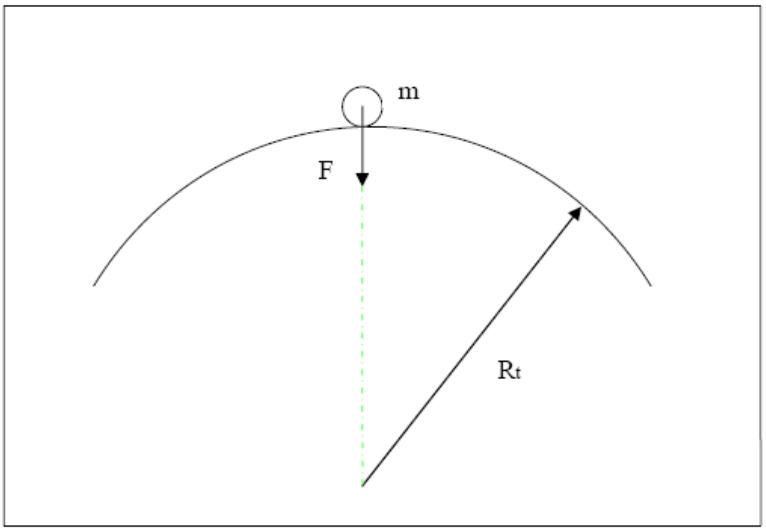

***Fig. 2.1**: Force exerted on mass m from Earth (considered as perfectly spherical)*

If we make the hypothesis that the surface is perfectly spherical, that the mass is homogenously distributed and that the sphere is not subject to rotation, the force F, directed toward the center of the sphere, has the same intensity in every point of the surface and its amplitude can be calculated using Newton law of universal gravitation:

$$|F| = G \cdot \frac{m \cdot M_t}{R_t^2} \tag{2.3}$$

Where F is the force exerted on mass m, G is the universal constant of gravitation, M_t=5,9736·10^{24} is the Earth's mass and R_t=6,37101·10^6 is the average Earth radius. Posing g=(m*M_t)/$R_t^{2,}$ equation 2.1 can be written as:

$$|F| = m \cdot g \tag{2.4}$$

where g represents the amplitude of the *gravity acceleration* on Earth's surface for a non-rotating, homogenous and perfectly spherical Earth. In this case, the vector **g** is directed toward the Earth's geometrical center corresponding to the Earth's center of mass**.** With the given values of Earth's mass and average radius, we obtain for g the value of 9,822 m·s^{-2}. This value represents only an estimation of the actual gravity acceleration on Earth's surface, because we must take into account the following aspects:

- The Earth is not homogeneous and is in fact made up of different materials that are not uniformly distributed. Specifically, the value of g depends both on the local geologic and topographic conditions at the point of measurement rather than on the global Earth inhomogeneities

- The form of the Earth is not a perfect sphere. It is more accurately represented (to first order) by an ellipsoid of rotation, which is flattened at the poles. Consequently, apparent gravity is a function of latitude: it is greater at high latitudes, where the distance from the Earth's center is lower. Obviously, because of the irregularity of the Earth surface, the locally measured value of g depends also on the height of the measurement point evaluated with respect to a reference equipotential surface (e.g. sea level).
- The Earth rotates on its axis. If we refer to a non-inertial rotating frame, a body lying on Earth surface's is subject to a centrifugal acceleration directed orthogonally to the rotation axis and decreasing with latitude. The actual value of g is the vector sum of the acceleration due to the Earth's gravity field and the centrifugal acceleration due to the Earth's rotation.

In conclusion, the value of the gravitational acceleration, g, on the Earth's surface depends on the location of the measurement point. It is usually made reference to an average value defined as the *standard gravity* g_o=9,80665 $m \cdot s^{-2}$.

To give the analytical expression of g at a defined point located on or above the Earth's surface, we make reference to a non-inertial frame centered at the Earth's center of mass and tied to Earth's surface (Figure 2.2). The forces acting on the reference point mass m on Earth's surface are the gravitational attraction and the centrifugal force. Considering an Earth elementary mass dm=ρ·dv, the Newtonian attraction exerted on dm by the mass m is expressed as:

$$d\vec{F}_g = -G \cdot \frac{m \cdot \rho \cdot dv}{l^2} \cdot \hat{l} \tag{2.5}$$

where l represents the distance between m and dm, $\hat{l}$ the unity vector on the direction m-dm and ρ the local volumic mass, function of the position. Integrating Equation 2.5 over the volume of the Earth, we obtain the total Newtonian attraction exerted by Earth on the mass m:

$$\vec{F}_g = \iiint_{V_t} -G \cdot \frac{m \cdot \rho \cdot dv}{l^2} \cdot \hat{l} \tag{2.6}$$

The centrifugal force acting on mass m is given by the expression:

$$\vec{F}_c = m \cdot \omega_t^{\,2} \cdot S \cdot \mathbf{i} \tag{2.7}$$

Where ω_t =7,292·10^{-5} rad·s^{-1} is the Earth's angular velocity, S the perpendicular distance between m and the rotation axis, Z, and **i** is the unit vector on X axis. The gravitational acceleration vector, **g,** is given by the expression:

$$\mathbf{g} = -G \cdot \iiint_{V_t} \frac{\rho \cdot dv}{l^2} \cdot \hat{l} + \omega_t^{\,2} \cdot S \cdot i \tag{2.8}$$

Generally, **g** is not directed toward the Earth's center of mass. The vector **g** at a specified point on the Earth's surface defines the local vertical.

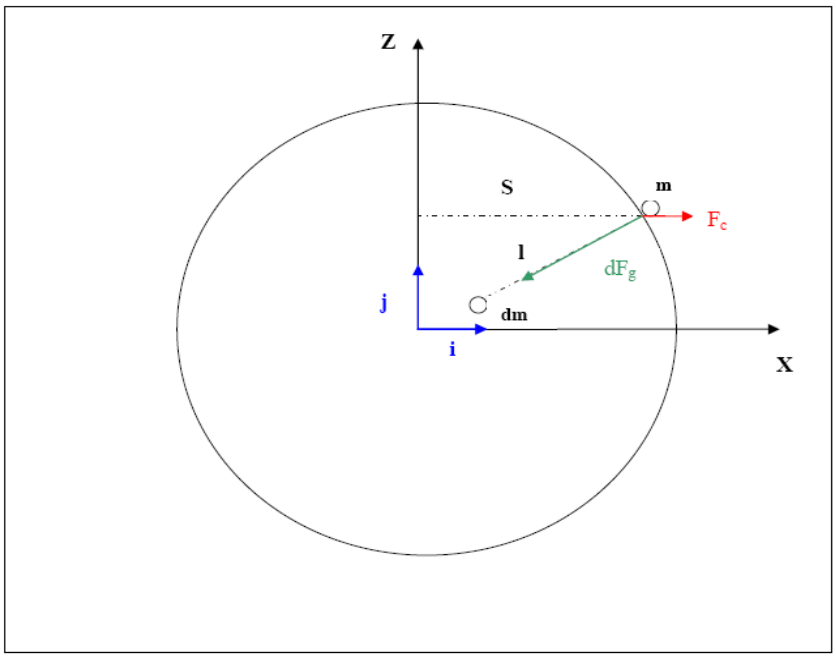

***Fig. 2.2**: Forces exerted on a point mass m located on Earth's surface (planar representation): dF_g is the gravity force exerted by an elementary mass dm, F_c is the centrifugal force in the non inertial rotating frame. Z is the rotation axis.*

Considering a point at a specified location, defined by its longitude, latitude and elevation, the gravitational acceleration is subject to time variability [*Melchior, 1971-1972*]. Some of the main causes of this variability are:

- Earth tides: Under the effect of the combined solar and lunar attraction, the Earth's visco-elastic body is subject to deformation, with consequent mass redistribution and gravity perturbation. The amplitude of the gravity effects of the Earth tides depends on location of the observation station, but is, in general, on the order of 300 μGal.
- Ocean loading effects: the combined effects of the solar and lunar attraction cause periodical variations of the ocean levels, with consequent perturbatiosn on the gravity field. The amplitude of ocean loading effects, depend on the location of the observation station, are on the order of 15 μGal.
- Polar motion effect: The Earth's instantaneous rotation axis moves with respect to the Earth's surface. This movement is evaluated with respect to a reference frame in which the Earth is fixed (ECEF), from a conventional rotation axis, the CIO (Conventional International Origin), and has three principal components: a quasi periodic free oscillation with a period of about 435 days (the Chandler wobble), a forced annual oscillation due to the seasonal air and water mass redistributions,

and a westward irregular drift of the mean pole. The amplitudes of polar motion effects are on the order of 10 μGal.

- Water and air mass redistributions related to the meteorological cycles. These effects are characterized by a large range of spatial and temporal scales.

2.4 Analytical computation of hydrological gravity perturbations: the disk model

The gravity perturbation produced by a thin, homogenous disk on a point located along the disk's axis (Figure 2.3) can be easily computed with the use of the Boguer's plate model. We choose a cylindrical reference frame centered on the axis of the disk and in line with the point where we want to calculate the gravity perturbation. We define this axis as the Z-axis along the local vertical direction. We consider a disk, having radius R and thickness s. G is a point at the disk's geometric center, corresponding to the center of mass in the case of homogeneity. Z_1 is the distance from the point mass m and the disk center G.

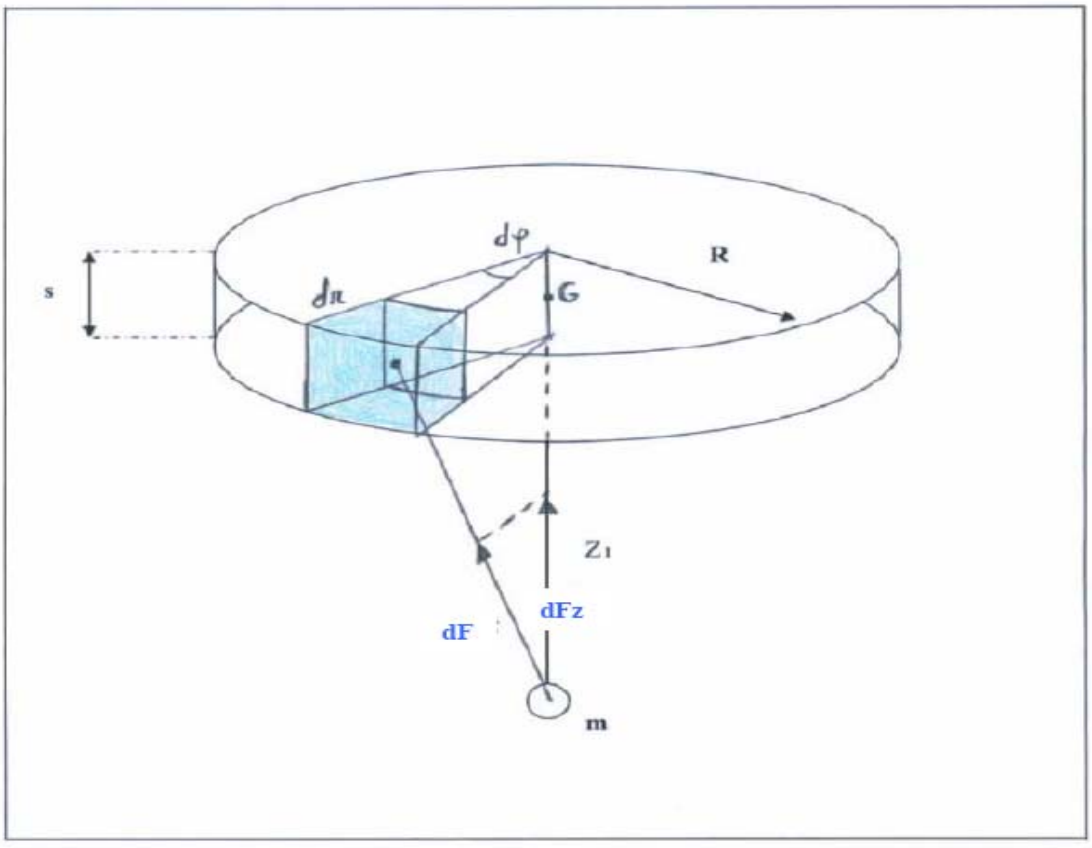

Fig. 2.3*: The disk model is used to compute the gravity perturbation produced by a thin homogenous disk on a point along the disk axis.*

The hypothesis of a thin disk implies that $Z_1 >> s$. This allows us to solve the problem by integrating over the surface instead of over the volume. Because of the cylindrical

symmetry, the total Newtonian attraction exerted by the disk on m has only a vertical component, which we define as F_z . We define as $\Delta g = F_z/m$ the corresponding gravity perturbation. In cylindrical coordinates, the elementary disk volume is defined as $dV = s \cdot r \cdot d\varphi \cdot dr$. This elementary volume exerts a force dF on mass m. θ is the angle between vector F and the vertical disk axis. The vertical component of dF is expressed as:

$$dF_z = dF \cdot \frac{Z_1}{(Z_1^{\,2} + r^2)^{1/2}} = dF \cdot \cos\theta \tag{2.9}$$

And the elementary gravity perturbation is $d(\Delta g) = dF_z/m$. The total gravity perturbation is computed by integrating over the surface of the disk:

$$\Delta g = G \cdot \rho \cdot s \cdot Z_1 \cdot \int_{r=0}^{R} \frac{r \cdot dr}{(Z_1^{\,2} + r^2)^{3/2}} \int_{\varphi=0}^{2\pi} d\varphi \tag{2.10}$$

where G is the Newtonian universal constant of gravity, ρ is the density of the disk and s the disk's thickness. We obtain:

$$\Delta g = 2\pi \cdot G \cdot \rho \cdot s \cdot \left(1 - \frac{Z_1}{(Z_1^{\,2} + R^2)^{1/2}}\right) = 2\pi \cdot \rho \cdot G \cdot s \cdot (1 - \cos\theta) \tag{2.11}$$

Equation 2.3 shows that the gravity perturbation, Δg, depends on the disk radius R and on the distance Z_1 between the disk center and the point on the disk axis where the perturbation is calculated. For $R \to \infty$, then cos(θ) goes to zero. Consequently, if the disk has an infinite extension, Δg does not depend on Z_1 and equation 2.11 becomes:

$$\Delta g = 2\pi \cdot \rho \cdot G \cdot s \tag{2.12}$$

If we consider a layer of water (water density $\rho_w = 1000\ kg \cdot m^{-3}$) having the thickness of 1 m, we obtain the value of the admittance $\alpha = 41{,}9\ \mu gal/m$.

The condition of infinite radius offers a good approximation to situations where the radius is significantly greater than the distance between the reference mass and the disk's center. The model can be extended to non-flat surfaces if the surface topography is small compared to the vertical distance between the measurement point and the surface. The gravity perturbation can then be evaluated using the height of precipitated water, even in absence of accurate information of the actual subsurface water distribution. But the model depends also on a further simplification:

- The precipitated water has a symmetric and homogenous distribution with respect to the measurement point, corresponding to the gravimeter position (the reference mass m in Figure 2. 2).
- The parameters related to the recharge-discharge process are uniform in the area of water penetration.

For non-thin disks, a volume integral must be computed. In cylindrical coordinates, the integral is expressed by [*Talwani, 1937*]:

$$\Delta g = G \cdot \rho \cdot \int_0^{2\pi} d\theta \int_{z_o}^{z_o+h} dz \int_0^R \frac{r \cdot z}{(r^2 + z^2)^{3/2}} dr \tag{2.13}$$

where z_o represents the vertical distance between the position of the measurement point and the disk's inferior face, R is the disk radius and h represents the disk's thickness. The result is:

$$\Delta g = 2 \cdot \pi \cdot \rho \cdot G \cdot (((z_o + h)^2 + R^2)^{1/2} - ({z_o}^2 + R^2)^{1/2} - h)) \tag{2.14}$$

In Figure 2.4, we display the values of the gravitational perturbation ($m \cdot s^{-2}$) produced by a 1 m thick disk as a function of the distance from the disk's surface (expressed in cm), for the values of the radius of 10 m, 100 m, 1000 m and 10000 m. When the radius tends to infinity, the gravity perturbation asymptotically approaches the constant value $4.19 \cdot 10^{-7}$.m/s^2.

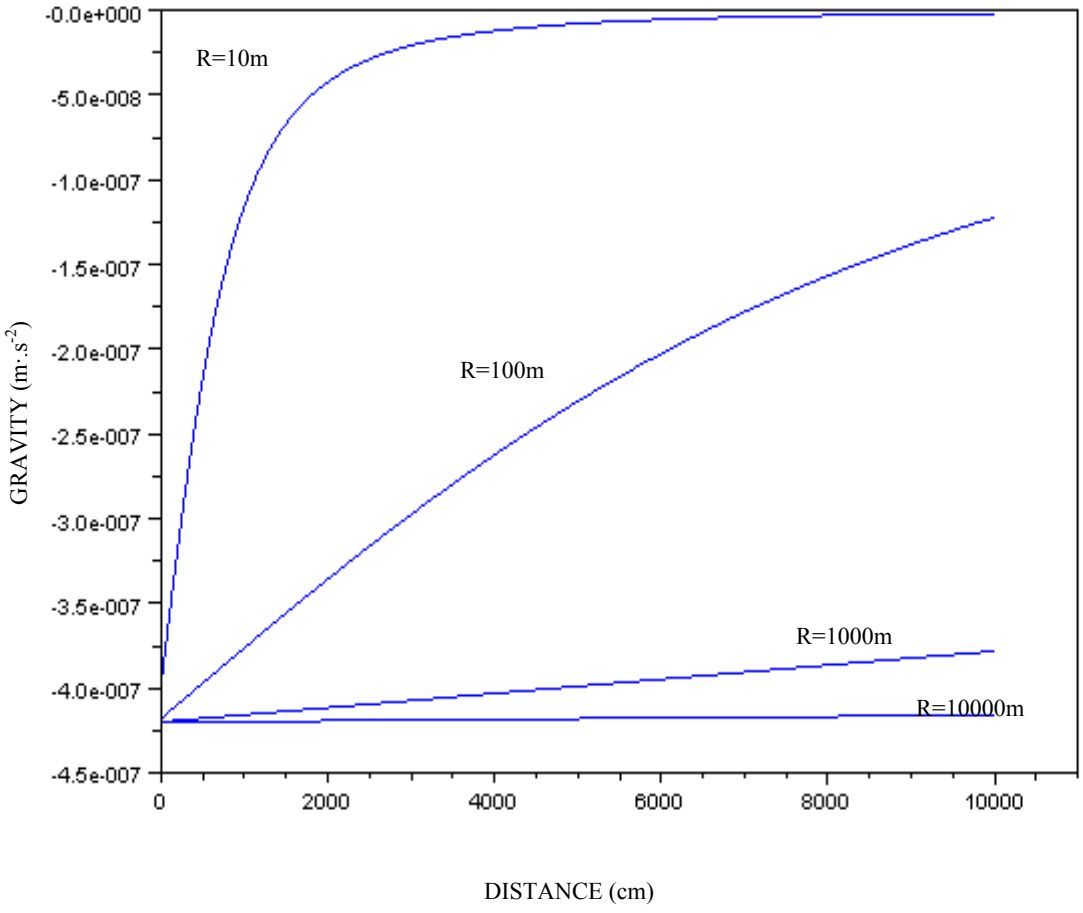

***Fig. 2.4**: Gravity perturbation ($m \cdot s^{-2}$) produced by a 1 m thick disk as a function of the distance from the disk's surface for different values of the disk radius.*

2.5 Numerical computation of the hydrological gravity perturbation: Digital Elevation Models (DEM)

The value of the admittance obtained with infinite plate model (α=41.9 μgal for 1 m of thickness) is often used for estimating the hydrological mass effects on gravity, especially for the evaluation of large and medium wavelength effects, where the infinite plane assumption is justified.

Our goal is to implement a local model, using the local precipitation as input. In our case, the infinite plane assumption is no longer appropriate. Therefore, it is more accurate to consider the actual topography of the area receiving the rainfall and affecting the gravity signal.

The gravity effect of our defined area can be calculated using Digital Elevation Models (DEM). The surface above the gravimeter, the weathered zone, is discretized into a number of prismatic elements [*Van Camp et al., 2006; Banerjee and Das Gupta, 1977; Talwani, 1973*]. The gravity effect Δg_e of a single element is given by:

$$\Delta g_e = G \cdot \rho_{wet} \cdot \int_{x_1}^{x_2}\int_{y_1}^{y_2}\int_{z_1}^{z_2} \frac{z}{(x^2+y^2+z^2)^{3/2}} \cdot dx \cdot dy \cdot dz \qquad (2.15)$$

where G is the Newtonian universal constant of gravity ($G=6.7428\cdot10^{-11}\pm0.00067\cdot10^{-11}$ N m^2 kg^{-2}) and ρ_{wet} is the density of the wet component of the layer (mass/volume). (We do not need to consider the mass of the weathered zone itself as this does not change with time.) The integration is carried out over the prism's volume, which is defined by the coordinates (x_1, y_1, z_1) and (x_2, y_2, z_2) in a Cartesian reference frame centered at the location of the gravity station.

In the absence of accurate information about ρ_{wet} in the weathered zone above the WULG, the calculation is made directly on prismatic water elements having the precipitation height as thickness. This simplification is adopted because the thickness of the weathered zone appears to be significantly smaller than the distance between the gravity sensor and the surface.

We make reference to a local Cartesian frame, where Z has the direction of the local vertical. We want to calculate the gravity perturbation exerted by a volume of water, V, on the point mass, M, having the coordinates x_m, y_m, z_m. The vertical component (Figure 2.5) of the force exerted by an elementary mass, $dm=\rho\cdot dx\cdot dy\cdot dz$, on mass M is given by:

$$dF_z = G \cdot \frac{M \cdot \rho \cdot (z - z_m)}{((x-x_m)^2 + (y-y_m)^2 + (z-z_m)^2)^{3/2}} dxdydz \qquad (2.16)$$

where ρ(x,y,z) is the density of the element. Dividing by M and integrating over the volume, V, we obtain the total gravity perturbation exerted by V on M:

$$\Delta g = \int_V G \cdot \frac{\rho(x,y,z)\cdot(z-z_m)}{((x-x_m)^2+(y-y_m)^2+(z-z_m)^2)^{3/2}} dxdydz \qquad (2.17)$$

This expression will be applied to the calculation of the admittance between precipitation height and gravity perturbation at the location of the WULG.

The region above the gravimeter has a topographically variable nature (hilly(, with significant height gradients. The surface cannot be analytically described with continuous functions. Thus, the calculation has to be performed numerically. We decompose the weathered layer above the gravimeter into a discrete number of prismatic elements (Figure 2.6) and evaluate their gravity effect at the location of the gravimeter. The 2000 m x 2000 m zone above the gravimeter is divided into 10,000 prismatic elements, each of dimensions 20 m x 20 m. The map projection of the discretized layer (Figure 2.7) defines a grid of 100 x 100 square units. The square elements of the grid are identified by the indices i and j, corresponding to the coordinates in meters x_i=20i, y_j=20j and elevation z_{ij}=0 in a local Cartesian frame (the coordinates are referred to the element central points). The gravimeter is located at (x_g, y_g, z_g).

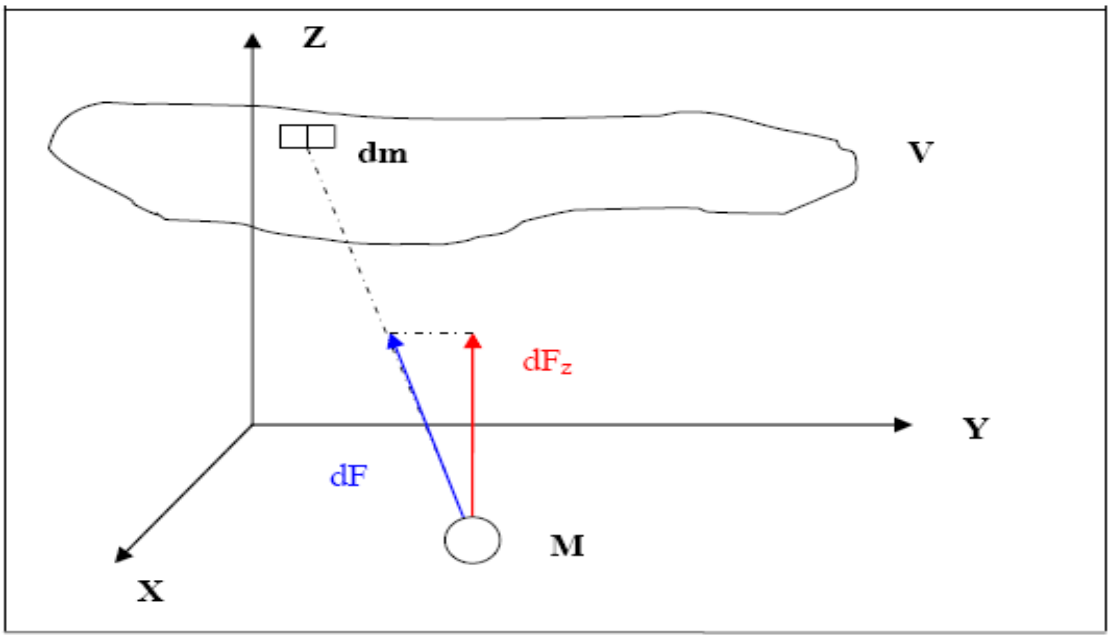

***Fig. 2.5.**: The vertical force dF_z exerted by the elementary mass dm=ρdx·dy·dz on the reference point mass M.*

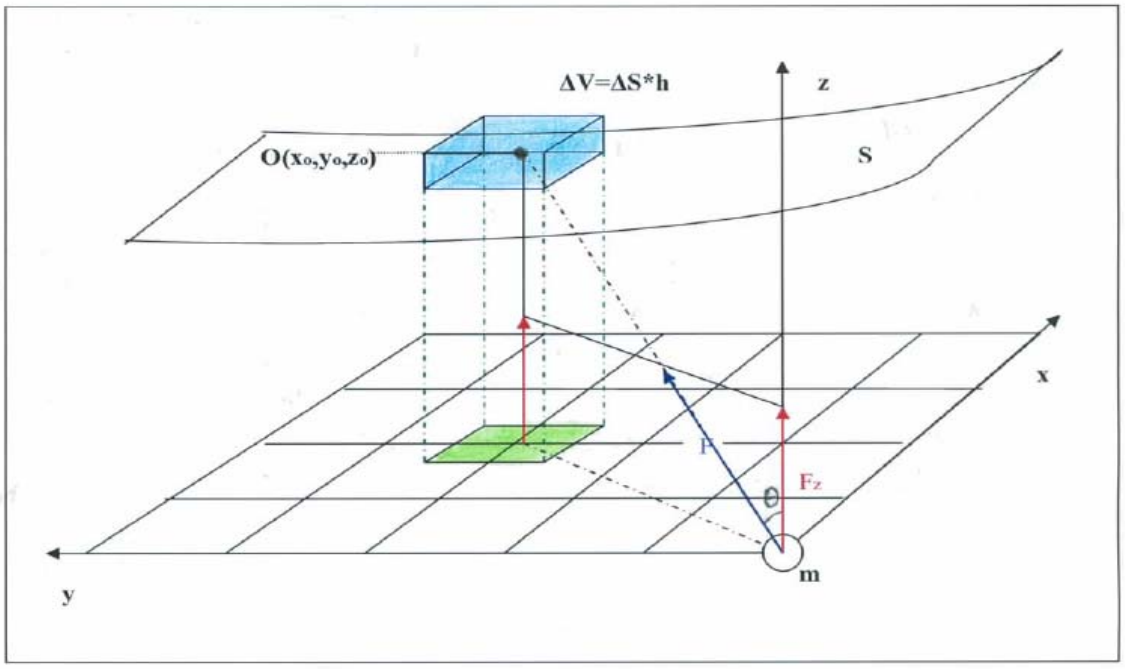

Fig. 2.6*: Point mass model for the calculation of the gravity perturbation of a water layer. The layer is subdivided into various prismatic elements with the mass concentrated at their centers of mass O. F is the attraction exerted by the element ΔV on the point mass m. F_z is the vertical component of the force.*

With the use of the Newtonian law of universal attraction, the gravity effect of the element identified by the coordinates (x_i, y_j ,$z_{i,j}$) by its center of mass is given by:

$$\Delta g_{ij} = G \cdot \Delta S \cdot \rho \cdot l_e \cdot \frac{z_{ij} - z_g}{((x_i - x_g)^2 + (y_j - y_g)^2 + (z_{ij} - z_g)^2)^{3/2}} \tag{2.18}$$

In Equation 2.18, ΔS represents the element base surface and h the element height, corresponding to the precipitated water height. The total layer effect is given by the sum of the elements' effects.

$$\Delta g = \sum_{i=1}^{100}\sum_{j=1}^{100} G \cdot \Delta S \cdot \rho \cdot l_e \cdot \frac{z_{ij} - z_g}{((x_i - x_g)^2 + (y_j - y_g)^2 + (z_{ij} - z_g)^2)^{3/2}} \tag{2.19}$$

The admittance, α, between a gravity change (μGal) and a precipitation height (m) is directly calculated with Equation 2.19, by defining l_e=1 m and by expressing the gravity in μGal. The result is α=35.9 μGal m^{-1}.

. In Figure 2.8, we display the topography of the area above the gravimeter (A) and the elements' gravity effects at the gravimeter location, as a function of their horizontal distance from the gravimeter (B).

The DEM takes into account only the surface topography. We observe that:

- The area above the gravimeter has a hilly configuration with significant height gradients. Because of the slope differences, the runoff coefficients are a function of space: the rate of precipitation infiltrating the soil is greater in the low slope zones.
- The soil is non homogenous [*Hecimovic and Basic, 2005*]. Part of the area is covered with low vegetation (grass other bushes), another part is covered with high vegetation (woods), and in a third part there is a significant presence of human artifacts.
- The precipitation events can have an important time and space variability at different scales. The precipitation intensity during a shower is a function of both time and space

The consequence is that the DEM provides only an estimation of the actual local admittance.

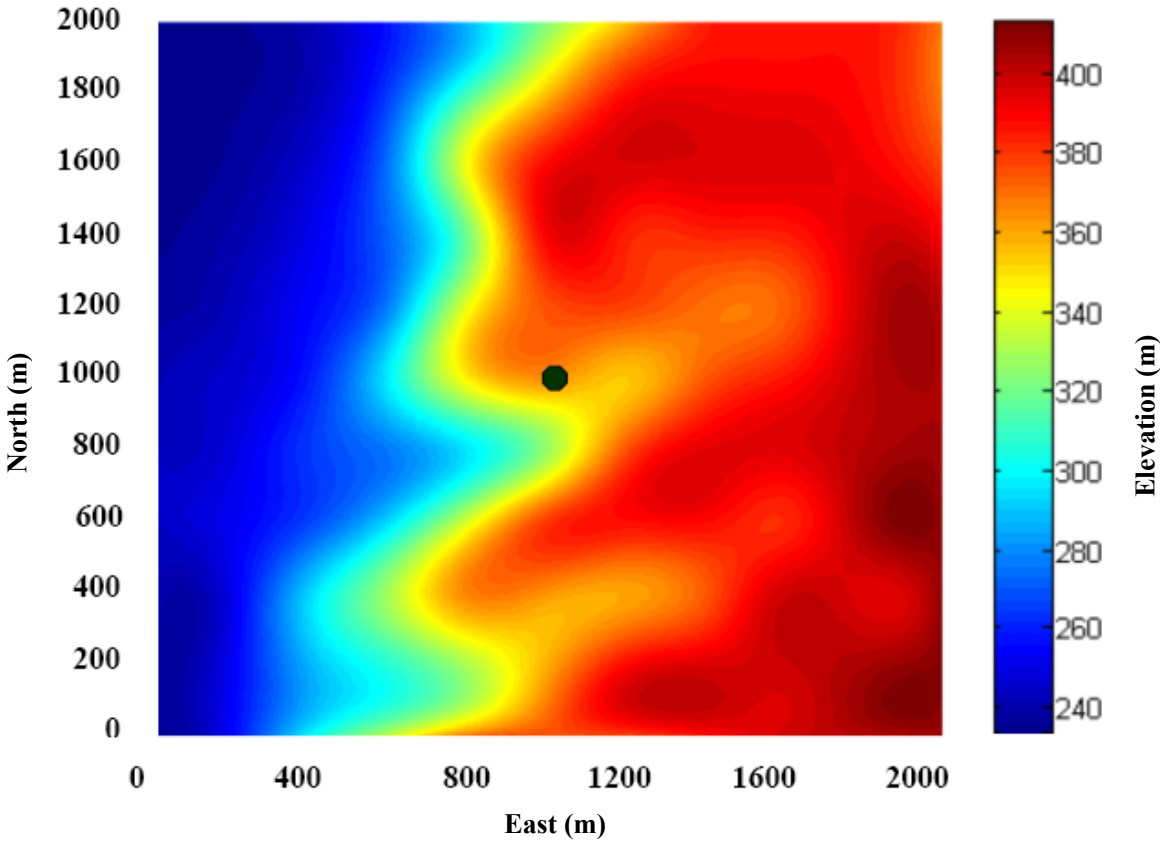

Fig. 2.7*: Map projection of the area above the gravimeter given over a 2 km x 2 km area centered on the position of the gravimeter (black dot). The distances and topography are expressed in meters.*

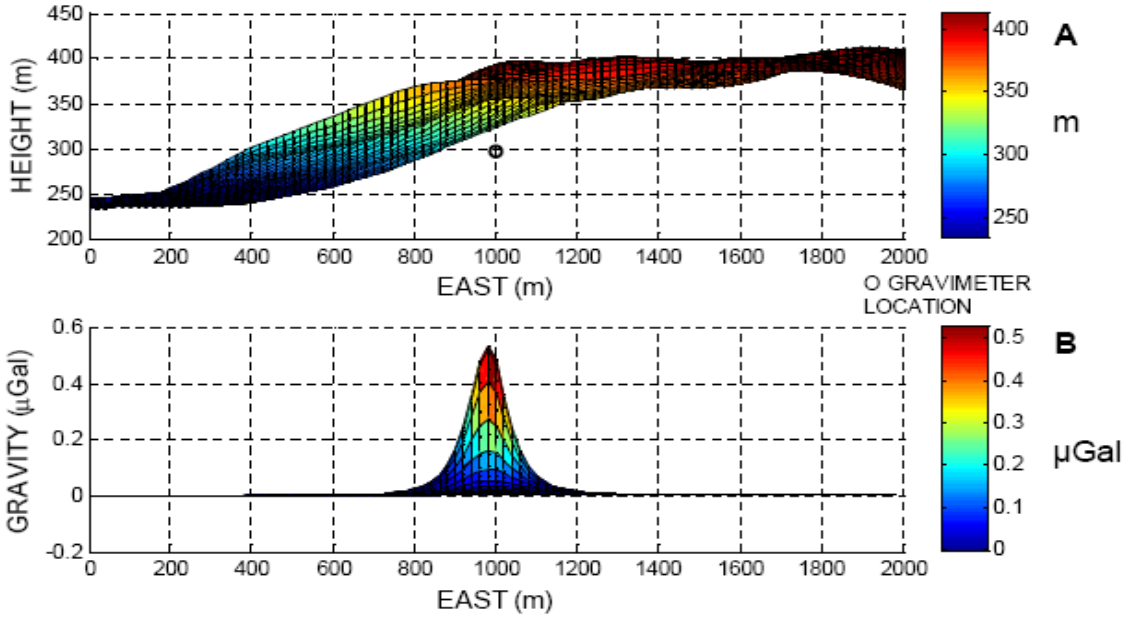

***Fig. 2.8**: Gravity effect of a uniform water layer:*

A. Topography of the area above the gravimeter (elevation in meters). The area is subdivided into prismatic elements whose horizontal projections are 20 m sided squares.

B. Gravity perturbation: The gravity effect of the surface elements displayed as a function of their horizontal distances from the gravimeter location.

Let's supposing we have the case of a uniform infiltration. We can estimate the error on gravity calculation due to the DEM model to the precipitation height (and not on the actual infiltrated zone). Simplifying, a uniform infiltration can be represented as a vertical downward translation of the water layer. In the DEM, this can be simply expressed with the variation of the coordinate z_g of the gravimeter, x_g and y_g being fixed. In Figure 2.9 we display the gravity perturbation as a function of the height above the sea level (the SG is 295 m above the sea level).

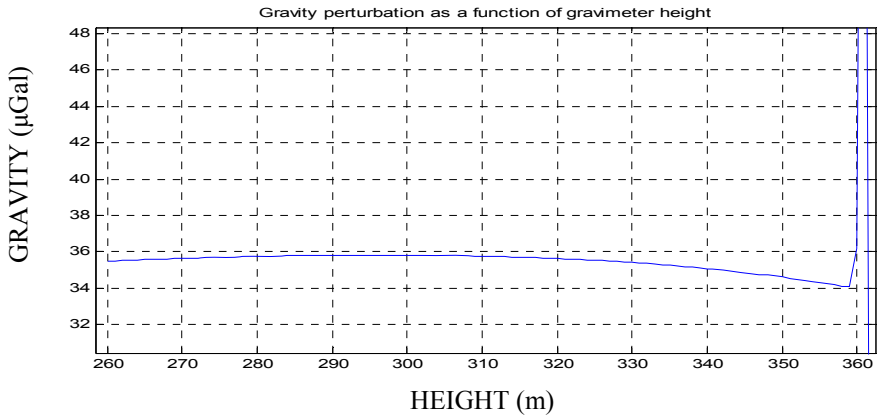

***Fig 2.9**: Gravity perturbation due to a 1 m thick water layer as a function of the gravimeter height above sea level,*

Estimating a maximal depth of infiltration of 20 m (this corresponds to a value of z_g of between 295 and 315 m), the gravity perturbation varies from 35.9 μGal to 35.6 μGal, resulting in an 0.8 % error. On the local surface, which lies at about 360 m above sea level, this model of calculation diverges.

The error due to the uncertainties in the gravimeter's horizontal coordinates is more relevant. Assuming a 20 m uncertainty in the gravimeter's horizontal position, we calculate using the DEM a 3.5 % relative error.

In Figure 2.10 we display the values of the gravity perturbation as a function of the radius of the integration area.

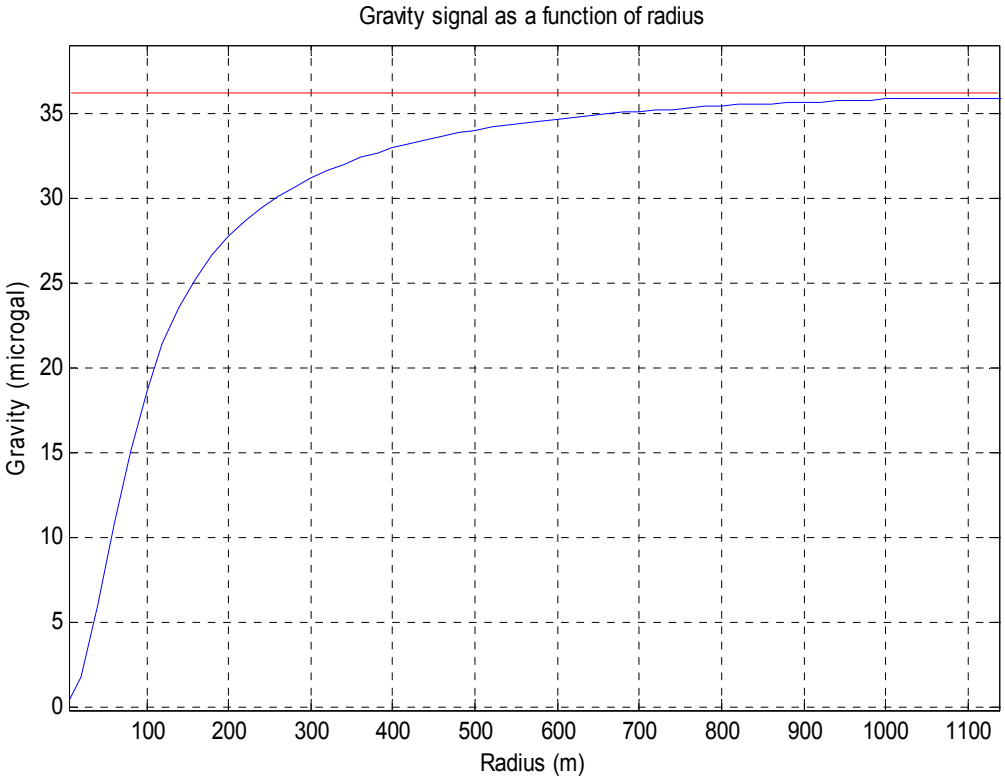

***Fig. 2.10**: Gravity perturbation as a function of the radius of the integration area.*

The main effect can be ascribed to an area delimited by an 800 m radius circumference. Comparing the values obtained for the integration on 800 m and 1000 m radius, we see that for an area increment of 57%, the gravity perturbation increment is of 1,1%.

2.6 The tank model expressed in terms of gravity changes

The value of the admittance derived in Section 2.5 allows us to rewrite the tank model (Equation 1.59) in terms of gravity variations. The admittance represents the

proportionality between the water level and the gravity perturbation at a point along the tank axis (Figure 2.11). This is expressed by:

$$\Delta g=\alpha\cdot h \tag{2.20}$$

where Δg represents the gravity perturbation, h the water level and α the admittance between gravity and water level. The gravity effect of layer with elementary thickness dh is expressed by:

$$d(\Delta g)=\alpha\cdot dh \tag{2.21}$$

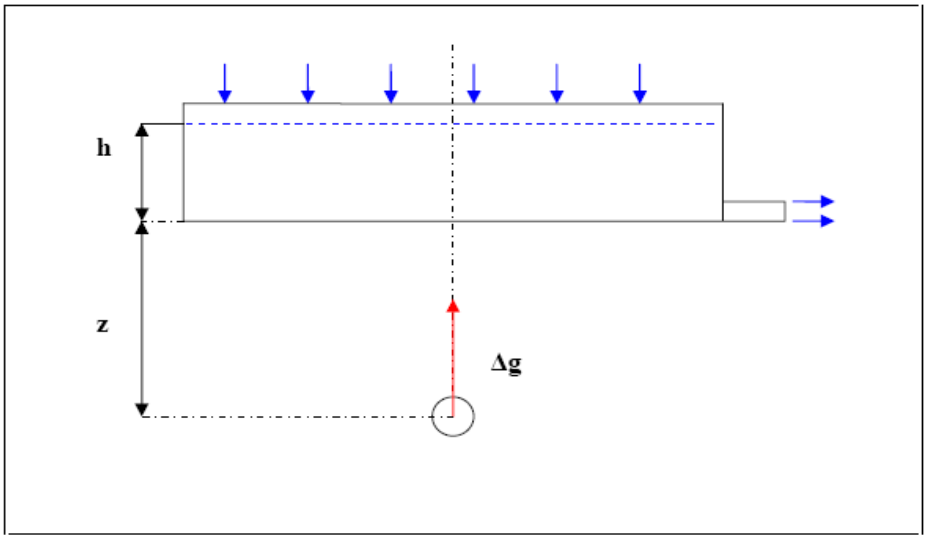

Fig. 2.11: *The tank model in terms of gravity: the effect of gravity is determined for a point lying on the tank axis. If z>>h, there is a simple proportionality between the water level, h, in the tank and the gravity perturbation Δg.*

The Tank Model equation can be rewritten in terms of gravity changes by multiplying both sides of Equation 1.59 by the admittance value, α, and changing the sign of the term α·r. This last step is required due to the fact that the gravimeter is located in an underground laboratory: an increase of the stored water level above the gravimeter will produce a reduction of the gravity signal. Applying these changes we obtain:

$$\alpha\cdot\frac{dh(t)}{dt}=-\gamma\cdot h(t)\cdot\alpha-\alpha\cdot r(t) \tag{2.22}$$

Substituting Equations 2.20 and 2.21 into Equation 2.22, results in

$$\frac{d(\Delta g(t))}{dt} = -\gamma \cdot \Delta g(t) - \alpha \cdot r(t) \tag{2.23}$$

where r(t) represents the rainfall rate (length/time) and γ is defined as the recovery rate after rainfall (time^{-1}), corresponding to c in Equation 1.59. Equation 2.23 represents the analytical formulation of the problem [*Imanishi et a,* 2004]. Obviously, the rainfall rate cannot be expressed as a continuous function of time. The precipitation time series (hyetograms) represent the precipitation heights integrated on discrete time intervals, and are referred to discrete time indexes. Equation 2.23 must be consequently rewritten in numerical form to be implemented. The numerical form of Equation 2.23 is expressed as:

$$\Delta g(i+1) = (1-\gamma) \cdot \Delta g(i) - \alpha \cdot r(i) \tag{2.24}$$

where γ is now a non dimensional parameter and i a discrete time index. r(i) has the dimensions of a length, representing the amount of water precipitated in the time Δt between (i-1)·Δt and i·Δt. The relation between r(i) and r(t) is expressed by:

$$r(i) = \int_{(i-1)\Delta t}^{i\Delta t} r(t)dt \tag{2.25}$$

In order to give a physical interpretation to Equation 2.23, we consider the case of no precipitation, with an initial water level h_0 in the tank. In this configuration, the mass of water present in the tank exerts an initial gravity perturbation on the reference point, m, given by:

$$\Delta g_0 = h_0 \cdot \alpha \tag{2.26}$$

If r(t)=0, Equation 2.23 becomes:

$$\frac{d(\Delta g)}{\Delta t} = -\gamma \cdot dg \tag{2.27}$$

which can be immediately integrated analytically using separation of variables and assuming as initial conditions $\Delta g = \Delta g_0$ for t=0.

$$\int_{\Delta g_0}^{\Delta g} \frac{d(\Delta g)}{\Delta g} = \int_0^t -\gamma dt \qquad \rightarrow \qquad \Delta g = \Delta g_0 \cdot e^{-\gamma * t} \tag{2.28}$$

The result is an expression for the gravity perturbation that is an exponential decay of time resulting after a given initial perturbation Δg_0. The inverse of γ, denoted τ, is a characteristic time parameter of the process, representing the time for the gravity perturbation to decrease from the initial value, Δg_0 to the value 0,37 Δg_0. The gravity recovery rate γ depends on the hydrogeological parameters, such as porosity and hydraulic conductivity [*Delcourt-honorez, 1986*].

In Figure 2.12 we display the gravity change following a precipitation event as described by the tank model. We observe that only the recovery phase is illustrated. The gravity decrease is represented as occurring instantaneously or, more precisely, as having a duration on the order of the reference interval Δt. When a precipitation event occurs, the rainfall height is simply added to the current water level, producing an instantaneous gravity change.

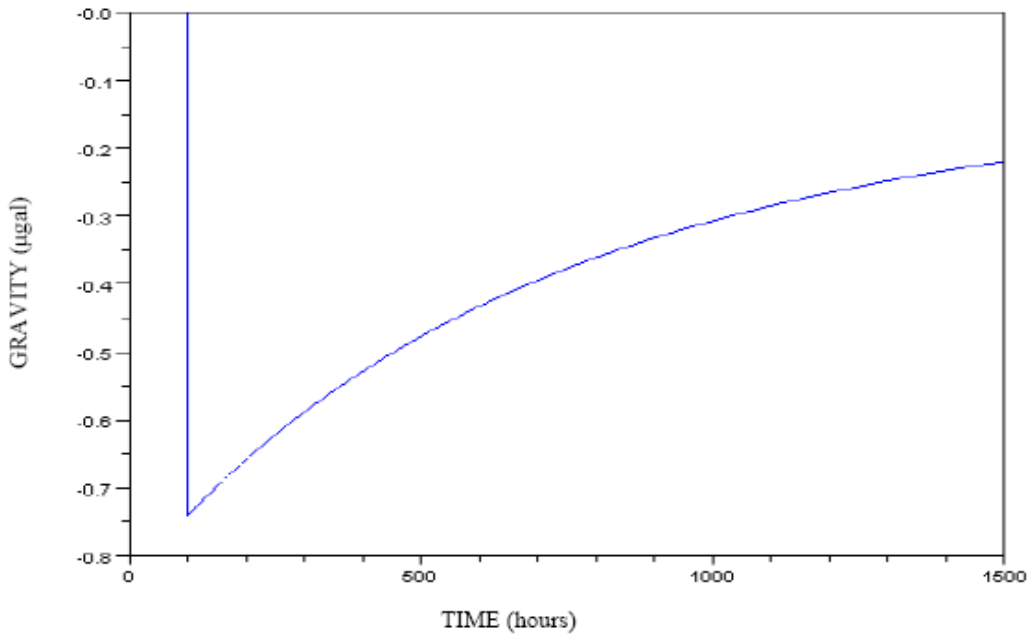

***Fig. 2.12**: Time evolution of the gravity signal after a single precipitation event, described by the Tank Model The gravity decrease is described as occurring instantaneously.*

2.7 Seasonal variation of the gravity recovery rate γ

Equation 2.23 has been previously implemented by Imanishi et al. (2004) to calculate the gravity effect of underground water in Matsuhiro (Japan), with a constant value of γ.

We have shown that the gravity recovery rate γ corresponds to parameter c in Equation 1.60. This parameter (Section 1.11) depends on the hydrogeological parameters, such as hydraulic conductivity, designed as K. K depends both on the fluid characteristics, e.g., the fluid viscosity, and on the solid matrix characteristics, e.g. the medium porosity. In Section 1.8 we have underlined the dependency of K on groundwater temperature and, in the case of the superposition of non-homogenous geologic layers, on the subsurface water distribution.

For these reasons, we modify the basic tank model by introducing the idea that the recovery rate has a seasonal dependence. We assume that the variability of γ can be expressed by a sinusoidal function with the following form:

$$\gamma(t) = \gamma_o \cdot (1 + A \cdot \cos(\frac{2 \cdot \pi}{T} \cdot t + \varphi)) \quad (2.29)$$

where $\gamma(t)$ represents the gravity recovery rate (1/time), γ_o represents the yearly average value of the gravity recovery rate, and A and φ represent the amplitude and phase of the variation function, respectively. We remind the reader, that in the absence of available information about local hydrological parameters, the model has to be empirically parameterized in order to obtain the best fit with the observed gravity data (see Section 3.5).

By allowing the gravity recovery rate γ to vary seasonally, we can absorb part of the seasonal variations of the hydrological gravity residuals. But, because of this empirical approach, the model does not allow us to identify of the different components of the seasonal signal. This seasonal variability could be explained by four different factors.

First, seasonality in γ could be due to variability of the hydraulic conductivity K, which is related to the parameter γ [*Van Camp et al., 2006, Falleiros et al. 1998*]. K can be expressed in the form $K=k \cdot \rho \cdot g \cdot \mu^{-1}$, where k (length^2) is the permeability of the solid matrix, which depends only on the characteristics of the porous medium. The term $\rho \cdot g \cdot \mu^{-1}$ depends only on the fluid characteristics, where ρ and μ represent the density and the viscosity of the fluid, respectively. The viscosity depends on groundwater temperature. At mid-latitude locations such as Walferdange, groundwater temperature has a definite seasonal variability, even if it is less sensitive in the saturated zone. *Bartolino* (2003) investigated the annual groundwater temperature fluctuations as a function of depth below the surface beneath the Rio Grande in New Mexico. He estimated an annual groundwater temperature range varying from 22°C at 1 m depth below the surface to 4°C at 15 m depth below the surface (see Section 1. 8).

A second seasonal effect, justifies imposing a seasonal dependence on γ, could be due to the infiltration variability. The runoff coefficients, and consequently the fraction of precipitation infiltrating the soil, can have a significant seasonal variability, related to the degree of saturation of the root zone [*Theis, 1935*].

Thirdly, seasonality in γ could result from seasonality in evapotranspiration [*Hupet and Vanclooster, 2005*]. The process of evapotranspiration has a strong dependence on air and soil surface temperatures that are subjected to significant seasonal oscillations.

Finally, seasonality in γ could be due to regional effects. Our model is based on local precipitation. However, the gravity recovery rate variability hypothesis may absorb longer wavelength seasonal effects as well [*van Dam et al., 2001*; *Crossley et al., 2005, Llubes et al. 2004*].

Now, the equation describing the gravity variations can be obtained by substituting the expression of $\gamma(t)$ given by Equation 2.29 into Equation 2.23:

$$\frac{d(\Delta g)}{dt} = -\gamma_0 \cdot (1 + A \cdot \cos(\frac{2 \cdot \pi}{T} \cdot t + \varphi)) \cdot \Delta g - \alpha \cdot r(t) \quad (2.30)$$

As already pointed out, the rainfall rate r(t) is not defined by a continuous function of time but by a discrete set of values. To allow us to solve the equation using finite

difference algorithms, Equation 2.30 has to be rewritten as a discrete expression. We define the terms of a progression:

$$\Delta g(i+1) = (1-\gamma_o \cdot (1 + A \cdot \cos(\frac{2 \cdot \pi}{T} \cdot i + \varphi)) \cdot \Delta g(i) - \alpha \cdot r(i) \tag{2.31}$$

where i represents the non-dimensional time indices, $\gamma(i)$ is the non dimensional recovery rate and r(i) are the precipitation heights. The time variable t in Equation 2.30 is given by $t=\Delta t \cdot i$, where Δt is the reference time interval (1 hour in the hourly implementation), and the recovery rate function $\gamma(i)$ is formally identical to $\gamma(t)$.

2.8 The Double Exponential Model

As pointed out in the previous Section, the Tank Model describes only the hydrological discharge process. Other models have been developed, such as the double exponential model [*Harnisch and Harnisch, 2002*], which desribes both the gravity decrease phase and the gravity recovery phase following a precipitation event.

The double exponential model computes the convolution of the precipitation height, (the input signal), with the product of two exponential functions describing the hydrological recharge phase and the hydrological discharge phase, respectively. The gravity variation at time i is defined as $\Delta g(i)$ and it is computed through the cumulate effect of all the precipitation events, which have occurred before the instant i. The Double Exponential model is expressed by:

$$\Delta g(i) = -\alpha \cdot \sum_{J=1}^{i-1} r(j) \cdot (1 - e^{\frac{-(i-j)}{\tau'}}) \cdot e^{\frac{-(i-j)}{\tau''}} \tag{2.32}$$

where α represents the admittance between the gravity variation and the precipitation (See Section 2.6), $\Delta g(i)$ represents the hydrological part of the gravity variation at time i, τ' and τ'' represent the hydrological recharge and discharge temporal parameters, respectively. The negative sign before α on the right side of the equation depends on the fact that that the gravimeter is located underground, and as in Walferdange, a precipitation induces a gravity decrease.

Like the gravity recovery rate γ of the Tank Model, the recharge and discharge time parameters depend on hydrogeological parameters, subject to seasonal fluctuations. For this reason, we introduce the hypothesis of seasonal variability in both τ' and τ''.

$$\tau'(i) = \tau_0' \cdot (1 - c' \cdot (\cos\frac{2 \cdot \pi}{T} \cdot i + \varphi') \tag{2.33}$$

$$\tau''(i) = \tau_0'' \cdot (1 - c'' \cdot (\cos\frac{2 \cdot \pi}{T} \cdot i + \varphi'') \tag{2.34}$$

where τ_o' and τ_o'' represent the average yearly values of the gravity decrease time parameter and the gravity recovery time parameter, respectively and φ' and φ'' represent

the phases of the gravity decrease temporal parameter and the gravity recovery temporal parameter variation functions, respectively.

If the parameter τ' tends to 0, we can write:

$$\lim_{\tau' \to 0} e^{\frac{-(i-j)}{\tau'}} = 0 \qquad (2.35)$$

and Equation 2.35 becomes:

$$\Delta g(i) = -\alpha \cdot \sum_{J=1}^{i-1} r(j) \cdot e^{\frac{-(i-j)}{\tau''}} \qquad (2.36)$$

Equation 2.36 corresponds to a single exponential model, which similar to the tank model, provides only a description of the gravity recovery phase. This model can be adopted when the duration of the recharge process is significantly shorter than the duration of the discharge process.

In Figure 2.13, we display the gravity decrease phase and the gravity recovery phase following a single precipitation event, as described by the double exponential model, for three different values of the discharge time parameter τ' (1, 150 and 300 hours) and a single value of parameter τ'' (700 hours). The model is implemented without the hypothesis of the seasonal variation of the time parameters. It can be remarked that for τ'=1 hour, the model output appears similar to the output of the tank model.

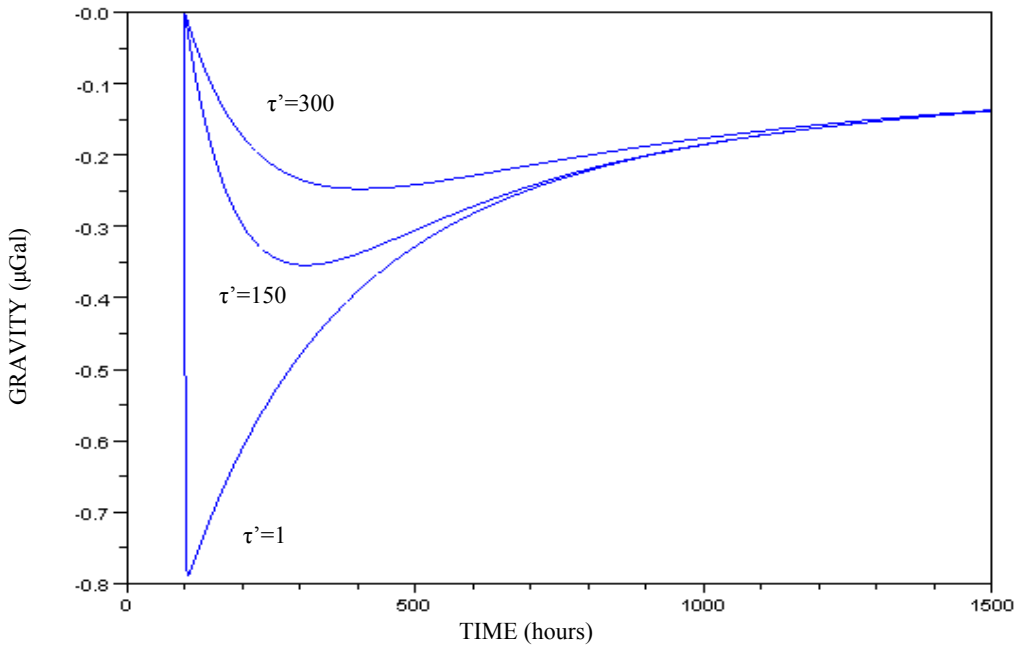

***Fig. 2.13**: Time evolution of the gravity signal described by the exponential model, for three different values of the recharge time parameter τ' (1 hour, 150 hours and 300 hours). The value of the discharge parameter is τ'' = 700 hours.*

2.9 Correspondence between the Tank Model and the Exponential Model

The equivalence between the tank model and the Single exponential Model can be demonstrated in a particular configuration: i.e., the parameter γ of the Tank Model and the parameter τ" of the Exponential Model are constants.

In this case, we remember that Equation 2.23 describes the Tank Model (Section 2.6):

$$\frac{d(\Delta g(t))}{dt} = -\gamma \cdot \Delta g(t) - \alpha \cdot r(t)$$

To allow us to solve the equation using finite difference algorithms, we have seen that equation 2.23 has to be rewritten as the discrete expression 2.24. We remember this expression, which defines the terms of a progression:

$$\Delta g(i+1) = (1-\gamma) \cdot \Delta g(i) - \alpha \cdot r(i)$$

setting K=1-γ, Equation 2.24 becomes:

$$\Delta g(i+1) = K \cdot \Delta g(i) - \alpha \cdot r(i) \qquad (2.37)$$

defining Δg(1) as the initial value of the gravity variation, and calculating the first terms of the progression, we obtain:

$$\Delta g(2) = K \cdot \Delta g(1) - \alpha \cdot r(1)$$

$$\Delta g(3) = K \cdot (K \cdot \Delta g(1) - \alpha \cdot r(1)) - \alpha \cdot r(2) = K^2 \cdot \Delta g(1) - K \cdot \alpha \cdot r(1) - \alpha.r(2)$$

$$\Delta g(4) = K \cdot (K^2 \cdot \Delta g(1) - \alpha \cdot r(1) - \alpha \cdot r(2)) - \alpha \cdot r(3) = K^3 \cdot \Delta g(1) - K^2 \cdot \alpha \cdot r(1) - K \cdot \alpha \cdot r(2) - \alpha \cdot r(3)$$

Finally, the general form of the progression can be expressed by:

$$\Delta g(i+1) = (1-\gamma)^i \cdot \Delta g(1) - \alpha \cdot \sum_{j=1}^{i} (1-\gamma)^{i-j} \cdot r(j) \qquad (2.38)$$

defining $I_c=(1-\gamma)^i \cdot \Delta g(1)$ as the initial conditions, and considering that, for γ<<1, we can make the approximation[1]:

$$(1-\gamma)^{i-j} =\sim e^{-(i-j)\cdot\gamma} \qquad (2.39)$$

[1] From $e=\lim_{n\to\infty}(1+1/n)^n$, posing n=-1/γ and considering γ<<1, we can approximate $(1-\gamma)^{-1/\gamma}=\sim e$ and finally $(1-\gamma)=\sim e^{-\gamma}$. It is important to note that the terms with little values of i-j offer the greater contributions to the gravity changes at time i.

Equation 2.43 can then be written:

$$\Delta g(i+1) = -\alpha \cdot \sum_{j=1}^{i} e^{-\gamma(i-j)} \cdot r(j) + I_c \qquad (2.40)$$

Equation 2.40 corresponds to Equation 2.36 of the Single Exponential Model. Consequently, in this configuration the gravity recovery rate γ of the Tank Model corresponds to the inverse of the recovery time parameter of the Exponential Model:

$\gamma = 1/\tau''$

Thus, in this configuration, the Exponential Model is formally equivalent to the Tank Model.

2.10 Conclusion

In order to express the groundwater storage variations in terms of gravity changes, we have estimated the value of the admittance between the gravity signal and the precipitation height at the SG location. This has been realized with the use of a Digital Elevation Model (DEM) of the area above the gravimeter. The area has been discretized into an ensemble of finite elements each having a prismatic form, and their effect at the gravimeter location computed using Newton's law of attraction. We have obtained a value of the admittance of 35.9 μGal/m.

In order to describe the hydrological gravity variations at the SG location, we have introduced two basic models: the Tank Model (derived in Chapter 1) and the Double Exponential Model. Both the models describe the groundwater storage variations due to the local precipitation. The Tank Model describes only the hydrological discharge phase following a precipitation event (the recharge phase is considered as instantaneous). The Double exponential model describes both the hydrological recharge and discharge phases following a precipitation event.

We have shown that in the Tank Model, the duration of the discharge phase is characterized by the parameter γ (gravity recovery rate). In the Double Exponential Model, the duration of the recharge and discharge phases are characterized by the time parameters τ' and τ'', respectively.

In the absence of accurate information about the local hydrogeological conditions, both models must be empirically parameterized.

We have thus modified the two basic models by introducing the hypothesis of seasonal variability of the parameters γ, τ' and τ'': these parameters depend on hydrogeological conditions, which are subject to seasonal fluctuations.

This hypothesis allows the models to absorb part of the seasonal components of the hydrological gravity variations. Nevertheless, with our empirical parameterization, it does not allow us to identify the different parameters driving these seasonal variations (global

effects, hydraulic conductivity changes, evapotranspiration rates changes, water table fluctuations, etc.).

We have then demonstrated that when τ' is significantly smaller than τ'', the Tank Model and the double exponential model provide similar results. Finally, we have demonstrated that in the particular case when τ' is equal to zero and τ'' and γ are constants (not subject to seasonal fluctuations), the models are formally equivalent

Chapter 3

Chapter 3: Gravity data, input data and model output

3.1 Introduction

We will use the local precipitation time series as input for the Tank Model and the Double Exponential Model, both described in Chapter 2. The model outputs, representing the modeled hydrological gravity time series, will be compared to the observed gravity time series.

Before analyzing the results, we will describe the methods of acquisition of the precipitation data and of the gravity data.

Two different sources were available for the precipitation time series: the WULG pluviometer and the Walferdange Meteorological Station (WMS) pluviometer. The series are qualitatively similar. However, they are quantitatively different, the cumulative precipitation registered by the WULG instrument is approximately 10% greater than that registered by the WMS instrument. This difference will be used to assess the uncertainties on the input data.

Because of the different periods of availability of the WULG and the WMS data, a combination of the two series will be used as input for the models. This combined series covers the period January 2003 to January 2010.

The gravity data are provided by the Superconducting Gravimeter OGCT040 (SG) operating from December 2003 in the WULG. In order to establish the quality of the SG, we will determine two important instrument characteristics: the SG transfer function and the SG instrumental drift.

The SG transfer function will be determined by injecting in the SG control electronics with both sine waves and step functions. We will then observe the system response.

The long term instrumental drift will be determined by comparing the SG relative gravity series with the absolute gravity measurements provided by the free-fall gravimeter, FG5, located in the WULG, at a few meters distant from the SG. We are not able to model the short-term initial instrumental drift.

In the absence of accurate information regarding the local hydro-geological parameters, both the Tank Model and Double Exponential Model will be empirically parameterized using a least square residual adjustment.

The model outputs, representing the modeled gravity time series, will be subtracted from the observed gravity time series for the period May 2004 to January 2009. The first months after the start of operating of the SG will be excluded from the calculation because of the substantial initial instrumental drift.

The reduction of the signal scatter will be computed for both the models. The results will be compared and discussed. The physical significance of the model parameterization will be analyzed.

Finally, we will estimate the gravity effect of the excavation of the Stafelter tunnel just above the SG location. The mass removal due to the excavation, which started in March

2009, may partly explain an upward drift of the gravity residuals observed over the same period.

3.2 Input data: rainfall time series at Walferdange

The Luxembourg climate can be defined as semi-continental, and is conditioned by two principal influences:

- Oceanic influences, due to the west and south-west winds. These influences determine precipitation throughout the year.
- Continental influences, because of the cold north-east winds and streams. The continental influence is particularly strong in the winter months.

Walferdange is located about ten kilometers north of the city of Luxembourg, the capital of the Grand Duchy of Luxembourg, at a latitude 49.6700^{o} N and 6.1500^{o}E. From a hydrological point of view, both Walferdange and the city of Luxembourg are included in the experimental Alzette catchment basin. The Alzette catchment basin covers a 1172 km^2 area in the south-western part of the Grand Duchy. (Figure 3.1).

The Alzette River has its source in France, about 4 km south from the border of Luxembourg, and crosses the Grand Duchy for 70 km in almost a south-north direction before joining the Sûre River, which crosses the Grand Duchy in almost a west-east direction. Currently, the Alzette Valley includes about two-thirds of all the Grand Duchy population, and hosts the most significant part of the country industrial implants.

The precipitation levels show a significant spatial variation along the area of the Alzette catchment, especially in the west-east direction. Maximal amounts are registered at the western border of Luxembourg, where the water saturated winds blowing off the ocean encounter the Ardennes, a region of rolling hills and Devonian mountains in the northern part of the country, and the Mousel heights in the southern part of the country. Here the annual precipitation varies between 900 mm and 1000 mm. The lowest amounts are registered at the eastern border of the Alzette catchment basin. Here the annual precipitation varies between 700 mm and 800 mm.

For the precipitation data in the locality of Walferdange, two different sources are available: the Walferdange Meteorological Station (WMS) pluviometer and the WULG pluviometer (Figure 3.2). Both the instruments provide precipitation heights with 1 min. temporal resolution.

A comparison between the two time series indicates a qualitative similarity. A significant quantitative difference exists as well. The cumulative precipitation provided by the WULG is approximately 10% greater than that provided by the WMS. In Figure 3.4 we show the precipitation time series (integrated to hourly values) provided by the two pluviometers, for the period December 2005 to March 2007. In Figure 3.5 we display the cumulative rainfall provided by the two pluviometers for the same period.

Because of the different periods of availability of the WMS data and the WULG data, we used a combination of the two series as input for the models. From January 2003 to December 2005, the WMS series was adopted. From December 2005 to January 2010 the WULG time series was adopted. The quantitative difference between the series was used to assess the uncertainty on the input data. Both the series are integrated to hourly values and referred to the end hour points.

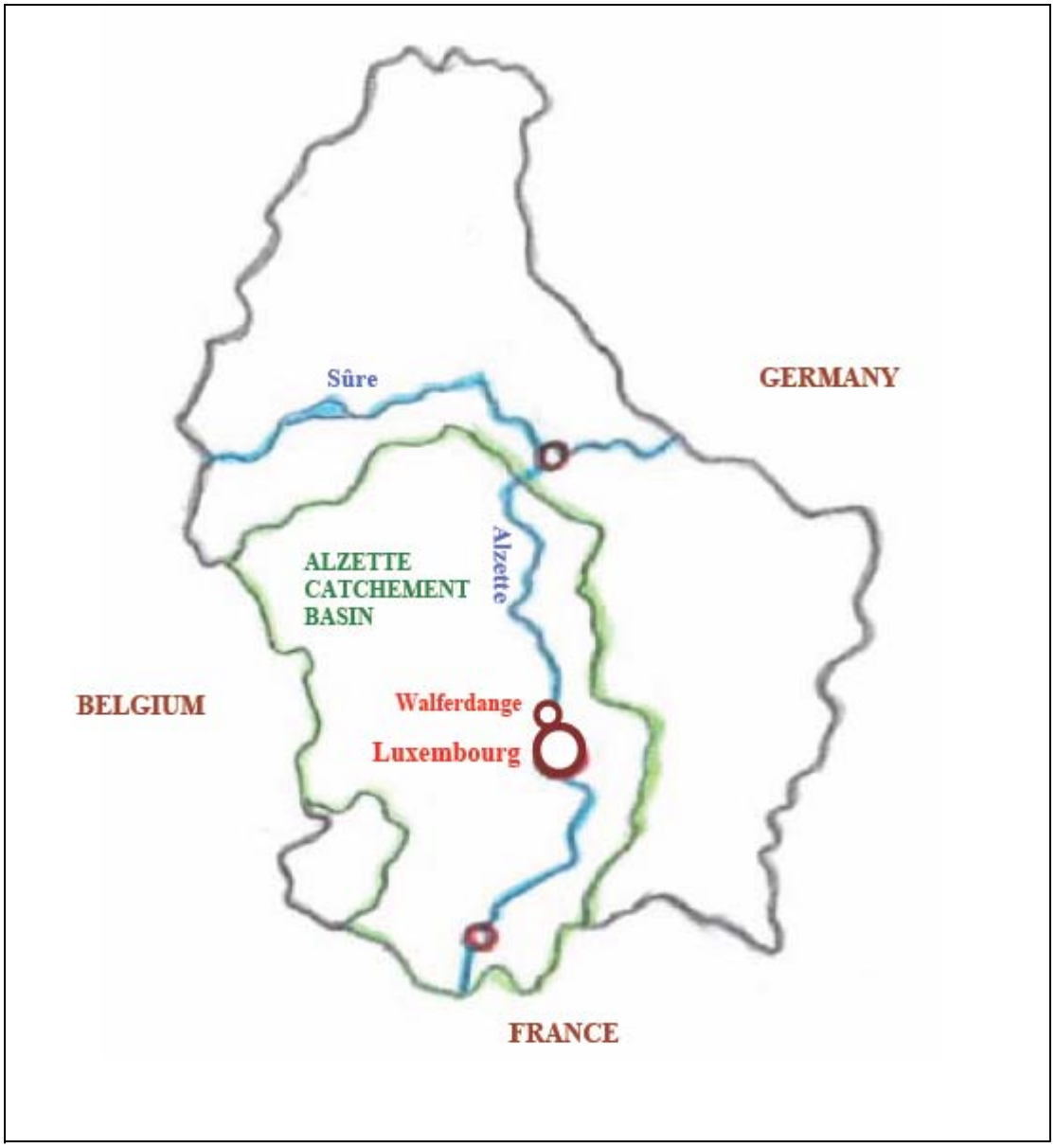

***Fig. 3.1**: Grand Duchy of Luxembourg, Alzette River, Sûre River and localities of Luxembourg and Walferdange. The Alzette River crosses the Ground Duchy of Luxembourg in an almost south-north direction before joining the Sûre River. The green contour includes the Alzette experimental basin.*

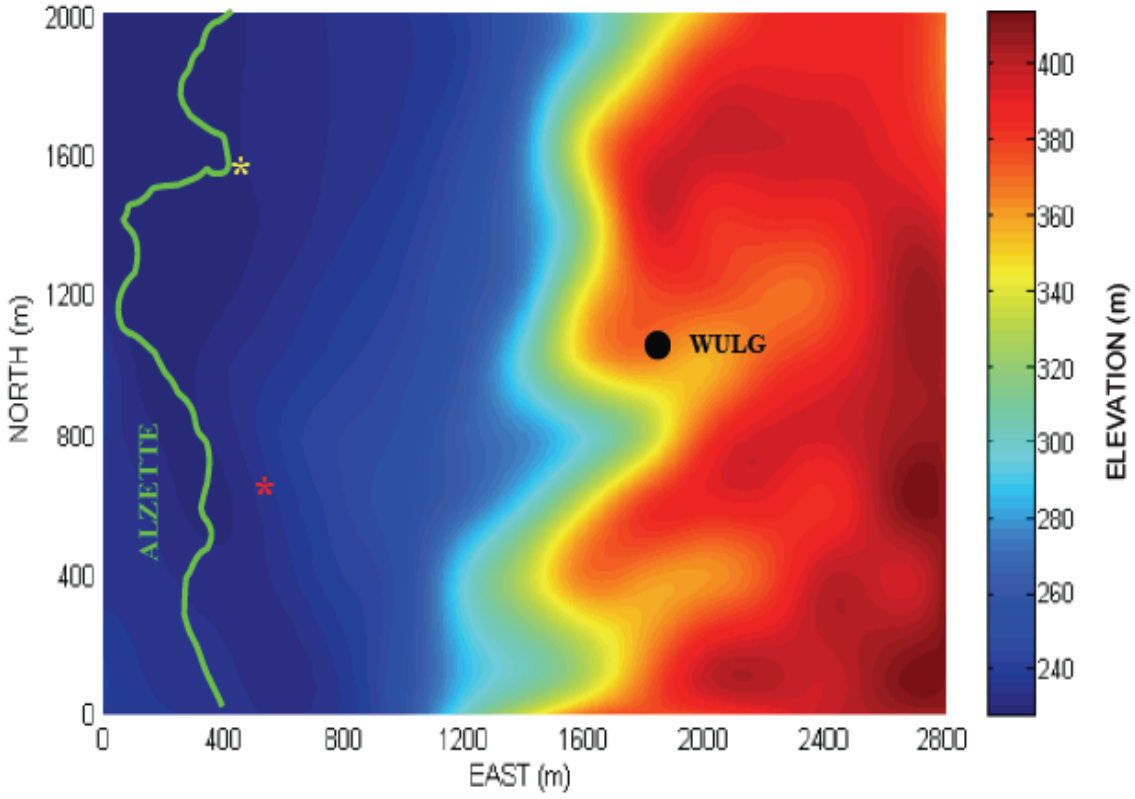

Fig. 3.2*: Locations of the WMS pluviometer (yellow asterisk) and the WULG pluviometer (red asterisk). The black dot represents the WULG. The green line represents the Alzette River.*

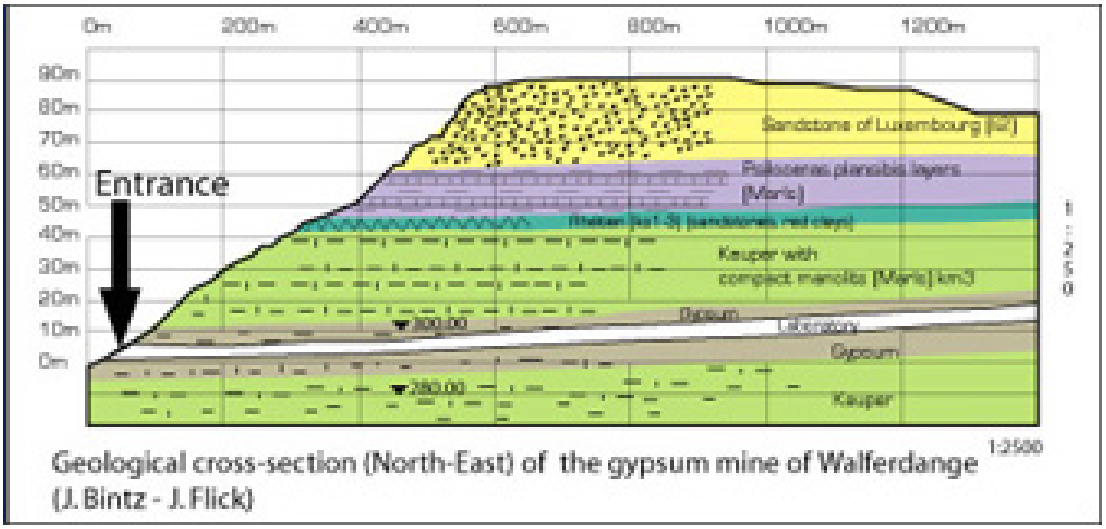

Fig. 3.3: *Geological cross-section of the old gypsum mine of Walferdange, presently hosting the Walferdange Underground Laboratory of Geodynamics (WULG).*

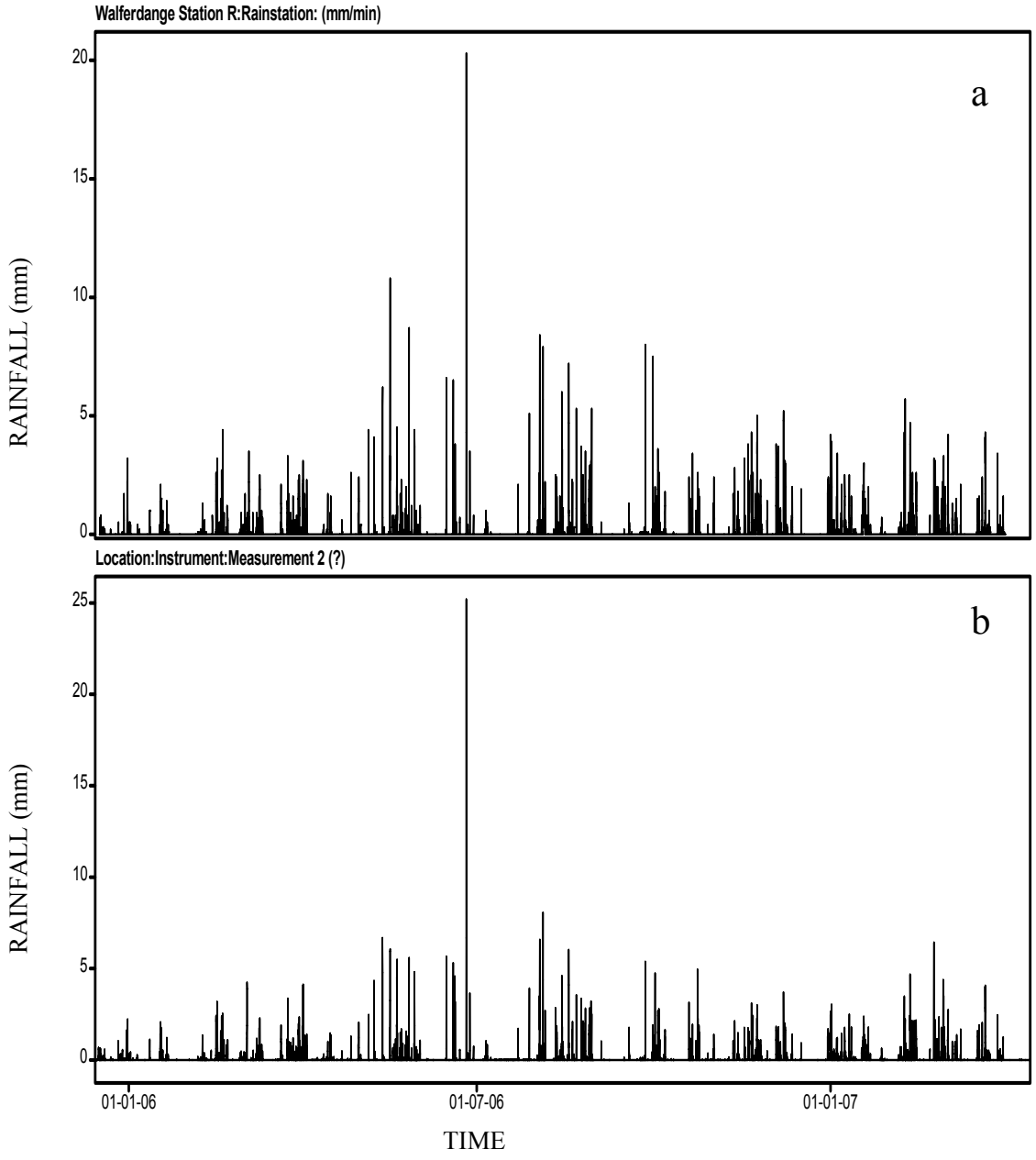

Fig. 3.4*: Rainfall time series (mm/hour) provided by the Walferdange Meteorological station (a) and the WULG pluviometer (b) for the period December 2005 to March 2007*

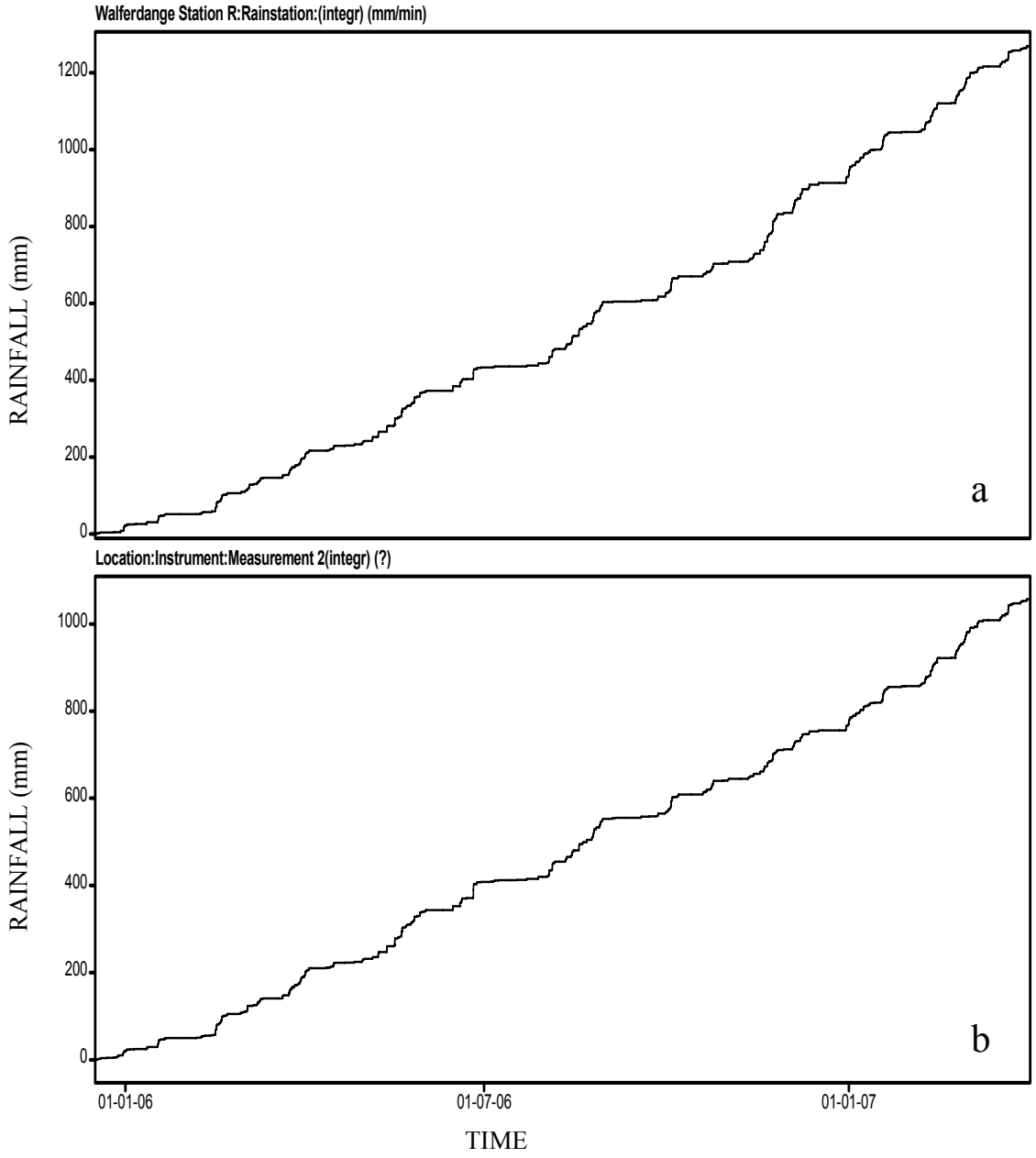

***Fig. 3.5**: Cumulative rainfall (mm) provided by the Walferdange Meteorological station (a) and the WULG pluviometer (b) for the period December 2005 to March 2007*

The combined series, covering the period January 2003 to January 2010 (Figure 3.6) represents the input of Equation 2.26 of the Tank Model and Equation 2.35 of the double Exponential Model.

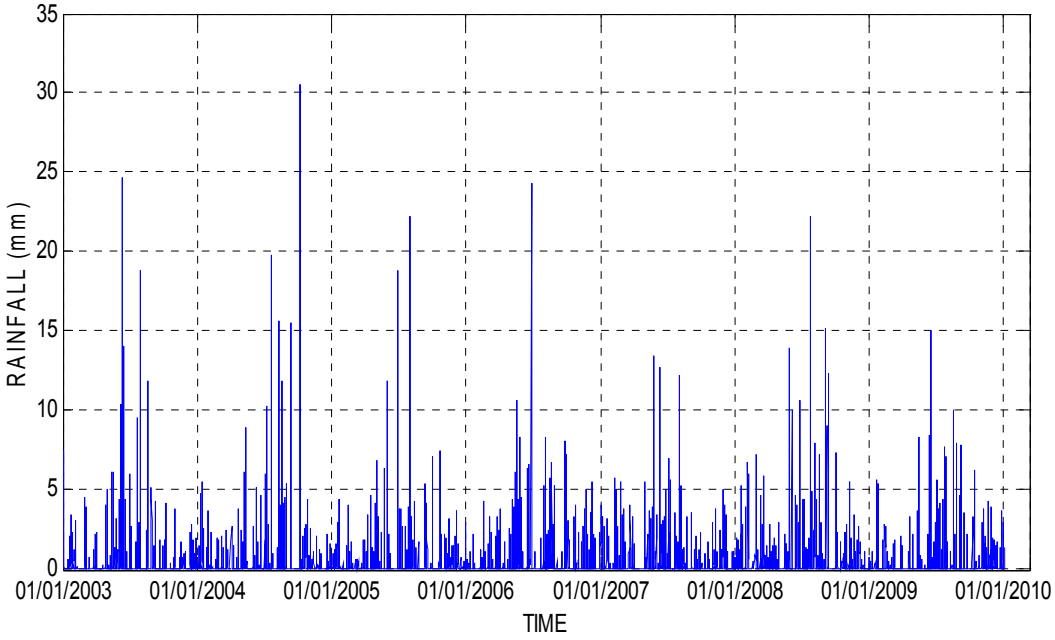

Fig. 3.6*: Input data: precipitation time series (mm/hour) provided by the WMS (January 2003 to December 2005) and the WULG (December 2005 to January 2010). The precipitation time series represents the input for both the Tank Model and the Double Exponential Model.*

3.3 Relative gravity measurements: the Superconducting Gravimeter OSGCT040

The output of Equation 2.33 and Equation 2.35 represent the modeled hydrologic gravity time series. These series must be compared to the observed gravity series, which is registered by the SG in the WULG.

The WULG is locatd underground in a derelict gypsum mine beneath the hills surrounding the locality of Walferdange (see Figure 3.3). The gypsum mine offers multiple advantages as a host of the laboratory:

- A stable temperature of about 13°C;
- Absence of running water and of anthropogenic disturbances;
- Facility of access;
- and Seismilogical stability.

SG's represent an evolution of the classical static spring gravimeters. Schematically, a static spring gravimeter can be represented as a test mass suspended to a spring. We refer to a zero length spring (having length equal to zero when it is not submitted to forces). The weight of the mass is balanced by the elastic force exerted by the spring. If k is the spring elastic constant, the equilibrium equation in the vertical direction in the location a (Figure 3.7) is given by:

$$k \cdot z_a = m \cdot g_a \tag{3.1}$$

where g_a is the gravity acceleration in location a (Figure 3.7) and z_a the spring elongation in location a. If the gravity acceleration in location b has a different value, g_b, the equilibrium equation in b is given by:

$$k \cdot z_b = m \cdot g_b \tag{3.2}$$

or

$$k \cdot (z_a + \Delta z) = m \cdot (g_a + \Delta g) \rightarrow k \cdot \Delta z = m \cdot \Delta g \tag{3.3}$$

where Δg is the gravity acceleration difference between the locations a and b and Δg the difference in the spring elongation at the locations a and b.

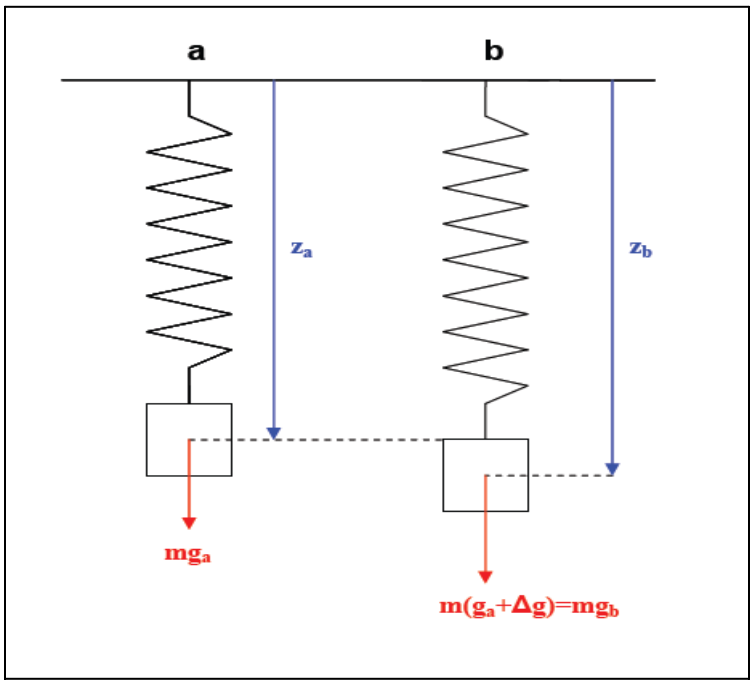

***Fig.3.7**: Functioning principle of the static spring gravimeter. A test mass m is suspended on a zero length spring. The spring deformation is proportional to the gravity field variation (for little variations, the relation between the spring deformation and the gravity force can be considered as linear).*

In SGs [*Goodkind, 1999, Richter, 1987; Crossley et al., 2005*], the mechanical spring is replaced by a magnetic field. The test mass is a hollow superconducting niobium sphere, which is in equilibrium under the combined action of the gravity force (sphere weight) and of the vertical upward levitation force due to the magnetic field induced by a permanent electric stream circulating in two superconducting coils. The vertical position

changes are detected by an electrostatic device and a feedback force maintains the sphere at a defined position. The feedback integrator voltage is proportional to changes in the acceleration of gravity. The functioning principle of the superconducting gravimeter (we display a single coil) is shown in Figure 3.8.

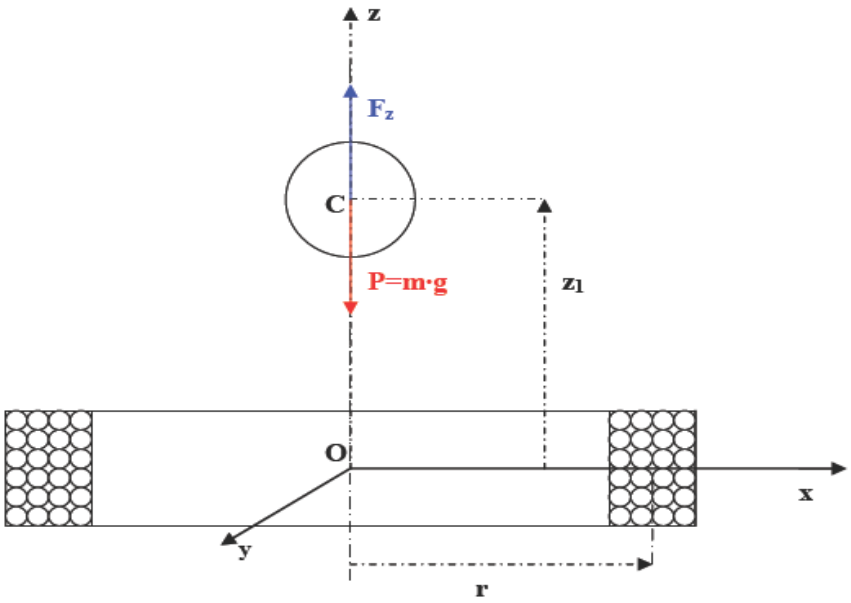

***Fig. 3.8**: Functioning principle of the superconducting gravimeter: a hollow superconducting niobium sphere is in equilibrium under the combined action of the gravity force (sphere weight) and of the vertical upward levitation force due to the magnetic field induced by a permanent electric stream circulating in two superconducting coils*

To allow the levitation phenomenon to occur, the ensemble constituted from the sphere and the coils must be maintained in a condition of superconductivity, at a temperature of about 4°C above the absolute zero (-273 °C).This is realized by placing the ensemble sphere coils in a bath of liquid helium.

With reference to Figure 3.7, we choose a Cartesian reference frame centered in the coil center of symmetry. The magnetic levitation force is vertically directed upward along the coil axis and is given by the expression:

$$F_z = \alpha \cdot \frac{z}{(r^2 + z_l^{\,2})^4} \cdot I_o \qquad (3.4)$$

where F_z represents the vertical levitation force, $\alpha=1.25\cdot10^{-12}$ $N\cdot m^7\cdot A^{-2}$ is a constant, r represents the coil medium radius (expressed in m), z_l the sphere center of mass elevation with respect to the chosen Cartesian frame (expressed in m) and I_o represents the electric stream traversing the coil.

Finally, the equilibrium condition in the vertical direction is expressed by:

$$F_z = m \cdot g \rightarrow m \cdot g = \alpha \cdot \frac{z}{(r^2 + z_l^{\,2})^4} \cdot I_o \qquad (3.5)$$

A change in the value of g produces a vertical displacement of the sphere until a new force balance is reached. A change in the stream I_o, and consequently in the voltage of the electrostatic feedback device, is required to bring the sphere back in the original balance position. With an adequate calibration, the voltage change can be interpreted as gravity variations.

The advantages of the Superconducting gravimeters lie in the measurement continuity, the linearity, the very high sensitivity (on the order of 10^{-11}m·s^{-2} or 10^{-4}μGal) and a limited long-term drift [C*rossley et al., 1998*].

The disadvantages lie in the fact that a very low temperature is required to maintain the state of superconductivity. The ensemble constituted by the superconducting sphere and the superconducting coils must be maintained at a temperature of about 4^{o}C above absolute zero. Consequently, a thermic optimal isolation is necessary. The consequence of these characteristics is the non-transportability of the instrument. In Figure 3.9 we display the cryogenic part of the SG.

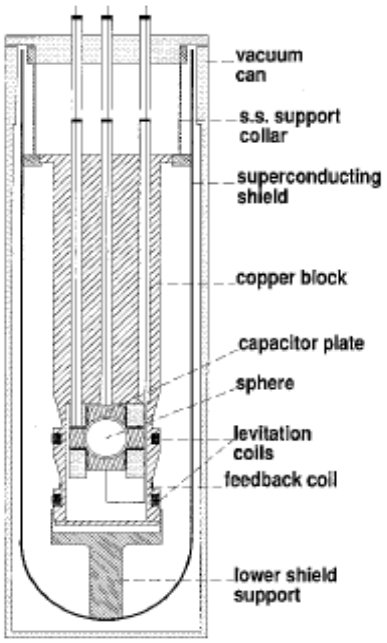

Fig. 3.9*: Cryogenic part of a Superconducting Gravimeter. To maintain a condition of superconductivity, the ensemble sphere-coils must be maintained at a temperature of about 4 ^{o}C above absolute zero [from Goodkind, 1999].*

As already pointed out, the Walferdange Underground Laboratory for Geodynamics (WULG) is located underground in a derelict gypsum mine, at latitude 49.6700°N, longitude 6.1500°E. The laboratory housing the SG lies at the end of an 800 m long tunnel cut into the side of a ridge. The gravity sensor is 295 m above sea level and about

80 m below the local surface. The area above the gravimeter has significant topographic gradients (See Figures 3.2 and 3.3), and is covered by uneven vegetation. The closest human artifacts (i.e. roads and buildings) are located at about 500 m from the gravimeter. All of these factors contribute to making the WULG seismically quiet. The OSGCT040 (Figure 3.10) provides high resolution relative gravity measurements from the 19th December 2003.

Fig. 3.10: *The superconducting gravimeter OSGCT040 located in the Walferdange underground Laboratory for Geodynamics. The instrument provides high-resolution relative gravity measurements from the 19-12-2003.*

3.4 Determination of the transfer function of the Observatory Superconducting Gravimeter OSGCT40 located in the WULG

3.4.1 Introduction

In order to determine the quality of the superconducting gravimeters, the experimental determination of their frequency response and the corresponding transfer function represents an important issue [*Van camp et al., 2000; Van Camp, 1998*]. This response can be significantly different for different gravimeters. The frequency response of the OSGCT40 is experimentally determined by injecting sine waves and step functions into the control electronics of the instrument. The procedure described by *Van Camp and al.* [2000] has been repeated reaching a precision of better than 0.01 sec in the phase response of the instrument. The zeros and poles of the transfer function have also been determined.

3.4.2 The Laplace Transform

The Laplace transform represents a powerful differential instrument for the analysis of Linear Time Invariant systems (LTI), such as electronic circuits [*Bertoni et al. 2003*]. The Laplace operator acts on functions represented in the time domain, transforming them into functions in the frequency domain, where the system input and output are functions of the complex angular frequency or Laplace variable, usually indicated with s, expressed in radians per unit of time.

If f(t) represents a real function of time defined for positive values of the time variable t, the Laplace Transform of f(t) is defined by:

$$\mathcal{L}[f(t)] = F(s) = \lim_{\substack{T\to\infty \\ \varepsilon\to 0}} \int_{\varepsilon}^{T} f(t)\cdot e^{-st}\,dt = \int_{0+}^{\infty} f(t)\cdot e^{-st}\,dt \qquad 0<\varepsilon<T \qquad (3.6)$$

where s is a complex variable defined by $s=\sigma+i\cdot\omega$, σ and ω being real variables.

The Laplace operator $\mathcal{L}$ is a differential operator with the property of linearity. This implies that if $F_1(s)$ and $F_2(s)$ are the Laplace transforms of the functions $f_1(t)$ and $f_2(t)$, then $c_1\cdot F_1(s)+ c_2\cdot F_2(s)$ is the Laplace transform of $c_1\cdot f_1(t)+ c_2\cdot f_2(t)$, where c_1 and c_2 are arbitrary constants.

The Laplace Transform of the time derivative of a function f(t) having F(s) as Laplace transform, is expressed by:

$$\mathcal{L}\frac{df(t)}{dt} = s\cdot F(s) - f(0^+) \qquad (3.7)$$

The Laplace Transform of the time integral of a function f(t) having F(s) as Laplace transform, is expressed by:

$$\mathcal{L}\left[\int_0^t f(\tau)d\tau\right] = \frac{F(s)}{s} \qquad (3.8)$$

Thus, the Laplace transform allows us to simplify the differential equations characterizing the LTI systems, reducing them to more easily solvable algebraic relations. The *inverse Laplace Transform* allows us to express the solutions again in the time domain.

3.4.3 Transfer function and frequency response for LTI systems

A transfer function (or network function) for an LTI system represents a mathematical expression, in the spatial or temporal frequency domain, of the relation between the model output and input. For a LTI system having a continuous time input signal x(t) and a continuous time output signal y(t), the transfer function is the ratio between the output Laplace transform Y(s) and the input Laplace transform X(s), having assumed zero initial conditions:

$$H(s) = \frac{Y(s)}{X(s)} \tag{3.9}$$

where $X(s) = \mathcal{L}[x(t)]$ and $Y(s) = \mathcal{L}[y(t)]$. The transfer function also corresponds to the Laplace transform of the system's impulse response, which is the output generated using a Dirac delta impulse as input. The Laplace transform of the Dirac delta is 1, and consequently we have $H(s)=Y(s)$.

For LTI systems, because of the previously underlined properties of the Laplace transform, the transfer function is generally represented by the ratio of two polynomials of the Laplace complex variable s:

$$H(s) = \frac{\sum_{i=0}^{m} b_i s^i}{\sum_{i=0}^{n} a_i s^i} \tag{3.10}$$

The poles are defined as the values of s for which the denominator of the transfer function is equal to zero, and the zeros represent the values of s for which the numerator of the transfer function is equal to zero. In the time domain, each pole is associated with a response mode of the system. The impulse response of the system is a linear combination of the different response modes. Thus, the transfer function completely defines the system response.

If the input of a linear time invariant system is a sinusoidal signal, it can be represented in complex form by:

$$x(t) = |X| \cdot e^{i(\omega t + \varphi_X)} = |X| \cdot e^{i\varphi_X} \cdot e^{i\omega t} = X \cdot e^{i\omega t} \tag{3.11}$$

where $|X|$ is the input amplitude, $\varphi(X)$ the input phase and i represents the imaginary number $(-1)^{1/2}$. The corresponding system output is also a sinusoidal signal with the same frequency ω but generally having a different phase and amplitude:

$$y(t) = |Y| \cdot e^{i(\omega t + \varphi_Y)} = |Y| \cdot e^{i\varphi_Y} \cdot e^{i\omega t} = Y \cdot e^{i\omega t} \tag{3.12}$$

The frequency response for the amplitude represents the amplitude change as a function of the frequency ω, and is defined as gain.

$$G(\omega) = \frac{|Y|}{|X|} = |H(i \cdot \omega)| \tag{3.13}$$

The frequency response for the phase represents the phase difference as a function of the frequency ω:

$$\phi(\omega) = \varphi_Y - \varphi_X = \arg(H(i \cdot \omega)) \tag{3.14}$$

The frequency response corresponds to the transfer function where the variable s is replaced with the variable (ω·i) and the variability of ω is limited to positive values.

From an experimental point of view, the amplitude and phase response of a given LTI system can be determined by injecting signals at different frequencies and analyzing the corresponding amplitudes and phases of the system output. The experimental frequency response in complex form is given by:

$$R(\omega_n) = \frac{|Y_n|}{|X_n|} \cdot e^{i \cdot \phi_n} = G_i \cdot e^{i \cdot \phi_n} = \frac{Y_n}{X_n} \qquad \textit{n=1: sample length} \tag{3.15}$$

where G_n represents the gain for the injected signal n having amplitude $|X_n|$ and frequency ω_n, $|Y_n|$ and Φ_n the amplitude and phase shift of the corresponding output signal, respectively. Sometimes, it is convenient to use input signals, which all have the same amplitude A. Thus, the complex experimental frequency response for signal i is expressed by:

$$R(\omega_n) = \frac{|Y_n|}{A} \cdot e^{i \cdot \phi_n}$$

Different mathematical algorithms allow us to determine the polynomial coefficients of the transfer function from the frequency response in complex form.

3.4.4 Experimental determination of the frequency response for the OSGCT40

The frequency response of the OSGCT40 is experimentally determined [*Olivier Francis, Gilbert Klein, Maren Westkott, and Laura Kipfstuhl, personel communication, 2009*] by injecting step functions and sine waves (as input signals) at defined voltages

into the control electronics of the gravimeter, and analyzing the response of the system (output signal).

With the step function method, the step response function is differentiated to obtain the impulse response function. The Fourier spectrum of the impulse response function corresponds directly to the transfer function of the system.

With the sine wave method, the transfer function is obtained by fitting the input signal (injected waves at different frequencies) and the output signal (instrument response) with a sinusoidal function. The amplitude ratios and phase differences as a function of the input frequencies correspond to the instrumental frequency response (Equation 3.15).

The gravimeter can be considered as a linear time invariant system, and therefore the observations made in the preceding section concerning the transfer function can be assumed as valid. Both sine waves and step functions should provide the same transfer function. Consequently, a comparison of the results obtained with the different types of input can offer an indication of the accuracy of the results.

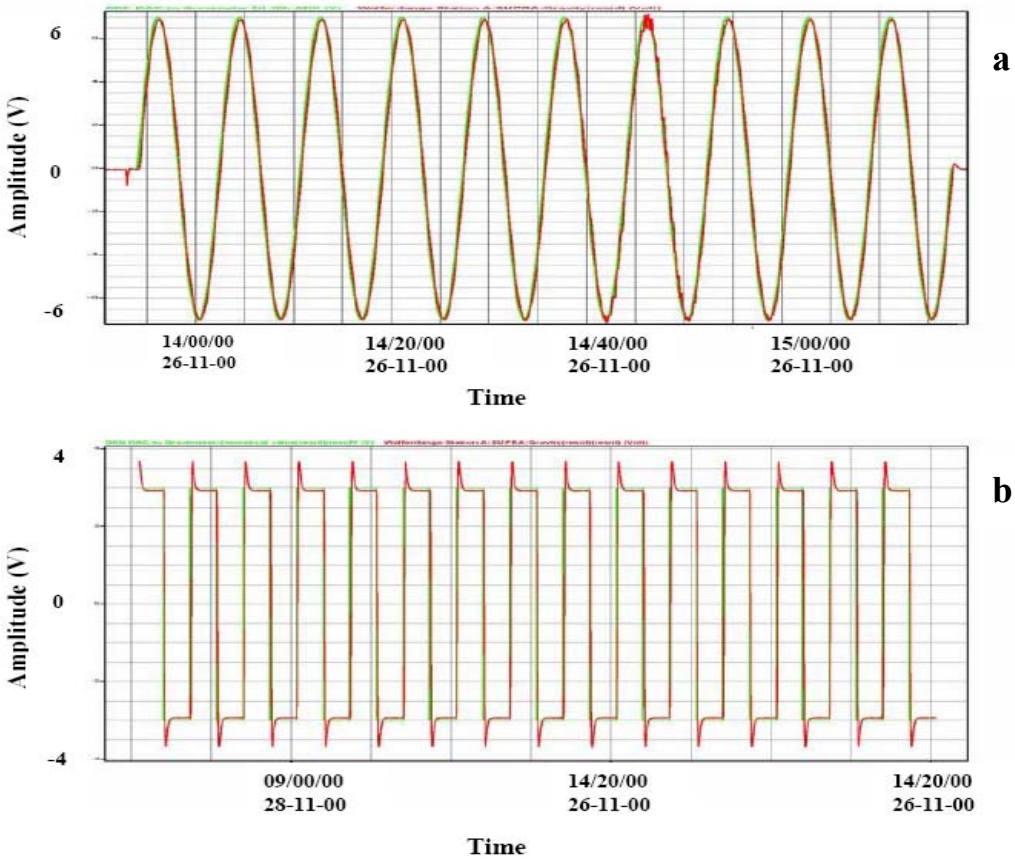

Fig. 3.11: *Voltages injected into the instrument control electronics.*

a) Sine waves with 500s period

b) Step functions

The experiment was conducted by injecting 29 time steps (Figure 3.11 b) and sine waves (Figure 3.11 a), which have an 8 Volt amplitude, at four different frequencies into the control electronics of the instrument. The periods corresponding to the different

frequencies are 200 seconds, 500 seconds (Figure 3.10 a), 1000 seconds and 2000 seconds. The instrument frequency response (amplitude and phase) obtained with the sine wave and the step function methods are displayed in Figure 3.12. In Table 3.1 we display the values of the phase shift (expressed in terms of time delay) obtained, for the four different periods, with the sine waves and the step functions, respectively.

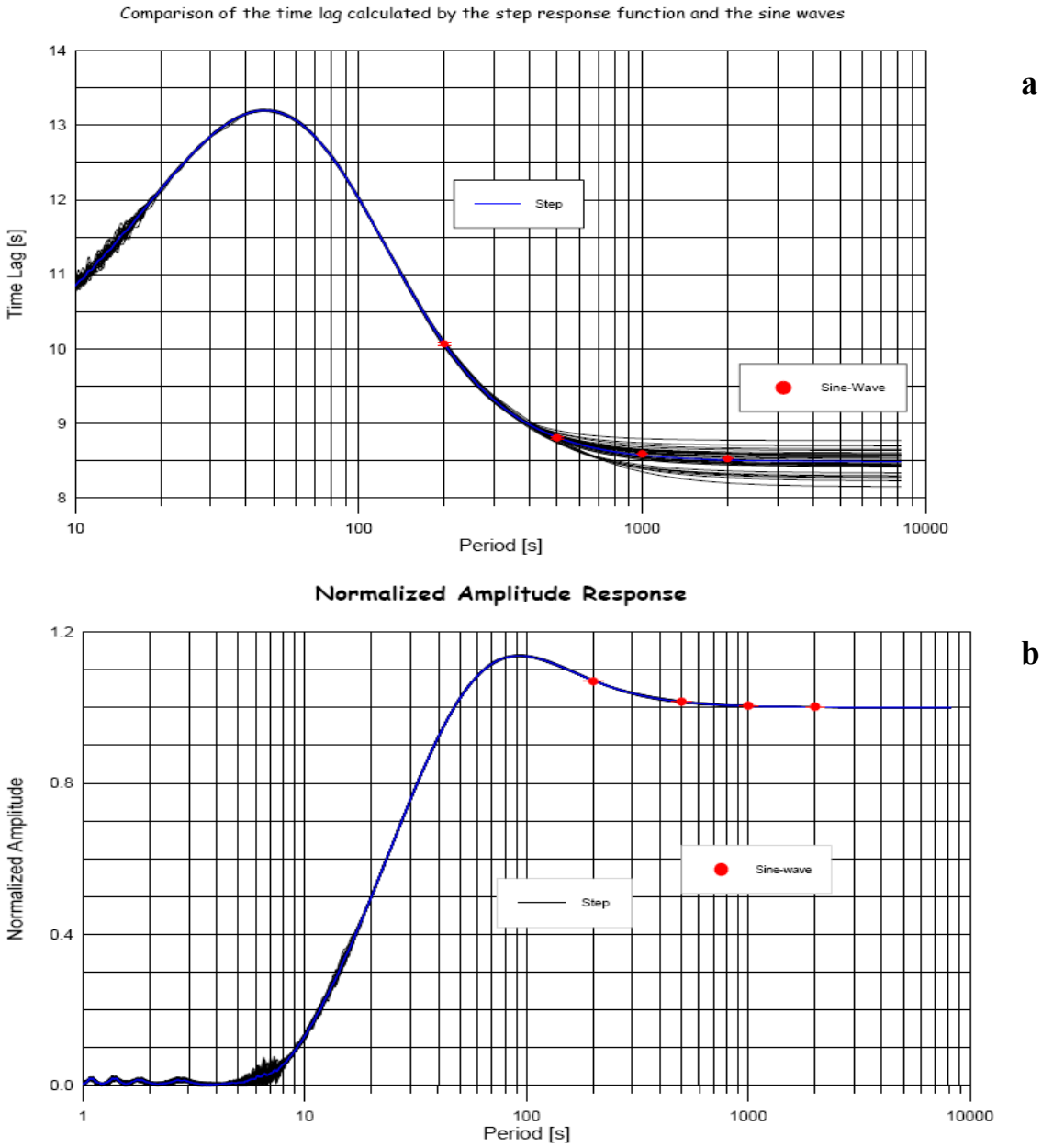

***Figure 3.12**: Frequency response of the OSGCT40 obtained by injecting sine waves (continuous line) and step functions (red dots) into the instrument electronics:*

a) Phase as a function of period represented in terms of time lag (s).

b) Normalized amplitudes a function of period.

Period (seconds)	Time lag (Sine Waves)	Time lag (Step Functions)
200	9.818+-0.011	9.823+-0.017
500	8.571+-0.011	8.554+-0.042
1000	8.343+-0.003	8.323+-0.111
2000	8.281+-0.02	8.256+-0.136

Tab. 3.1: *Values of the phase (expressed in terms of time lag) obtained, for the four different periods, with the sine waves and the step functions.*

In Table 3.2 we display the values of the normalized amplitudes obtained, for the four different periods, with the sine waves and the step functions, respectively.

Period (seconds)	Amplitude (Sine Wave)	Amplitude (Step Function)
200	1.044374+-0.000353	1.0469+-0.0004
500	0.990787+-0.000138	0.9892+-0.0130
1000	0.980199+-0.000022	0.9787+-0.0005
2000	0.977218+-0.000006	0.9759+-0.0001

Tab. 3.2: *Values of the normalized amplitudes obtained, for the four different periods, using the sine waves and the step functions.*

The determination of the transfer function determines the quality of the superconducting gravimeters. The frequency response can show significantly different shapes for different instruments. Therefore, it is important to determine the specific response of each instrument. As an example, a comparative investigation has been carried out on the frequency responses of the OSGCT40 and of the cryogenic gravimeter GWR-C021 located in Membach (Belgium). The amplitude and phase responses for the two instruments are displayed Figure 3.13. The normalized amplitude is here displayed in a log-log representation.

The polynomial coefficients of the transfer function of the OSGCT40 are obtained from the complex experimental frequency response with a least squares fit algorithm. The form of the transfer function is defined by the ratio of two polynomials of the complex Laplace variable s (Equation 3.10). The numerator and denominator of the transfer function are both modeled as 6^{th} order polynomials (Please note, that the order of the denominator must be superior or equal or superior to the order of the numerator). The fit-errors versus frequency are weighted with the use of a weighting vector. The fit provides the following transfer function:

$$H(s) = \frac{-0.03897s^6 + 0.08883s^5 - 0.1268s^4 + 0.1159s^3 - 0.06664s^2 + 0.01835s + 0.0010281}{s^6 + 1.744s^5 + 1.6s^4 + 0.8269s^3 + 0.2292s^2 - 0.0271s + 0.001028}$$

(3.16)

The transfer function *H(s)* allows us to calculate the instrument frequency response (amplitude and phase) by replacing the variable s with the variable (ω·i). In Figure 3.14, we display the observed phase and amplitude response (blue) and the phase and

amplitude responses calculated with the use of the transfer function. The agreement appears almost perfect.

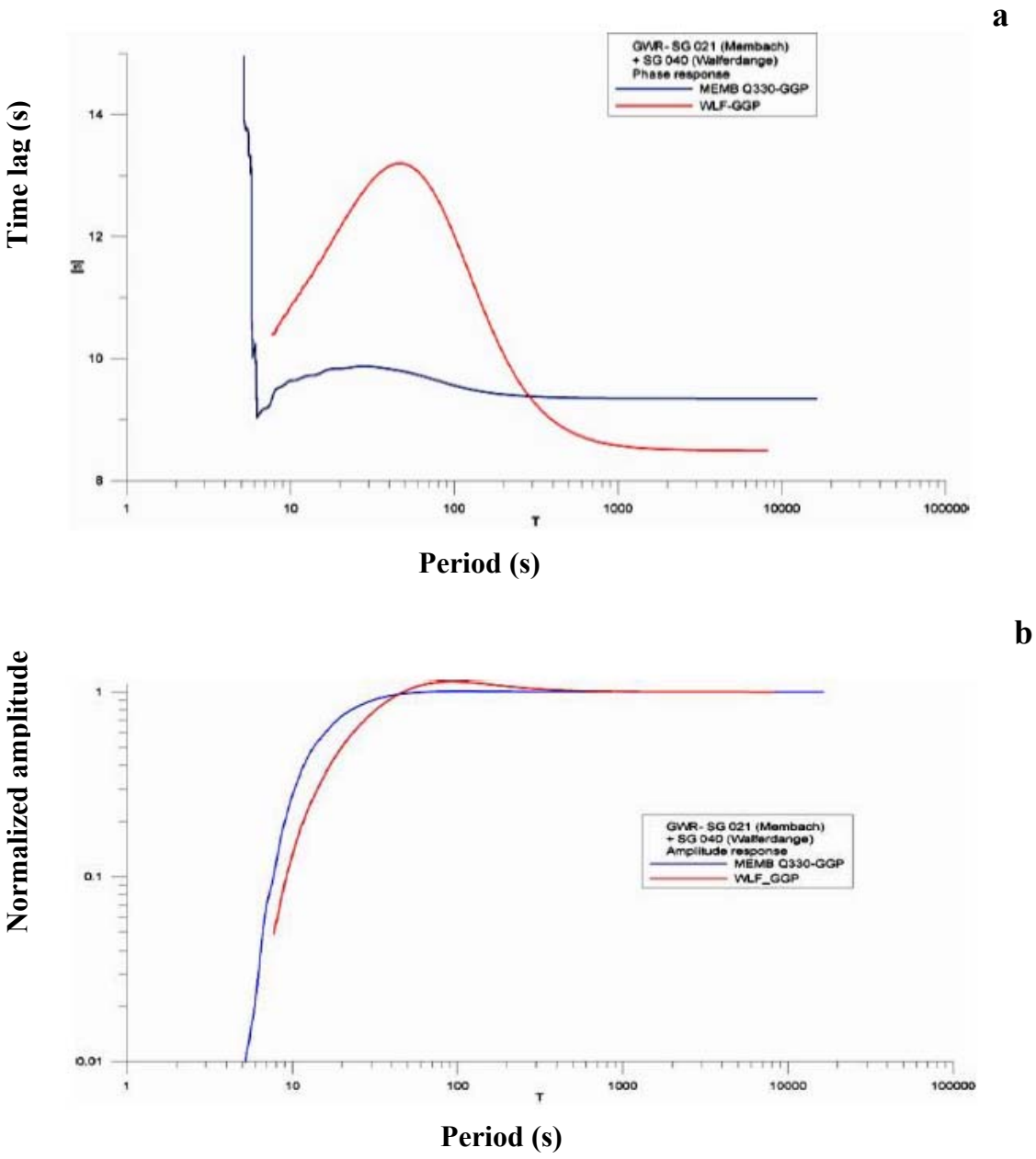

Fig. 3.13: *Comparison of the transfer functions of the OSGCT40 operating in the WULG (red line) and the GWR-C021 operating in Membach (blue line).*

a) Phase as a function of the period, T, expressed in terms of time lag (seconds)

b) Normalized amplitude as a function of the period T (log-log representation)

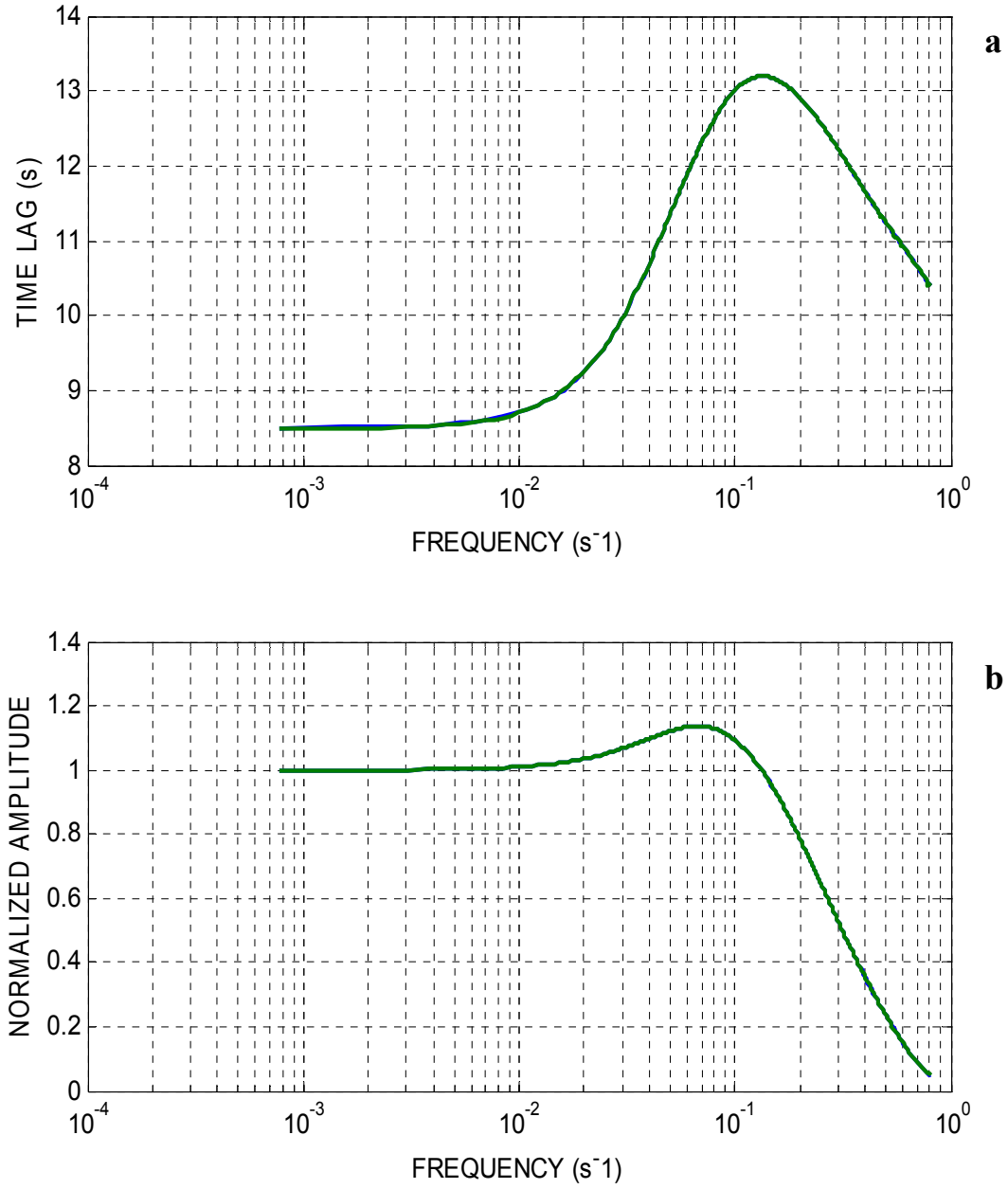

Fig. 3.14*: Phase response (a) and normalized amplitude response (b) of the OSGCT40. The observed response is represented with a green line; the response calculated with the use of the transfer function is represented with a blue line.*

In Figure 3.15 we show in the complex coordinate system the points representing the poles and zeros of the transfer function. The poles are the values of s, which make the denominator of the transfer function zero, and consequently correspond to the function points of divergence. As previously underlined, each pole is associated, in the time

domain, to a response mode of the instrument. The zeros are the values of s, which make the numerator of the transfer function zero, and the function equals zero at these points. The values of the poles and of the zeros are reported in table 3.3.

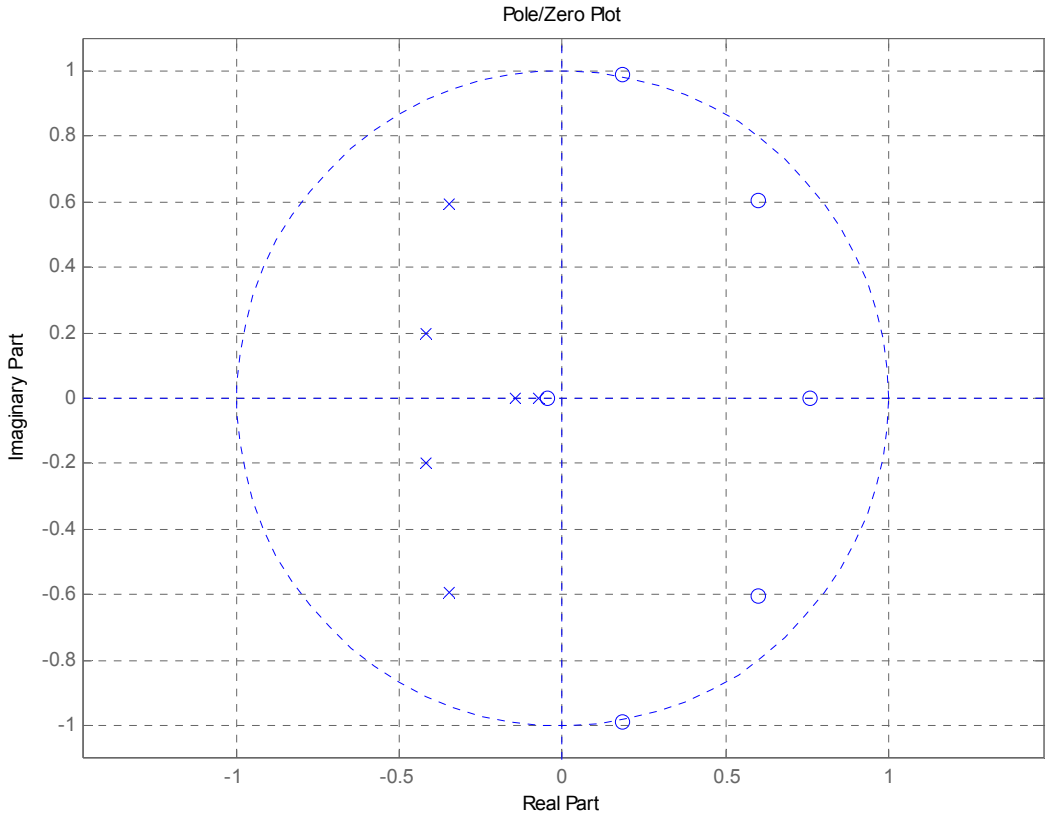

***Fig. 3.15**: Pole-Zero plot: representation in the complex coordinate system of the points corresponding to the poles and zeros of the transfer function. The poles are represented with blue crosses; the zeros are represented with blue circles.*

Poles	**Zeros**
-0.3455+0.590i	0.1820 + 0.9883i
-0.3455-0.590i	0.1820 - 0.9883i
-0.4187 + 0.1947i	0.5999 + 0.6044i
-0.4187 - 0.1947i	0.5999 - 0.6044i
-0.1446	0.7629
-0.0713	-0.0472

***Tab. 3.3**: Poles and zeros of the transfer function.*

3.5 Gravity time series provided by the OSGCT40 located in the WULG

The gravity time series provided by the SG for the period December 2003 to January 2010 have been filtered and decimated to hourly values. This series, corrected for the ocean loading, Earth tides and polar motion effects, represent the hydrological gravity variations still uncorrected for the instrumental drift (Figure 3.16, black line). Even if the drift is significantly reduced with respect to that of classical spring gravimeters, an instrumental drift is still present in superconducting gravimeters.

The causes of the drift are mainly related to variations in the magnetic field, possible absorption of gas from the levitating sphere and pressure variations of the helium gas used to maintain the sphere–coils ensemble in a superconducting state at low temperatures. Besides the transfer function, the characterization of the SG instrumental drift is important for interpreting gravity changes from the instrument.

Van Camp and Francis [2006] have investigated the behavior of the superconducting gravimeter operating in Membach (Belgium). They have presented two possible hypotheses about the kind of functions apt to model the drift. The first hypothesis is that the drift is a linear function of time. The second hypothesis is that the drift is an exponential function of time.

With a statistical analysis of the differences between absolute gravity measurements and the measurements done with the superconducting gravimeter, the authors reached the conclusion that at the long-term (periods > 10 years) the drift is best modeled with exponential functions of time. For periods not exceeding 10 years, the linear and Exponential Models appear to represent the drift with equal precision.

Similar to the treatment of *Van Camp and Francis* [2006], we compared the SG time series and absolute gravity measurements to assess the instrumental drift of the OSGCT40. The absolute gravity measurements were provided by the free fall absolute gravimeter FG5 located in the WULG in proximity of the SG (Figure 3.17) The SG time series cover a period of 6 years. Thus, following the conclusions of *van Camp* and *Francis,* the instrumental drift of the OSGCT40 is modeled with a simple linear function of time. The comparison with the absolute gravity data indicates a linear drift of 1.27 μGal/year. Finally, the function adopted to describe the drift is expressed by:

$$\Delta g(t) = 1.47 \cdot 10^{-4} \cdot t \qquad (3.17)$$

where $\Delta g(t)$ represents the instrumental drift as a function of the time t expressed in hours.

The absolute gravity measurements provided by the FG5 are displayed in Figure 3.16 (red dots, μGal). In the same Figure are displayed (black line, μGal) the SG residuals time series corrected for the linear drift expressed by Equation 3.17. The residuals from the drift represent the reference time series for the comparison with the hydrologically modeled gravity time series.

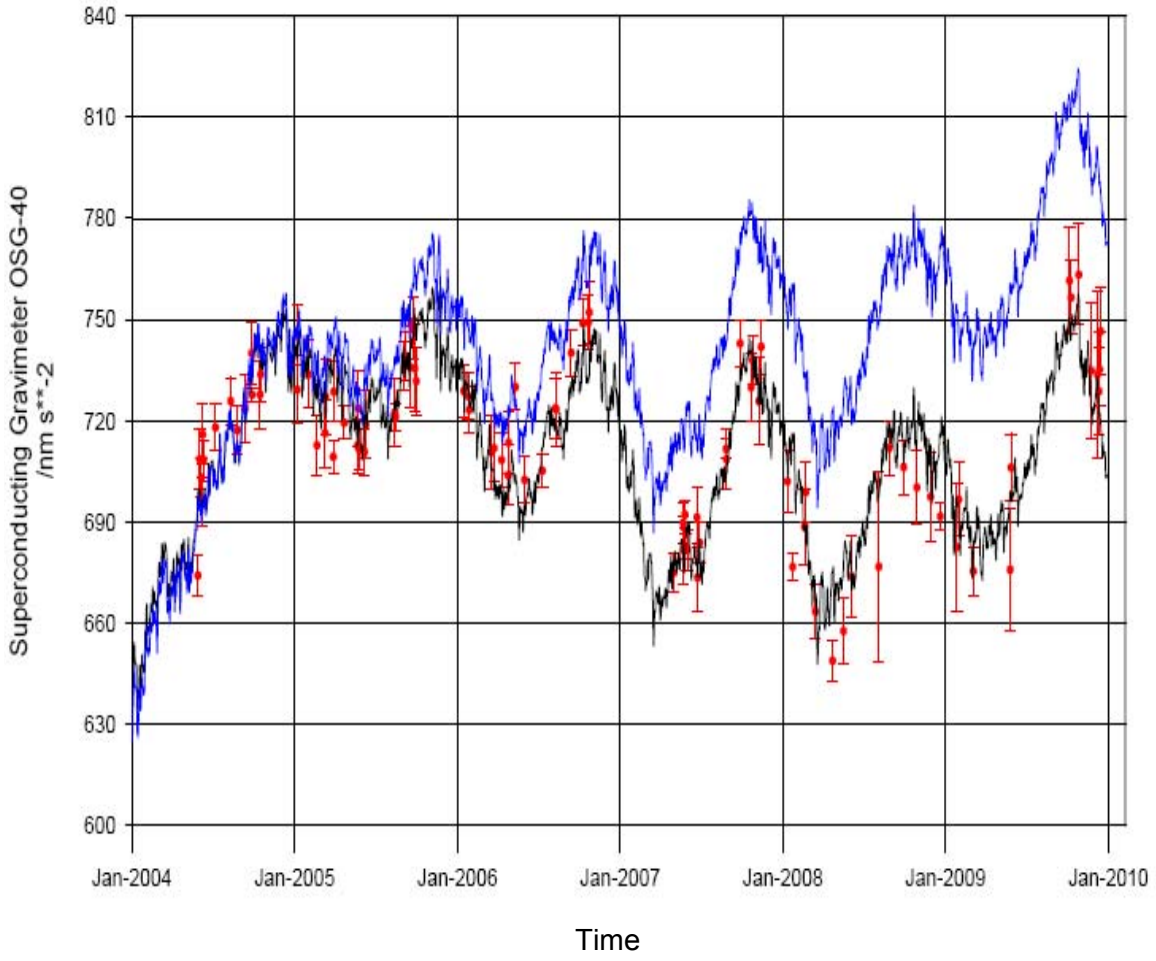

Fig. 3.16*: Hydrological gravity residuals provided by the* OSGCT40 *without correction for the linear long term instrumental drift of 1.27 μGal/year (blue, μGal), hydrological gravity residuals provided by the* OSGCT40 *after correction for the linear long term instrumental drift (black, μGal), and absolute gravity measurements provided by the free fall absolute gravimeter FG5 located in the WULG in proximity of the SG (red, μGal).*

The survey of the residuals shows the permanence of a significant initial short term (5-6 months) instrumental drift.

3.6 Tank Model implementation method

The 1st order differential equation, Equation 2.26, represents the Tank Model equation in its analytical form. The rainfall rate r(t) is here a theorical continuous function describing the incoming precipitation as a function of time. As already pointed out, the precipitation series are actually a discrete set of values referred to discrete time indices, i. Defining Δt as the sampling reference time interval, the relation between the actual numerical rainfall series r(i) and the theoretical analytical series r(t) is expressed by:

Fig. 3.17: *The free-fall absolute gravimeter FG5 located in the WULG at a few meters distant from the OSGCT40. The absolute gravity measurements provided by the FG5 have been used to asses the drift of the superconducting relative gravimeter.*

$$r(i) = \int_{(i-1)\cdot\Delta t}^{i\cdot\Delta t} r(t)dt \tag{3.18}$$

where r(t) is the continuous rainfall rate series (depth/time) and r(i) the discrete rainfall time series. Thus, r(i) represents the integrated amount of water precipitated between the epochs (i-1)·Δt and i·Δt, where i represent non-dimensional time indices.

First order differential equations [*Quarteroni et al. 2000, Quarteroni, 2003*] can be numerically solved using the Euler method. A fist order differential equation, defined on the interval $[t_o, t_n]$ is expressed as:

$$y'(t) = \frac{dy}{dt} = f(t, y(t)) \tag{3.19}$$

The initial conditions are expressed as:

$$y_o = f(t_o) \tag{3.20}$$

The value $y(t_i)$ for the instant $t_i \subset [t_o,t_n]$ can be approximated by subdividing the interval $[t_o,t_n]$ into n sub-intervals, each having a length $\Delta t=(t_n- t_o)/n$. We thus have:

$$t_{i+1}=t_o+i\cdot\Delta t \tag{3.21}$$

$$t_n=t_o+n\cdot\Delta t \tag{3.22}$$

Considering the finite increments Δy and Δx instead of the infinitesimal variations dy and dt, it is possible to write the following expression for each sub-interval :

$$\frac{y_{i+1}-y_i}{t_{i+1}-t_i}=f(t_i,y_i) \tag{3.23}$$

The approximation consists of replacing the function with the tangent to the function at the considered point. From Equation 3.23 we obtain:

$$y_{i+1}=y_i+\Delta t\cdot(f(t_i,y_i)) \tag{3.24}$$

where $\Delta t=t_{i+1}-t_i=(t_n- t_o)/n$ represents the sub-interval length. The error with the Euler approximation is then proportional to the length of the sub-intervals.
In Equation 2.25, the reference time interval is the sampling time series interval, assumed to be unity (1 hour for the hourly implementation). The averaging theorem allows us to write Equation 3.18 in the form:

$$r(i)=r_m(i)\cdot\Delta t \tag{3.25}$$

where $r_m(t)$ is the average value of r(t) in the interval $[t_{i+1}, t_i]$. Consequently, $r_m(t)$ has the same numerical value then r(i) but the dimensions of length instead of dimensions length/time. Equation 2.26 in numeric form is rewritten as:

$$\frac{\Delta g(i+1)-\Delta g(i)}{\Delta t}=\gamma_o\cdot(1-A\cdot\cos(\omega\cdot i-\varphi))\cdot\Delta g(i)-\alpha\cdot r_m(i) \tag{3.26}$$

Defining $\gamma_{oi}=\gamma_o\cdot\Delta t$ as the non dimensional recovery rate after a precipitation event, having the same numerical value as γ_o, , Equation 3.26 becomes:

$$\Delta g(i+1)=\Delta g(i)+\gamma_{oi}\cdot(1-A\cdot\cos(\omega\cdot i-\varphi))\cdot\Delta g(i)-\alpha\cdot r\ (i) \tag{3.27}$$

Equation 3.27 represents an iterative expression that can be implemented with the use of relatively simple algorithms. Preliminarily, some algebraical manipulations are carried out in order to simplify the equation. Finally, the Equation becomes:

$$\Delta g(i+1)=K\cdot(1-C\cdot\cos(\omega\cdot i-\varphi))\cdot\Delta g(i)-\alpha\cdot r(i) \tag{3.28}$$

where $C=(\gamma_o/(1-\gamma_o))\cdot A$ and $K=1-\gamma_o$ are two constants. The as the value of K approaches 1, the smaller the model errors become. The Tank Model was actually implemented in the form represented by equation 3.28.

3.7 Tank Model output and comparison between observed gravity and modeled gravity

The rainfall time series provided by the WULG, integrated to hourly values and referred to the end-hour points, are used as input for the Tank Model (equation 3.28). The rainfall heights are expressed in meters. An uncertainty of 10% is assigned to the rainfall data, as determined by the quantitative difference in the rainfall data from the two closely space pluviometers (see Section 3.2).

In the absence of direct information on local hydro-geological parameters, the model parameterization is determined empirically. The value of the admittance, $\alpha=36$ μGal m^{-1} derived in Section 2, has been used for the model parameterization in Equation (2.27). The parameters γ_o, A and φ in the same equation are obtained empirically by a least square adjustment. The gravity variations observed with the SG are compared with the values predicted by Equation 3.28 using the rainfall data, for the period 19 December 2003 to 1 December 2004. The parameters are determined from the data in order to minimize the residuals. The values of A=0.6, $\varphi= 2\pi/5$, and $\gamma_o=0.0011$ $hours^{-1}$ provide the best results. For reference, *Meurers* (2007) adopted the value $\tau=720$ hours for the discharge time parameter at the gravity station in Vienna, which corresponds to $\gamma_o=0.0015$ $hours^{-1}$ (see Section 1). The model outputs for the period 1st January 2003 to 1st January 2010 are displayed in Figure 3.18.

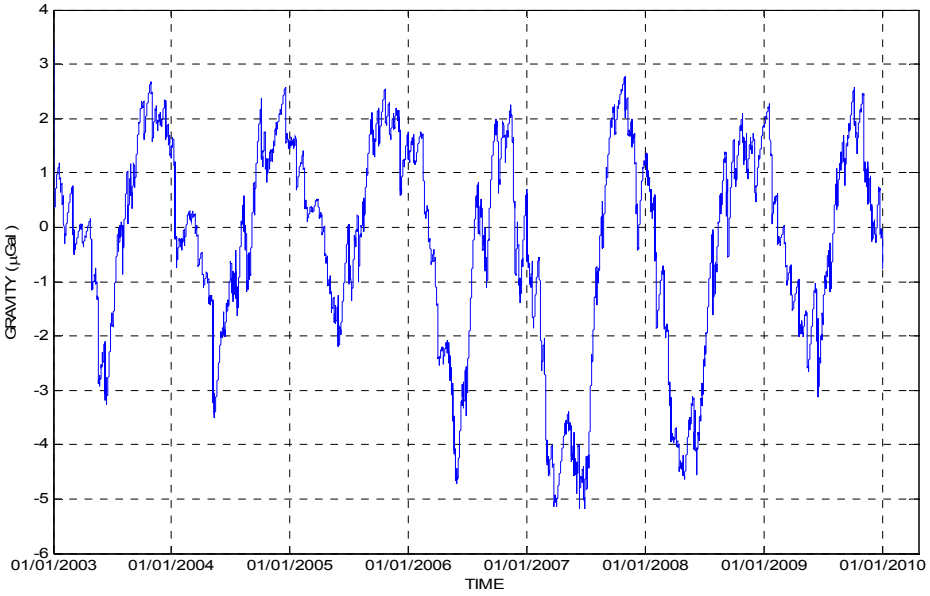

***Fig. 3.18**: Tank Model output (modeled gravity) in μGal for the period 1st January 2003 to 1st January 2009.*

The modeled hourly time series of the gravity (µGal) is compared with the observed hourly time series obtained from the SG for the period 19-December 2003 to 1-January 2010. The observed time series (green), the modeled (blue) time series for the specified period are displayed in Figure 3.19 A. The final residuals are displayed in Figure 3.19 B.

In order to quantify the entity of the signal reduction, we refer to the Root Mean Square (RMS. For a given set of values x_i with i=1:n, the root mean square is defined as:

$$RMS_x = \sqrt{\frac{\sum_{i=1}^{n} x_i^{\,2}}{n}} \tag{3.29}$$

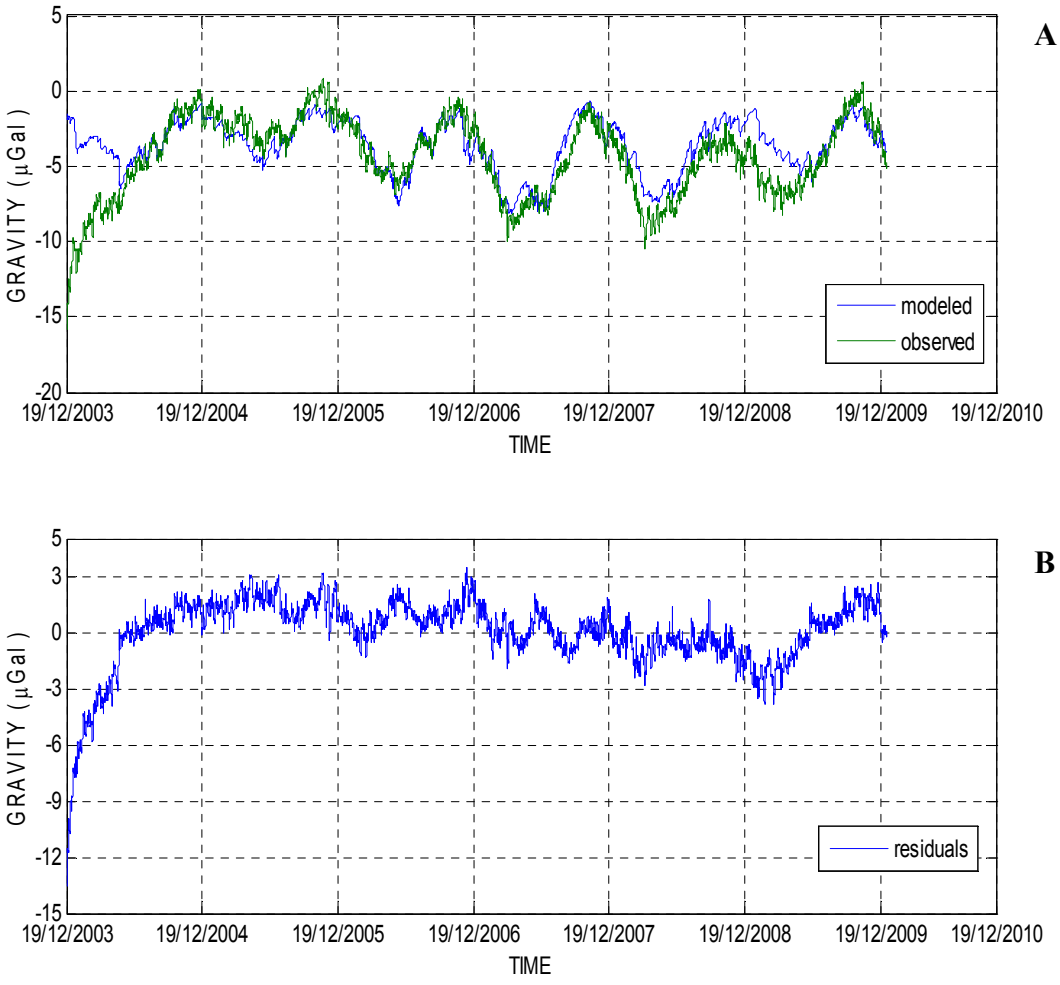

Fig. 3.19*: Comparison between observed and modeled gravity time series:*

A. Observed gravity (green, µGal), modeled gravity (blue, µGal) at Walferdange. The comparison period is 30-May, 2004 to 1-January, 2010.

B. Gravity residuals (µGal), representing the difference between the observed and modeled time series.

We obtain the final gravity residuals by subtracting the modeled gravity time series $\Delta g_m(t)$ from the observed gravity time series:

$$\Delta g_r(t) = \Delta g_o(t) - \Delta g_m(t)$$

where Δg_r represents the final residuals, Δg_o the observed residuals and Δg_m the modeled residuals. As already pointed out, a significant instrumental drift persists in the initial months of operating of the SG. Therefore, the calculation of the RMS values is made for the period 1st of May 2004 to 1st of January 2010.
The Root Mean Square (RMS_o) of the observed gravity time series is:

RMS_o=2.3 μGal

The Root Mean Square (RMS_r) of the final gravity residuals is:

RMS_r=1.19 μGal

corresponding to a 73% reduction of the signal scatter. In Figure 3.20 are displayed the modeled gravity (green, μGal), the observed gravity (red, μGal) and the rainfall (blue, mm) for the period May to September 2004.

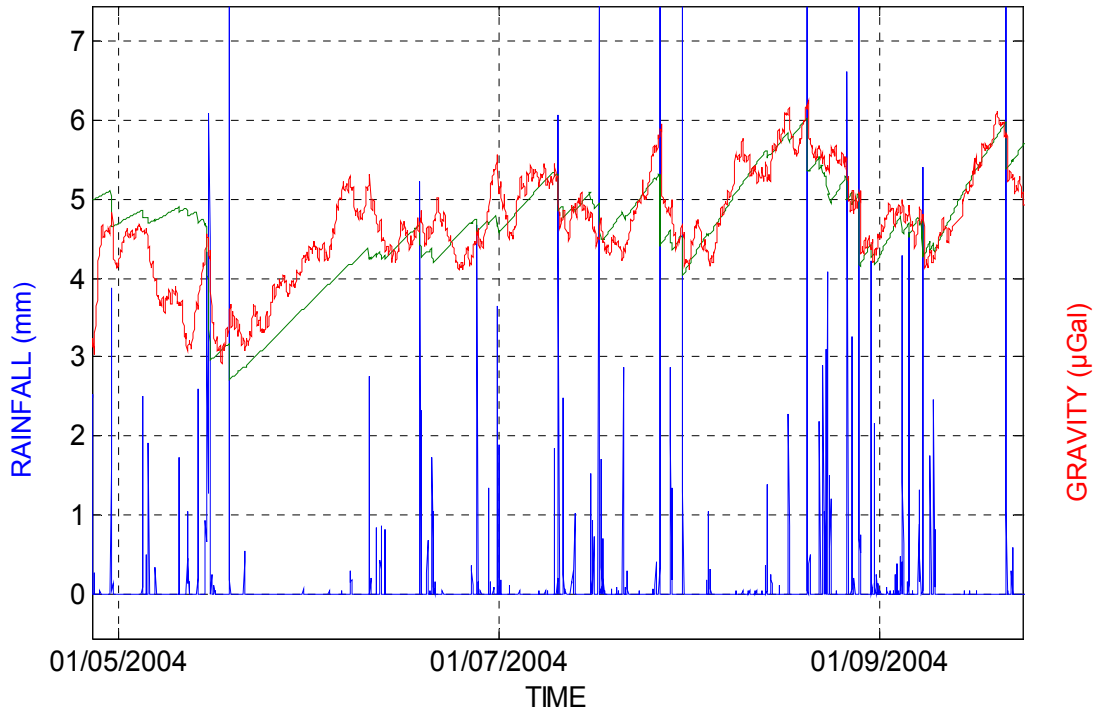

Fig. 3.20: *rainfall (blue, mm/hour), observed gravity (red, μGal), modeled gravity (green, μGal) for the period May to September 2004. The same scale is adopted for gravity and rainfall.*

Focusing on the period where we have high intensity precipitation events, we observe that the duration of the recharge phase (corresponding to the gravity decrease phase because the gravimeter is located beneath the mass increase) appears significantly shorter than the duration of the discharge phase (gravity recovery phase). Therefore, we conclude that the simplification assumed in the Tank Model (an instantaneous recharge phase) can reasonably be accepted at the location of Walferdange.

But the model does not take into account the gravity variations due to short time effects like air pressure changes and air mass redistribution related to meteorological events. [*Gerstenecker, 1978*] Consequently, during the gravity decrease (recharge) phase, it can sometimes be difficult to distinguish the component of the gravity variation due to the Newtonian attraction of the precipitation from gravity variations due to the other short-term mass effects.

In the gravity recovery phase (discharge phase), characterized by a significantly longer duration, it is easier to separate the gravity variation due to the groundwater storage decrease from the gravity variation due to other short-term mass effects.

In Figure 3.21 we display the precipitation series (blue, µGal), the modeled gravity series (green, µGal) and the observed gravity series (red, µGal) for the entire period January 2003 to January 2010.

The Figures 3.22 to 3.28 represent a zoom in on Figure 3.21. The annual precipitation series, modeled gravity series and observed gravity series are displayed from the year 2003 to the year 2009.

In Figure 3.23, the initial short term instrumental drift can be easily identified.

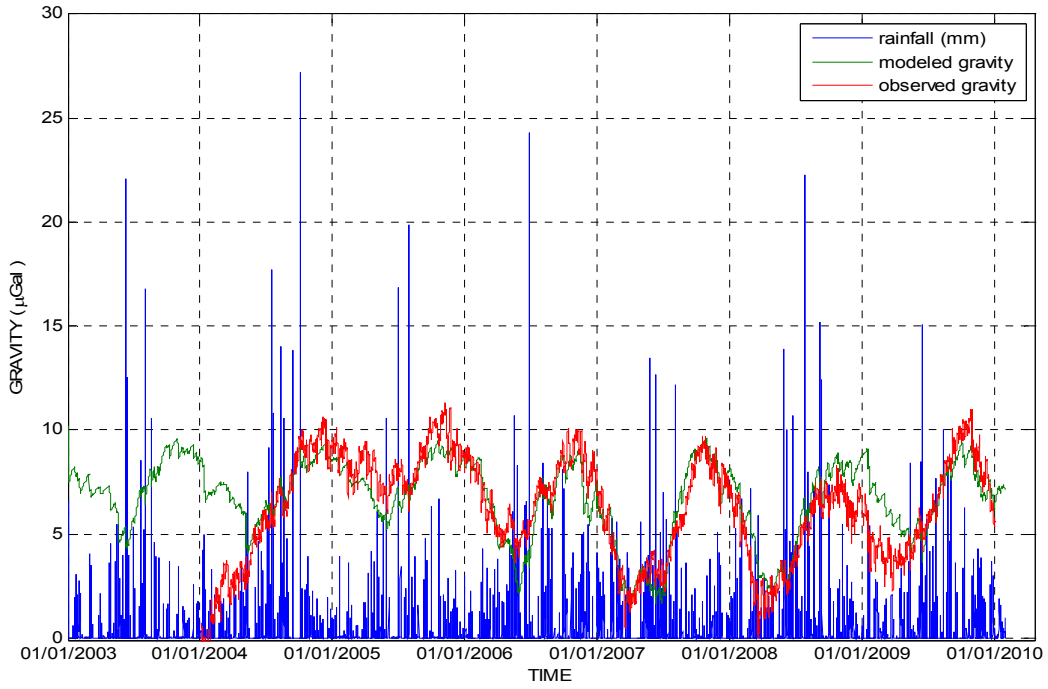

Fig. 3.21 *: Rainfall (mm), observed gravity (red, µGal), modeled gravity (green, µGal) for the period January 2003 to January 2010.*

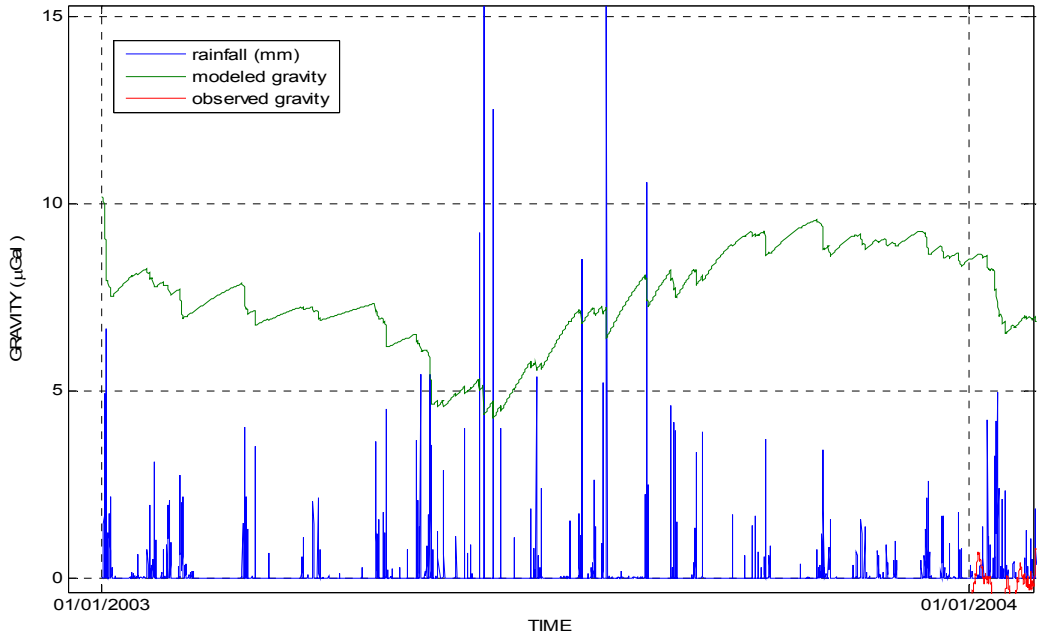

***Fig. 3.22**: Rainfall (mm), observed gravity (red, µGal), modeled gravity (green, µGal) for the year 2003.*

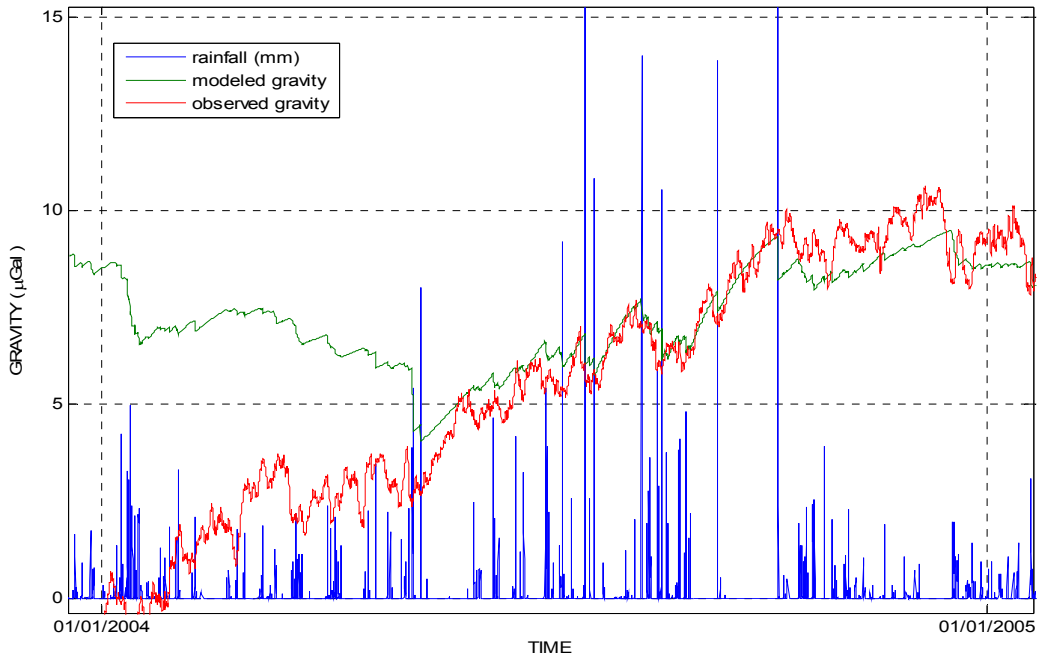

***Fig. 3.23**: Rainfall (mm), observed gravity (red, µGal), modeled gravity (green, µGal) for the year 2004.*

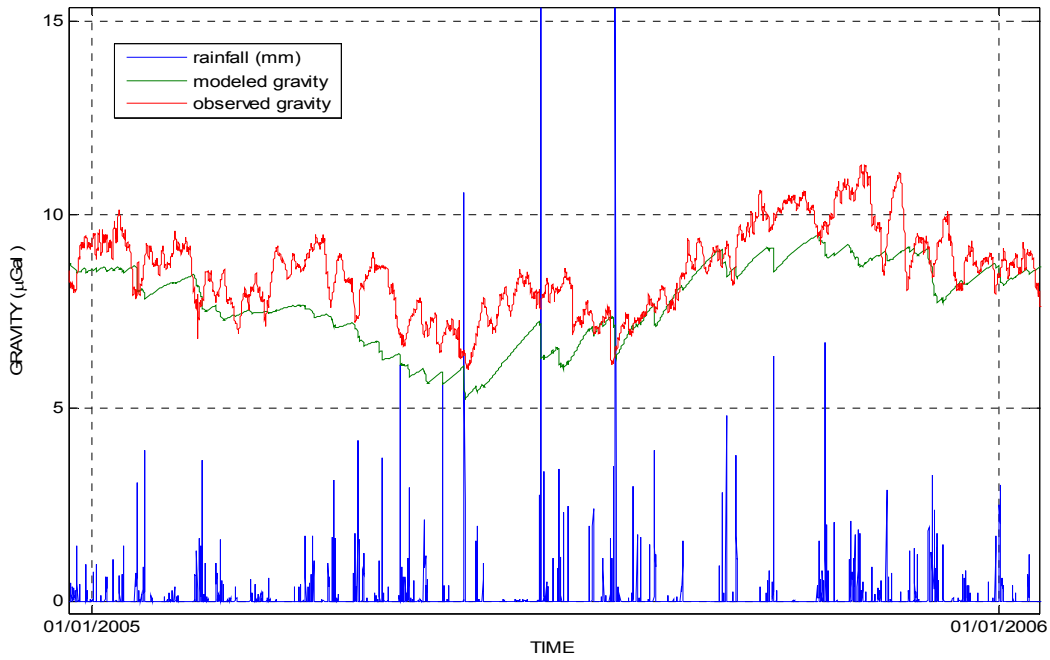

***Fig. 3.24**: Rainfall (mm), observed gravity (red, µGal), modeled gravity (green, µGal) for the year 2005.*

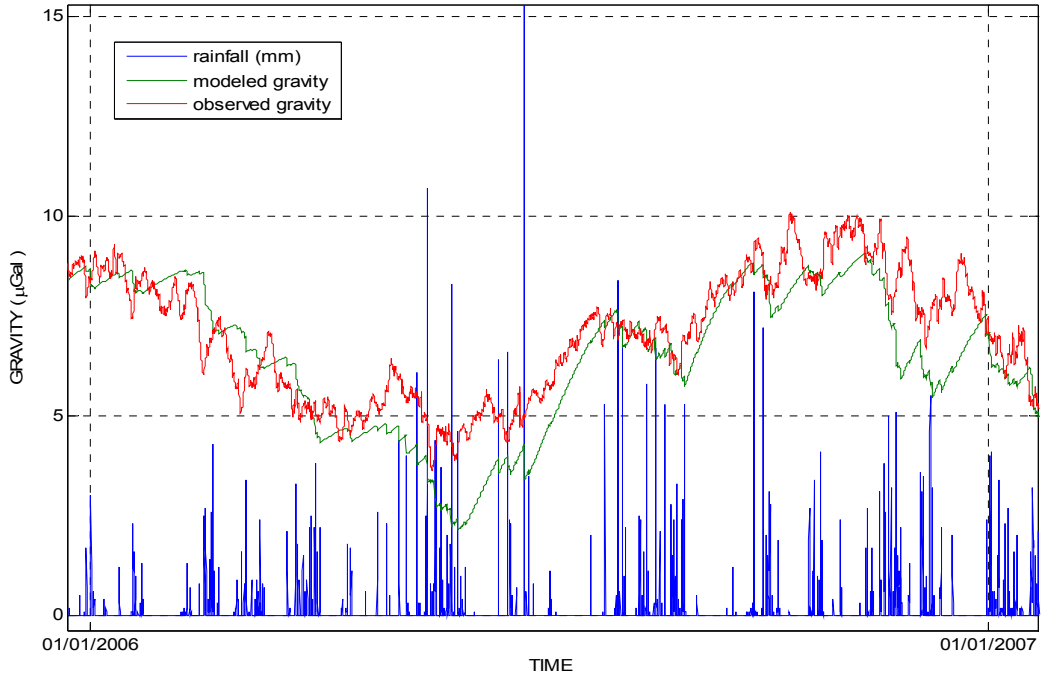

***Fig. 3.25** : Rainfall (mm), observed gravity (red, µGal), modeled gravity (green, µGal) for the year 2006.*

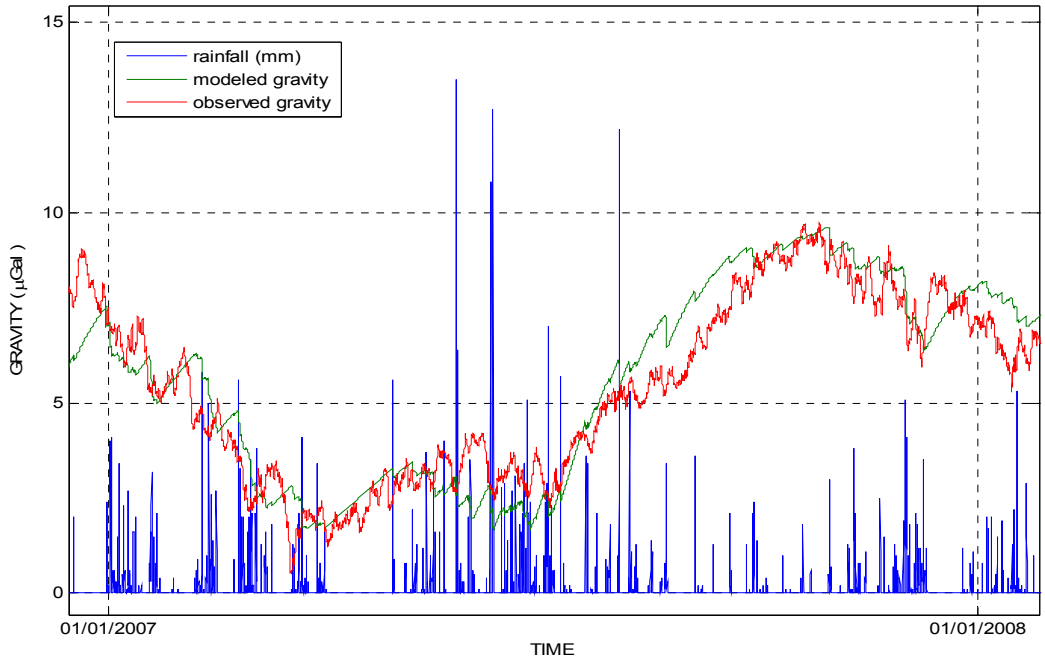

***Fig. 3.26**: Rainfall (mm), observed gravity (red, µGal), modeled gravity (green, µGal) for the year 2007.*

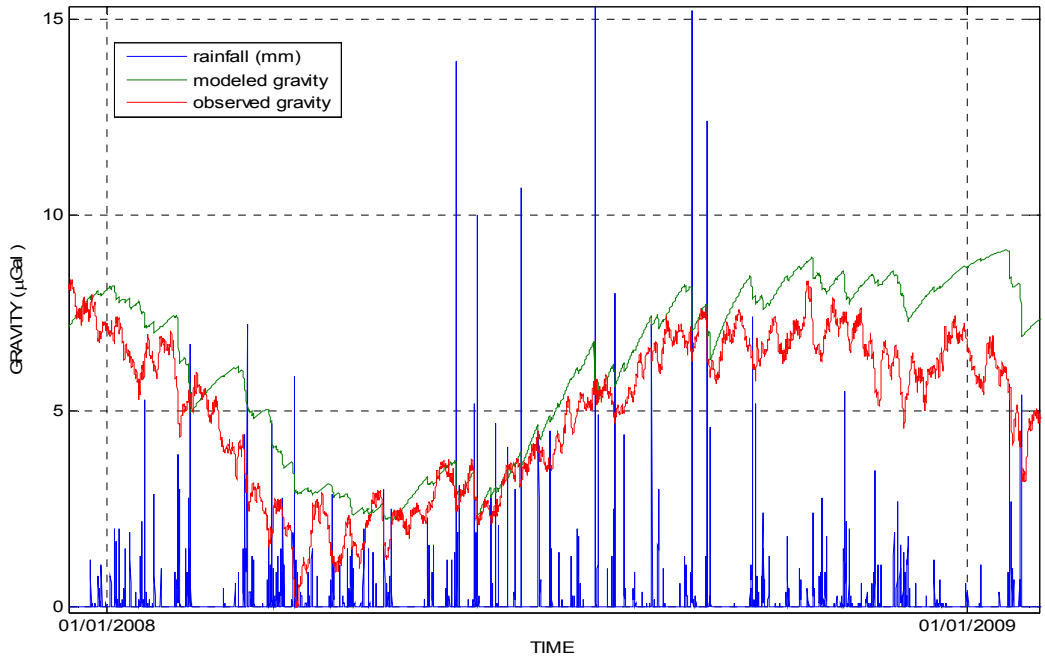

***Fig. 3.27** : Rainfall (mm), observed gravity (red, µGal), modeled gravity (green, µGal) for the year 2008.*

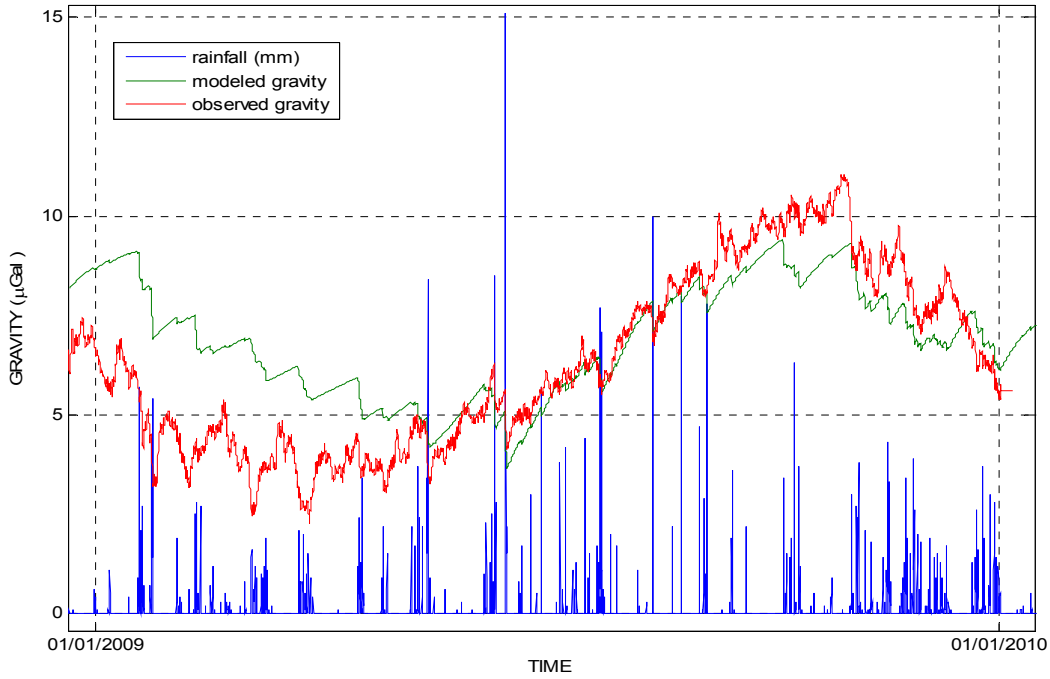

***Fig. 3.28**: Rainfall (mm), observed gravity (red, µGal), modeled gravity (green, µGal) for the year 2009.*

In Table 3.3, we display the RMS of the uncorrected gravity time series, the RMS of the gravity residuals (difference between observed and modeled gravity series), and the percentage of scatter reduction for the years 2004 to 2009. In 2009 the scatter reduction is only of 53%, compared to the values of 90% and 81% in 2007 and 2008, respectively A possible cause is the gravity perturbation due to the excavation of the Stafelter Tunnel, which started in March 2009. This effect is estimated in Section 3.9.

In 2004 the percentage of scatter reduction is only of 14%, because of the initial significant instrumental drift.

	2004	2005	2006	2007	2008	2009
RMS of observed gravity (µGal)	3.46	1.1	1.57	2.37	1.98	2.23
RMS of gravity residuals (µGal)	3.2	0.65	0.79	0.74	0.86	1.53
Scatter reduction (%)	14	65	75	90	81	53

***Table 3.3**: RMS of the uncorrected gravity time series, RMS of the gravity residuals (difference between observed and modeled gravity series) and percentage of scatter reduction, for the years 2004 to 2009. The RMS values are expressed in µGal.*

3.8 Comparison between the Tank Model and the Double Exponential Model

The Double Exponential Model allows us to describe both the recharge and discharge phase with exponential functions. The time parameter τ' characterizes the duration of the recharge phase, the time parameter τ" characterizes the duration of the discharge phase.

Similar to the case of the Tank Model, the Double Exponential Model is empirically parameterized. As for the Tank Model, the value of the admittance, α=36 μGal m^{-1} derived in Section 2, has been used. The other parameters are determined from the data in order to minimize the residuals. The values of τ'=1 hour, τ"=720 hours c"=0.6, φ= 2π/5, and γ_o=0.0011 $hours^{-1}$ provide the best results. In Figure 3.29, we display the Exponential Model output for the period 1-January, 2003 to 1-January, 2010.

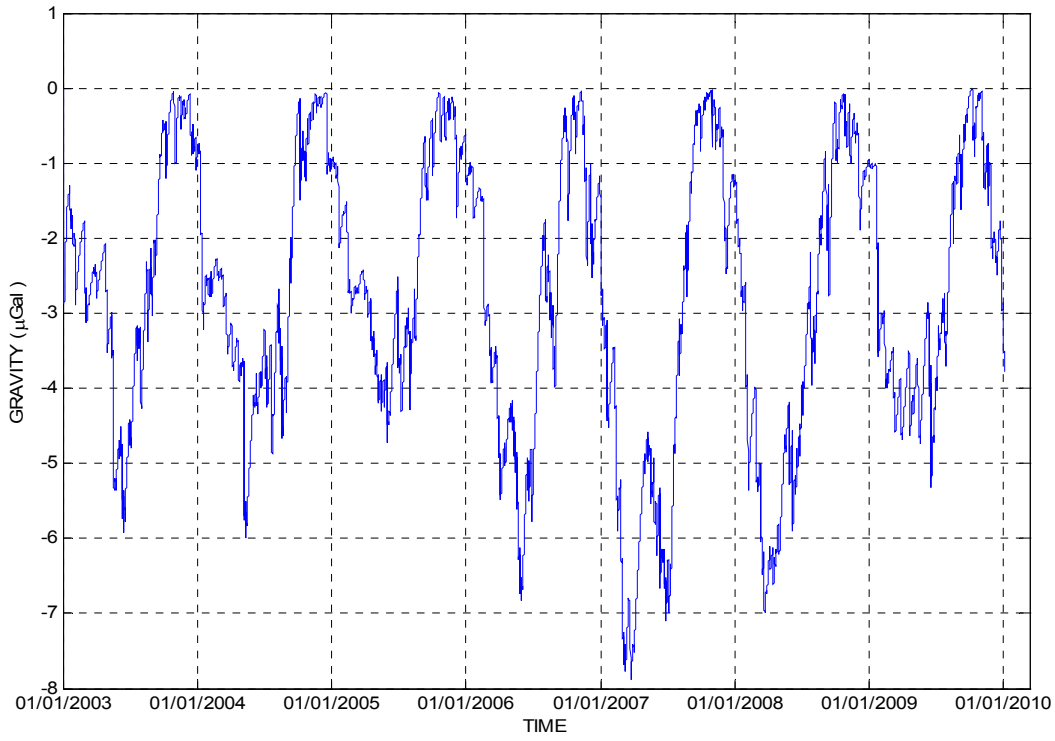

Fig. 3.29: *Exponential Model output (modeled gravity) for the period January, 2003 to January, 2010.*

The modeled hourly time series of the gravity (μGal) is compared with the observed hourly time series obtained from the SG for the period 19-December, 2003 to 1-January, 2010. The observed time series (green), the modeled (blue) time series for the specified period are displayed in Figure 3.30 A. The final residuals are displayed in Figure 3.30 B.

As for the Tank Model, the first months of operation are excluded from the calculation of the RMS values, because of the significant instrumental drift. The RMS values are evaluated on the period May, 2004 to January, 2010. The following results are obtained:

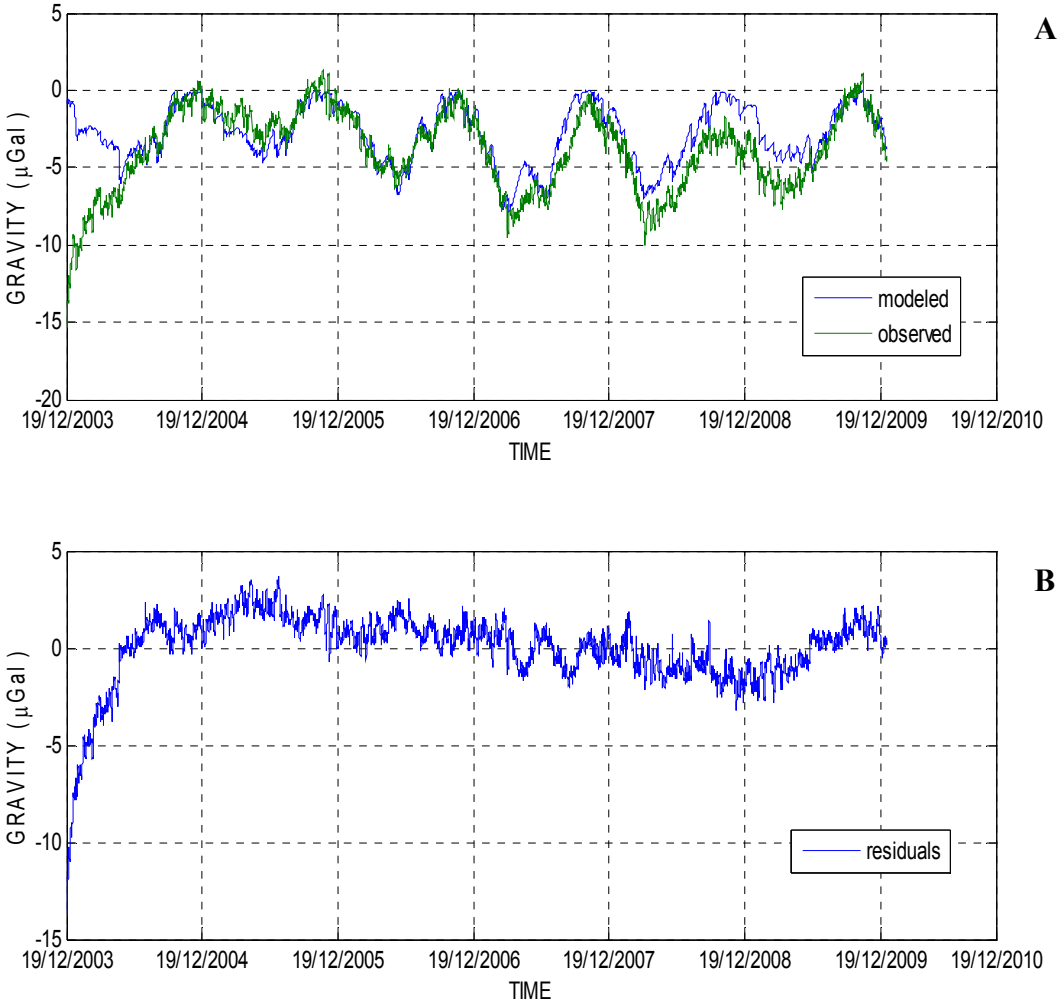

Fig. 3.30*: Comparison between observed and modeled gravity (Exponential Model) time series:*

A. Observed gravity (green, µGal), modeled gravity (blue, µGal) at Walferdange. The comparison period is 30 May 2004 to 1st January 2010.

B. Gravity residuals (µGal), representing the difference between the observed and modeled time series.

The Root Mean Square (RMS_o) of the observed gravity time series is:

RMS_o=2.3 µGal

The Root Mean Square (RMS_r) of the gravity final residuals time series is:

RMS_r=1.19 µGal

corresponding to a 73% signal scatter reduction.

These values correspond perfectly to the values obtained with the Tank Model. In Figure 3.31 are displayed the Tank Model output and the Exponential Model output for the period January 2003 to January 2010.

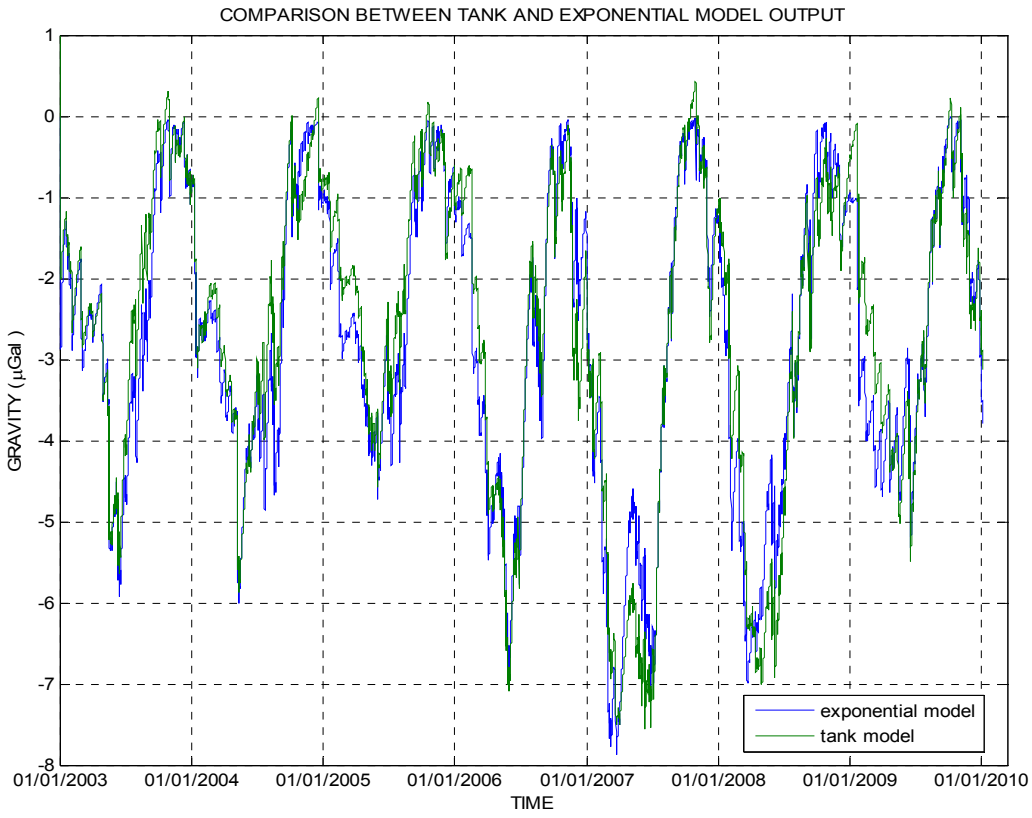

Fig. 3.31*: Tank Model output (green, µGal) and the Exponential Model output for the period 1-January, 2003 to 1-January, 2010.*

The model outputs, representing the hydrological gravity changes, appear significantly similar for the two models. The output similarity persists until $\tau' << \tau$".

The influence of the recharge time parameter τ' can be analyzed by implementing the Double Exponential Model with increasing values of τ'. In Figure 3.32, we display the outputs obtained by implementing the model with the values τ'=4 hours (blue, µGal), τ'=120 hours (green, µGal), τ'=240 hours (red, µGal) for the period January, 2003 to April, 2008. As previously demonstrated in Section 2.15 with a single test input, implementing the model with increasing values of τ' results in a 'smoothing' of the output curve. The greater the value of τ', the smaller the maximal gravity variation following the precipitation event becomes.

The analysis of the observed gravity time series in Walferdange seems to indicate that the duration of the gravity decrease phase (recharge phase) is actually observably shorter than the duration of the gravity recovery phase (discharge phase). Modeling also the

recharge phase, as in the Exponential Model, provides no significant improvement in the model outputs.

Consequently, the Tank Model, which requires significantly less computation time with respect to the Double Exponential Model, appears to be adequate for describing the hydrological effects on gravity in Walferdange.

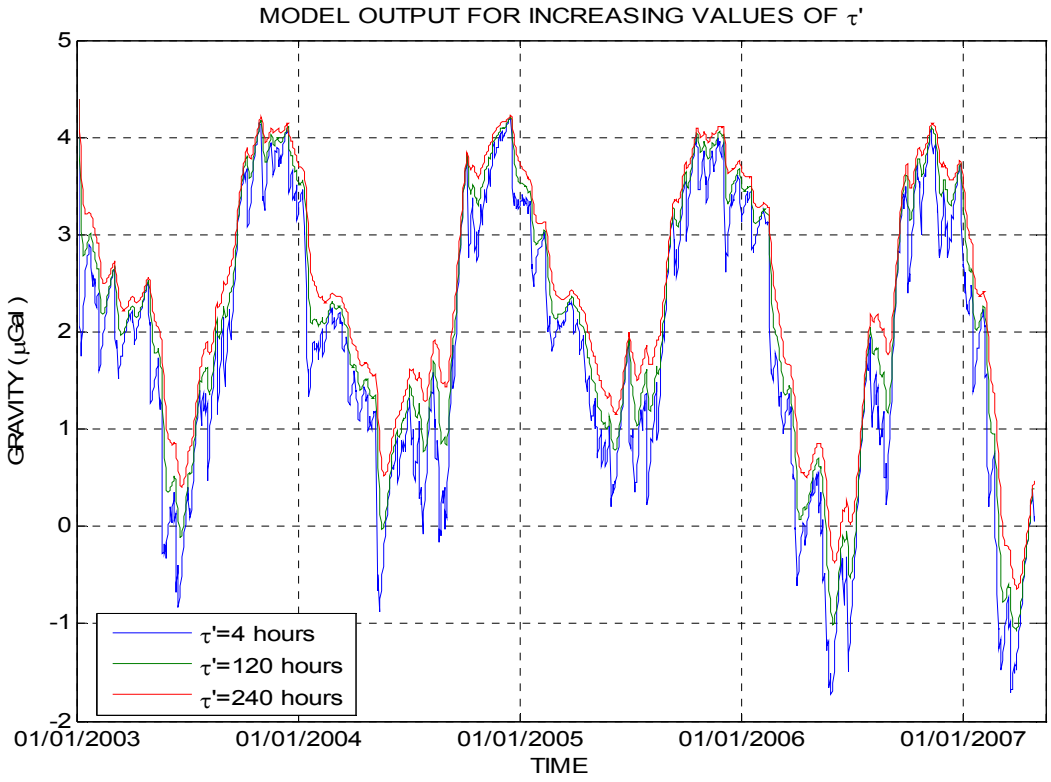

Fig. 3.32*: Double Exponential Model output with increasing values of τ'. The outputs with τ'=4 hours are displayed in blue, the outputs with τ'=120 hours are displayed in green, the outputs with τ'=240 hours are displayed in red. The gravity is expressed in μGal. Implementing the model with increasing values of τ' results in a 'smoothing' of the output curve.*

The validity of these conclusions is limited to the specific location of Walferdange. As previously discussed, the gravity variations driven by hydrological variations are site specific. Thus, it seems reasonable that applying the Double Exponential Model in different locations to describe the recharge phase may offer a better description of the local hydrological gravity variations.

3. 9 Estimation of the gravity signal produced by the works of excavation of the Stafelter Tunnel.

In the period between February and March of 2009, the hydrological gravity residuals show a distinctive upward trend. This positive trend appears after several years of a negative trend in the gravity residuals.

In the same period, February-March 2009, excavation of the Stafelter Tunnel were undertaken. The Stafelter Tunnel was forseen as part of the construction required to realize the 'Route du Nord', a major road connecting the southern and the northern part of the Grand Duchy of Luxembourg.

The tunnel extends from the rue de Echternach at the Southern extremity to "Maegrondt" at the northern extremity, which is situated on the plateau of Heeschdrëferbierg. Most of the tunnel, which strikes in an almost straight, lies under the forests of the Grëngewald. The tunnel lies in an almost horizontal plane at a vertical distance of about 100 m above the gravimeter.

The tunnel is composed of two galleries, each having a horseshoe profile, and a cross-section of 58.45 m^2. The excavation cross-section is approximately 75 m^2 for each gallery. The total length of the tunnel is of 1850 m.

The coincidence in time between the commencement and progress of the excavation and the drift of the gravity residuals may indicate that the mass distribution changes related to the excavation could have an effect on the gravity signal at the SG location. Therefore, we estimated the gravity effect due to the mass removal at the location of the SG.

The excavation started at the same time at both the extremities of the tunnel. The actual excavation of both of the galleries is still in progress at the southern extremity. At the end of 2009, 977 m of the north-south gallery and 1181 m of the south-north gallery have been excavated (Figures 3.33 and 3.34). At the northern extremity, which is the end closest to the gravimeter, a trench of 250 m length and approximately 500 m^2 in cross-section has been excavated. Almost all the extracted material is composed of Luxembourg sandstone, having a density of about 3 kg/m^3.

In order to estimate the gravity effect, the galleries and the trench have been mathematically represented as one-dimension rods. We have chosen a local Cartesian coordinate system centered on the gravimeter location, with the x-axis perpendicular to the tunnel direction, the y-axis parallel to tunnel direction and the z-axis corresponding to the local vertical (Figure 3.35).

The gravity effect has been computed using a numerical model. The galleries and the trench have been subdivided into 1 m length linear elements. The effect of each element is expressed by:

$$(\Delta g_e)_i = G \cdot \frac{\lambda \cdot z}{(x^2 + y_i^{\,2} + z^2)^{3/2}} \cdot \Delta y$$

where $\Delta(g_e)_i$ represents the gravity effect of the element i, G is the Newtonian constant of attraction, λ is the linear density (kg/m). In the chosen frame, x and z are constants and only y varies. We set $x=x_0$ and $z=z_0$. The value of Δy is 1 m.

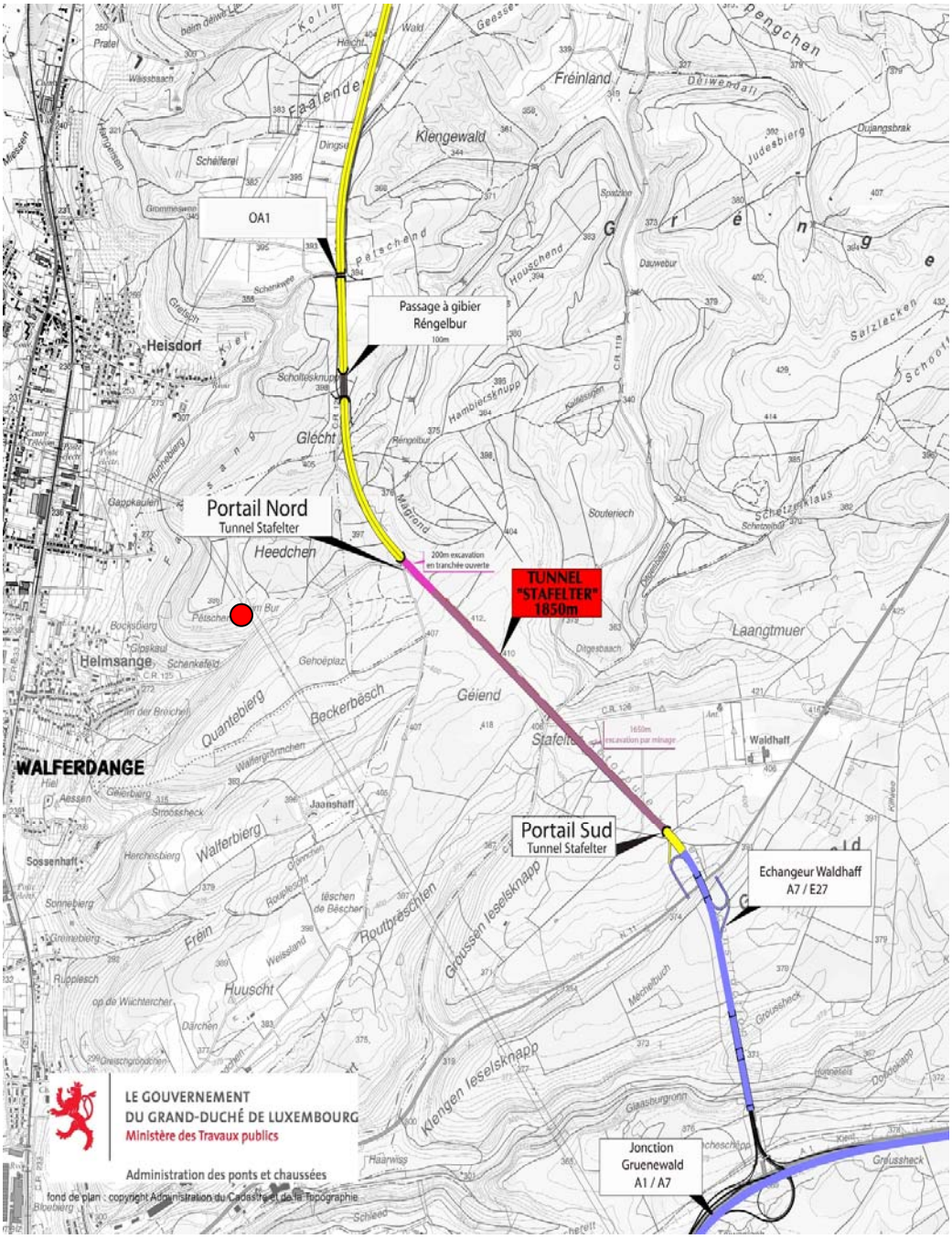

Fig. 3.33*: Position of the gravimeter OSGCT040 with respect to the Stafelter Tunnel. The red dot represents the position of the gravimeter, the pink segment represents the trench excavated at the tunnel's northern extreme (map provided courtesy of the "Administration des ponts et chaussées", Luxembourg, (www.pch.public.lu/projets/index.html)*

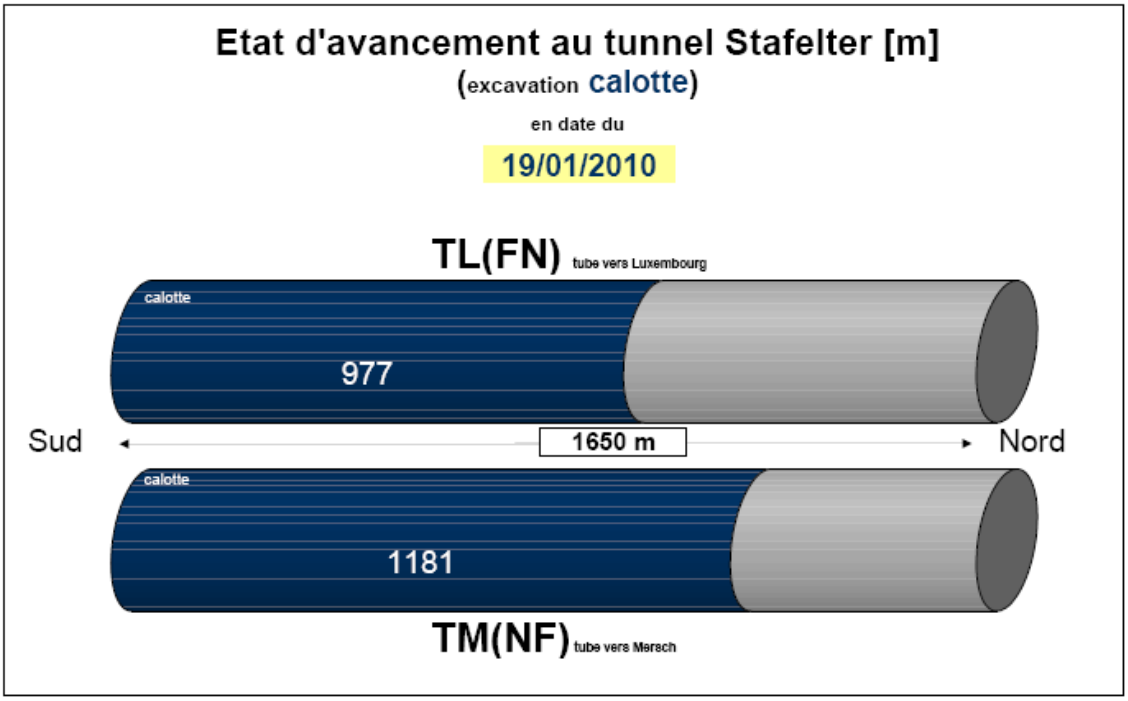

Fig. 3.34: *State of the excavation of the two galleries, which make up the Stafelter Tunnel. The excavation of both the galleries has started from the southern extremity (image provided courtesy of the "Administration des ponts et chaussées", Luxembourg, www.pch.public.lu/projets/index.html).*

Consequently, the gravity effect of a segment whose endpoints have the coordinates (x_0,y_m,z_0) and (x_0,y_n,z_0) is expressed by:

$$\Delta g_e = \sum_{y=m}^{n} G \cdot \frac{\lambda \cdot z_0}{(x_0^{\,2} + y^2 + z_0^{\,2})^{3/2}} \cdot \Delta y \qquad (3.33)$$

The numerical integration is made on varying values of y. x_0 represents the horizontal distance between the gravimeter and the tunnel direction. z_0 represents the vertical distance between the plan containing the tunnel and the gravimeter. We estimate the values of x_0=790 m and z_0=100 m. Thus Equation 3.33 becomes:

$$\Delta g_e = \sum_{y=m}^{n} G \cdot \frac{\lambda \cdot 100}{(100^2 + y^2 + 790^2)^{3/2}} \cdot \Delta y \qquad (3.34)$$

where Δg_e represents the total gravity effect of the segment. Estimating a cross-section of the northern trench of 500 m^2 and a medium density of 3 kg/dm^2, we calculate a linear density of $\lambda_1 = 1.5 \cdot 10^6$ kg/m. Similarly, using the cross-section for each gallery excavation of about 75 m^2, we estimate a linear density of $\lambda_2 = 2.4 \cdot 10^5$ for each gallery. Thus, the total effect is the sum of the effect of the three segments, which correspond to the trench, the north-south gallery and the south-north gallery, respectively. For the trench, y varies between 350 and 400 m. For the south-north gallery, y varies between 1019 and 2200 m.

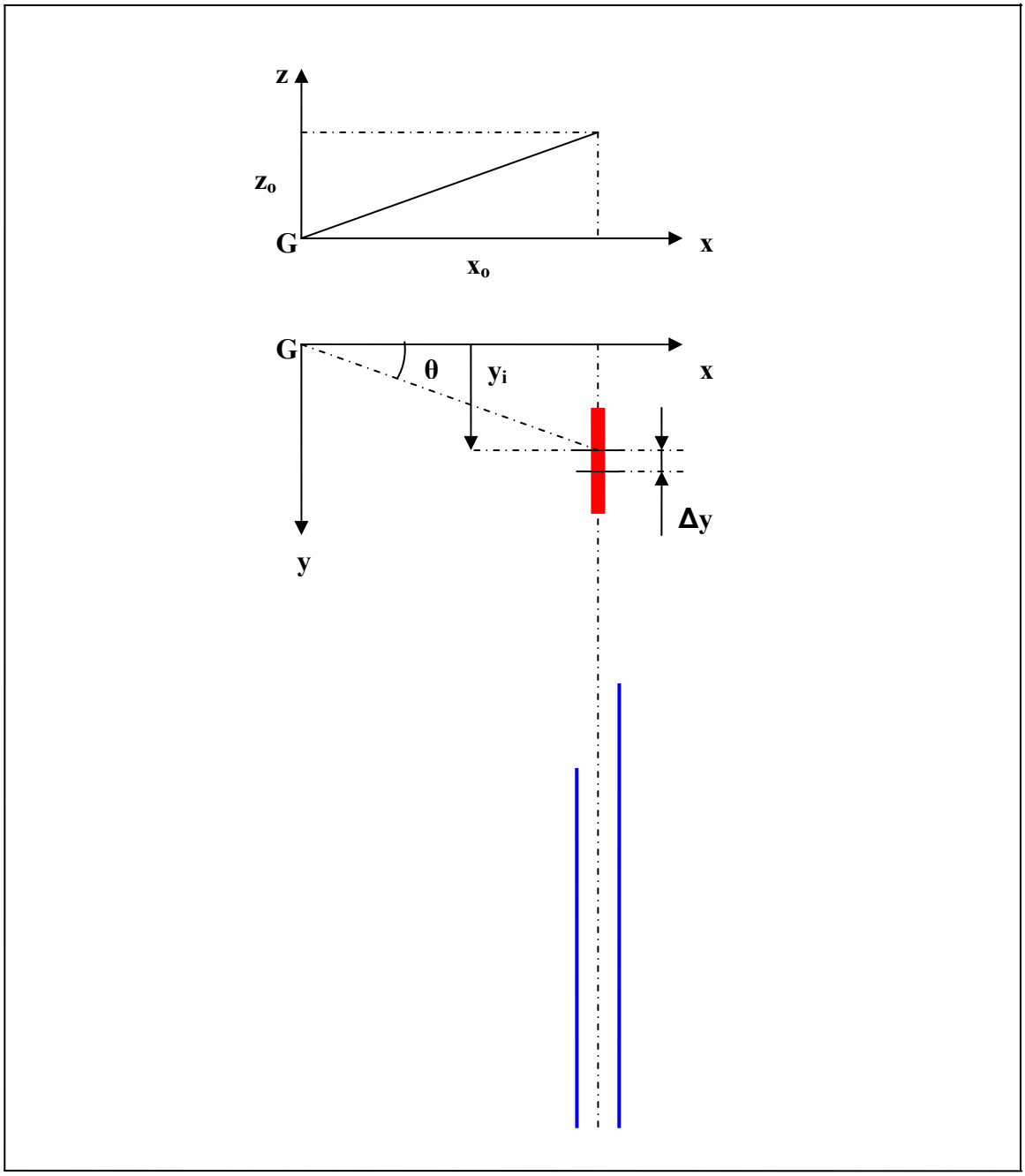

Fig. 3.35*: Graphical scheme for the calculation of the gravity effect of the excavation. A local Cartesian reference system is chosen with the x-axis perpendicular to the tunnel direction, the y-axis parallel to the tunnel direction and the z-axis. The frame is centered on the gravimeter location, indicated by G. The red segment represents the northern trench. The blue segments represent the part of the galleries excavated from the southern extremity on December, 2009.*

Finally, for the north-south gallery, y varies between 1223 and 2200 m. The values for x and z are 790 m and 100 m, respectively. We obtain the following results:

- Gravity effect of the trench $\Delta g_e = \sum_{y=350}^{600} G \cdot \frac{\lambda_1 \cdot 100}{(100^2 + y^2 + 790^2)^{3/2}} \cdot \Delta y$ =0.34 μGal

- Gravity effect of the north-south gallery

$$\Delta g_e = \sum_{y=1019}^{2200} G \cdot \frac{\lambda_2 \cdot 100}{(100^2 + y^2 + 790^2)^{3/2}} \cdot \Delta y \text{ =0.041 μGal}$$

- Gravity effect of the south-north gallery

$$\Delta g_e = \sum_{y=1223}^{2200} G \cdot \frac{\lambda_2 \cdot 100}{(100^2 + y^2 + 790^2)^{3/2}} \cdot \Delta y \text{ =0.023 μGal}$$

Consequently, the total effect of the excavation, on December 2009, on the SG is about 0.4 μGal. This result must be interpreted with some caution, as some of the parameters could have been underestimated or overestimated. The total effect of the galleries when the excavation will be complete is given by:

$$\Delta g_e = 2 \cdot \sum_{y=600}^{2200} G \cdot \frac{\lambda_2 \cdot 100}{(100^2 + y^2 + 790^2)^{3/2}} \cdot \Delta y \text{ =0.184 μGal}$$

Thus, we estimate the total effect of the excavation at completion of about 0.53 μGal. The values appear to only a partially explain the observed upward trend in the gravity residuals. However, as previously discussed, we may have underestimated the actual effect.

If, at the conclusion of the excavation, the gravity residuals should resume their previous downward trend, we may have an indication that the excavation is at least one of the causes of the observed upward trend at the beginning of 2009.

3.10 Conclusion

Before presenting the model output, we have discussed the methods of acquisition of the precipitation time series and of the gravity time series.

For the precipitation time series, two different sources were available: the Meteorological Station of Walferdange (MSF) pluviometer, providing the rainfall heights with 1 min. temporal resolution from January 2003, and the WULG pluviometer, providing the rainfall heights with 1 min. temporal resolution from December 2005.

We have shown that the two instruments provide qualitatively similar results, but that a quantitative difference is observed as well. The cumulative precipitation provided by the WULG pluviometer is about 10% greater than that provided by the MSF pluviometer.

For the period January, 2003 December, 2005 the MSF series has been used as input to the different models. From December, 2005, because of the direct availability of the data, the WULG time series has been adopted. The difference between the series has been used to assess the uncertainties in the input data.

The observed gravity time series were provided by the Superconducting Gravimeter OSGCT040 (SG) located in the WULG. In order to qualify the SG, we have determined two important instrumental characteristics: the instrument transfer function and the instrumental drift.

The SG transfer function was determined by injecting in the instrument control electronics both sine waves and step functions, and observing the system response. The poles and zeros coordinates of the transfer function were determined, providing a complete description of the instrument response.

We have compared the OSGCT040 frequency response to the response of the Superconducting Gravimeter GWR-C021 operating in Membach (Belgium), demonstrating that the frequency response can assume different shapes for different instruments. The frequency response is consequently a characteristic of each Superconducting Gravimeter.

The SG instrumental drift has been determined by comparing the SG time series to the absolute gravity measurements provided by the free-fall absolute gravimeter FG5 located in the WULG, located at a few meters distant from the SG. A long-term linear drift of 1.27 μGal/year has been estimated.

In the absence of accurate information about the local hydro-geological parameters, both the Tank Model and the Exponential Model have been empirically parameterized recurring to a least square adjustment. The comparison between the observed hydrological gravity residuals and the modeled hydrological gravity residuals has been carried out for the period May, 2004 to January, 2010. The initial period after the start-up of the SG (December 2003) have been excluded from the comparison because of the severe initial short-term instrumental drift.

Subtracting the modeled gravity time series from the observed time series, both models provide a reduction of the signal scatter of about 72%. The Exponential Model provides the best results with the values of the recharge and discharge time parameters τ' and τ'' of 2 hours and 720 hours, respectively. Thus, the recharge time parameter is significantly smaller than the discharge time parameter. In this case, the Tank Model and the Exponential Model give similar results.

We could conclude that the Tank Model, which describes solely the recovery phase, gives a reliable description of the local hydrological effects on gravity.

Finally, we have estimated the gravity effect due to the excavation of the Stafelter Tunnel, in the vicinity of SG. The final hydrological gravity residuals show, for the period February-March 2009, an upward trend, which follows a downward trend that has lasted four years. We postulate that this reversal in the trend may be due to the mass removal related to the excavation.

With a simple numerical model, we estimated that at the end of 2009, the effect of the excavation on the gravimeter observations was only between 0.4 and 0.5 μGal. When the excavation is completed, the gravity effect may reach 0.7 μGal. Monitoring the trend of the gravity residuals during the months following the excavation may provide additional information on this issue.

Chapter 4

Chapter 4: Correlation between gravity changes and variations of the Alzette River water level in Walferdange, Luxembourg

4.1 Introduction

This chapter, even if strictly related to the research previously discussed, must be considered as methodologically independent.

Using a purely statistical approach, we will investigate the correlations between gravity changes observed by the SG and the water level changes of the Alzette River, which correspond to a set of sampled shower events. The Alzette River level data (limnimetry) are provided by Walferdange Meteorological Station (WMS).

Because of the distance between the SG and the Alzette River, the direct effect of the water level changes on the gravity changes can be excluded. The motivation behind this investigation is that we would like to test whether the observed gravity changes are better correlated with the Alzette River level changes as compared to only the precipitation measurements. This is because both gravity changes and water level changes depend on the soil hydro-geological parameters (degree of saturation, hydraulic conductivity), whereas precipitation does not.

The investigation will be subdivided in two main parts. First, we will estimate the time delay between gravity variations and water level variations on the one hand, and between gravity variations and precipitation events on the other hand. To this purpose, we will refer to the time derivatives of the water level and gravity series. This will allow us to better identify the gravity variations driven by hydrological causes.

Secondly, we will calculate the correlations 1) between gravity changes and Alzette River level changes and 2) between Alzette River level changes and precipitation amounts.

The investigation will be carried out on a set of precipitation events sampled between 2004 and 2007

We will show that, for both parts of the investigation, the SG provides no additional information with respect to the pluviometer in enabling us to predict the Alzette River level variations.

Finally, we will determine values for the admittances between the gravity changes and Alzette River level changes and between precipitation heights and water level changes.

4.2 Relation between precipitation, Alzette water level changes and gravity variations in Walferdange

A drainage basin is defined as a land surface where all the various flows generated by precipitation are drained to the same outlet (river, lake, or sea). Generally, the basin is delimited by the heights crests (Figure 4.1).

The precipitation volume that is not retained by vegetation or subject to direct evapo-transpiration flows into the basin outlet. This flow can be subdivided into four main components, according to the course of the outlet:

- The direct precipitation, representing the volume falling directly on the water surface.
- The overland flow, representing the surface runoff.
- The subsurface flow, representing the volume subject to rapid flow in the superficial soil layers.
- The groundwater flow, representing the volume subject to slower flow in the deep soil layers.

The basin hydrological response is described by the time evolution of the flow rate (m^3/s), or the water level (cm), at the basin outlet, after precipitation events. It is graphically represented by hydrogramms. The response time parameter, t_r, represents the delay between the center of gravity of the precipitation event and the maximum value of the flow rate (or water level). This parameter characterizes the time scale of the basin response to precipitation events.

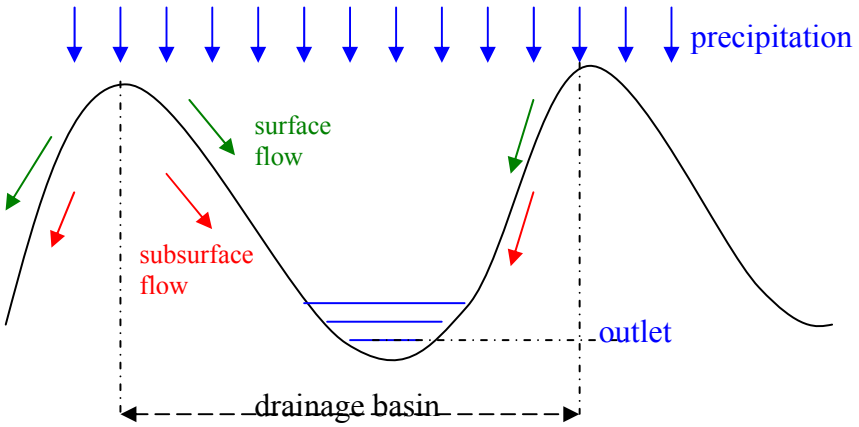

***Fig 4.1**: Scheme of a drainage basin. The various flows generated by a precipitation event are drained to the same outlet.*

The hydrological response can be significantly different for different catchments. The determining factors can be subdivided in two categories: the external factors and the internal factors. The external factors include:

- The general climatic conditions (average temperature, pressure, humidity, etc.).
- The precipitation characteristics (duration, intensity, space and time distribution).

The internal factors include:

- The catchment structure (topography, form, slopes, etc.).
- The physical properties (soil composition, vegetation coverage). These properties are quantified through parameters like porosity, permeability and hydraulic conductivity.
- The soil antecedent humidity degree, quantified by the Antecedent Precipitation Index (API) parameter.

These factors determine the relative portion of water going into the flow components, and consequently the catchment hydrological response. For instance, for catchments characterized by high slopes and low porosity soils, overland and subsurface flows dominate and the hydrological response time is rapid (low values of t_r). Conversely, for catchments characterized by low slopes and high porosity soils, groundwater flow

dominates and the hydrological response slower (high values of t_r). A qualitative example is displayed in Figure 4.2.

The Alzette hydrological basin covers an 1172 km^2 area in the south-eastern part of the Grand Duchy of Luxembourg (see Chapter 3). The basin soils are heterogeneous, with different hydrological characteristics. A hydro-geological map of Luxembourg is displayed in Figure 4.3. In the area of Walferdange, two principal classes of soils are present:

- Clay or clay loam soils, characterized by low permeability and porosity. These soils are subject to hydric excess in the winter.
- Silt or sand-silt soils (derived from Luxembourg sandstone), characterized by high porosity and permeability. These soils are subject to hydric deficit in the summer.

In the Alzette valley, recent alluvium soils are also present. These are low structured and have very heterogeneous hydrological characteristics.

Concerning the external factors, the Alzette basin's hydrological response is controlled by strong seasonal variability: A precipitation contribution dominates in the winter, while evapo-transpiration effects play the major role in summer.

Thus, the Alzette water level changes (hydrological response) depend both on the external factors (precipitation, climatic conditions) and on the internal factors (basin structure, soil composition).

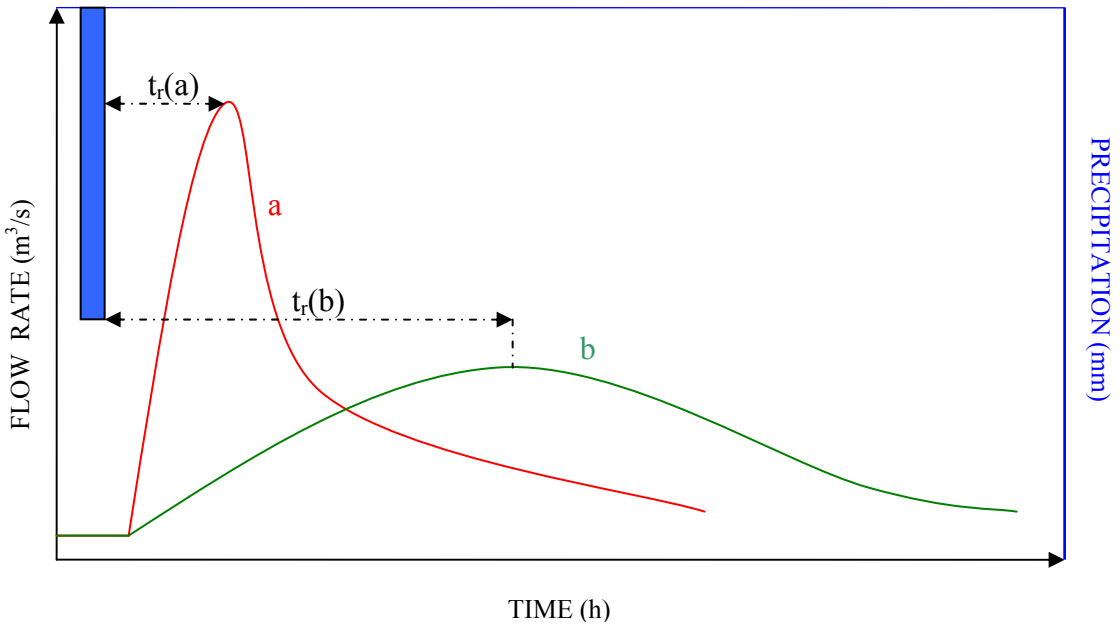

***Fig 4.2**: Qualitative examples of catchment hydrological responses (hydrogramms) to a precipitation event: The response time $t_r(a)$ (predominance of overland flow) is more rapid than the response time $t_r(b)$ (predominance of groundwater flow).*

The Alzette River flows at a minimum horizontal distance of 1700 m from the WULG gravimeter. This implies that the direct effect (the mass change) of the Azette River level changes on the gravity signal observed by the SG located in the WULG can be excluded (see Chapter 2).

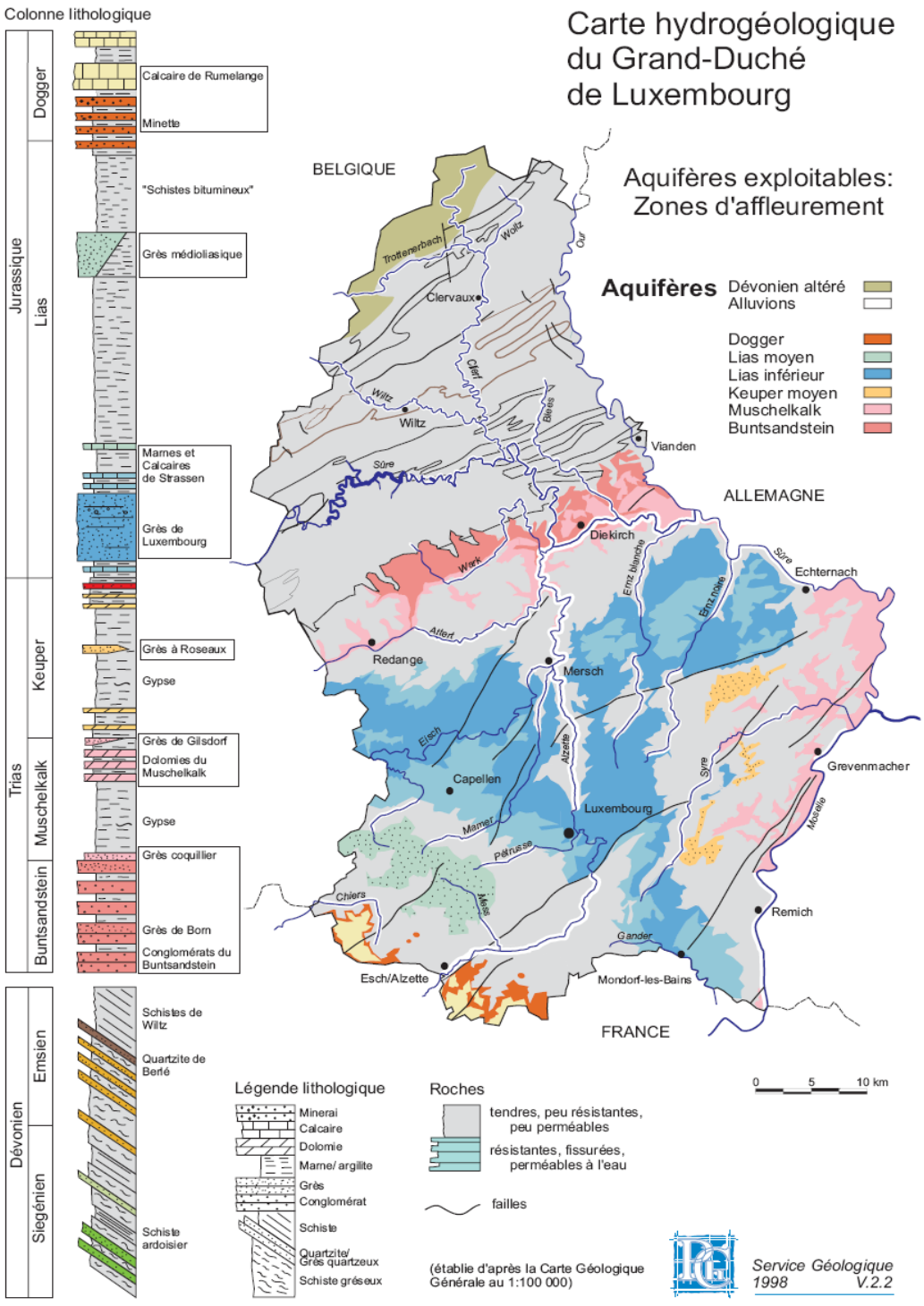

Fig 4.3: *Hydro geological map of the Grand Duchy of Luxembourg. (provided courtesy of the "Administration des ponts et chaussées", Luxembourg,* www.pch.public.lu/publications *).*

Nevertheless, the hydrological gravity signal, like the hydrological response, i.e. the Alzette River level changes, depends both on the external and on the internal factors. The duration of the hydrological recharge and discharge processes, which determine the gravity changes (see Chapter 2), depend on parameters like soil porosity, permeability and hydraulic conductivity.

This may indicate that we could expect a better correlation between the gravity changes and the water level changes, than between the precipitation levels and the river level changes.

In order to verify this hypothesis, we carry out a statistical investigation, divided into two parts:

- A preliminary statistical investigation of the time delays between the gravity changes, the Alzette River level changes and the precipitation events. The idea is that, particularly in the case of high intensity precipitation, the gravity signal change may precede the precipitation signal. If this were true, it may improve our ability to predict extreme events such as flooding.
- A comparative analysis of the correlation between 1) the integrated water content of the precipitation events and the water level changes on one, and 2) the correlation between the gravity variations and the water level changes.

4.3 Shower continuity parameters and quantitative parameters

The investigation is carried out on a set of sampled showers. A shower is defined as an ensemble of precipitation events related to the same meteorological perturbation. More precisely, a shower is specified by the continuity parameters Δh_o and Δt_o: two showers are considered distinct if, during a time period longer than a defined time Δt_o (multiple of the sampling time interval Δt), the precipitation height is inferior to a given value Δh_o for each interval Δt.

Some examples are displayed in Figure 4.4. Choosing the values Δh_o=1.5 mm and Δt_o=2 hours, the precipitations displayed in Figure 4.4 A and 4.4 D correspond to a single shower. On the other hand, the precipitations shown in Figure 4.4 B and 4.4 C correspond to two distinct showers.

The continuity parameters must define a clear correspondence between the processes under investigation. An example is given in Figure 4.5, where we display the rainfall heights (Figure 4.5 A) in mm and the Alzette water level (Figure 4.5 B) in cm for the ensemble of precipitation events occurring on 25-06-2006. The precipitation occurring between 3h and 9h appear to be related to the single water increase phase occurring between 6h and 11h. Consequently, it is reasonable to choose the parameters Δh_o and Δt_o in order to define a single shower.

The water level increase duration Δt_i is defined as the time delay between the start of river level increase and the maximum river level increase due to a particular shower. The mean water level increase duration $<\Delta t_i>=185\pm35$ min is calculated for 45 showers sampled between January 2004 and April 2007. In general the same value can be adopted for the parameter Δt_s.

The value of Δh_s is the minimum continuous precipitation for which a water level increase can be observed.

The values of 3 hours and 0.5 mm hour^{-1} are adopted for Δt_s and Δh_m, respectively.

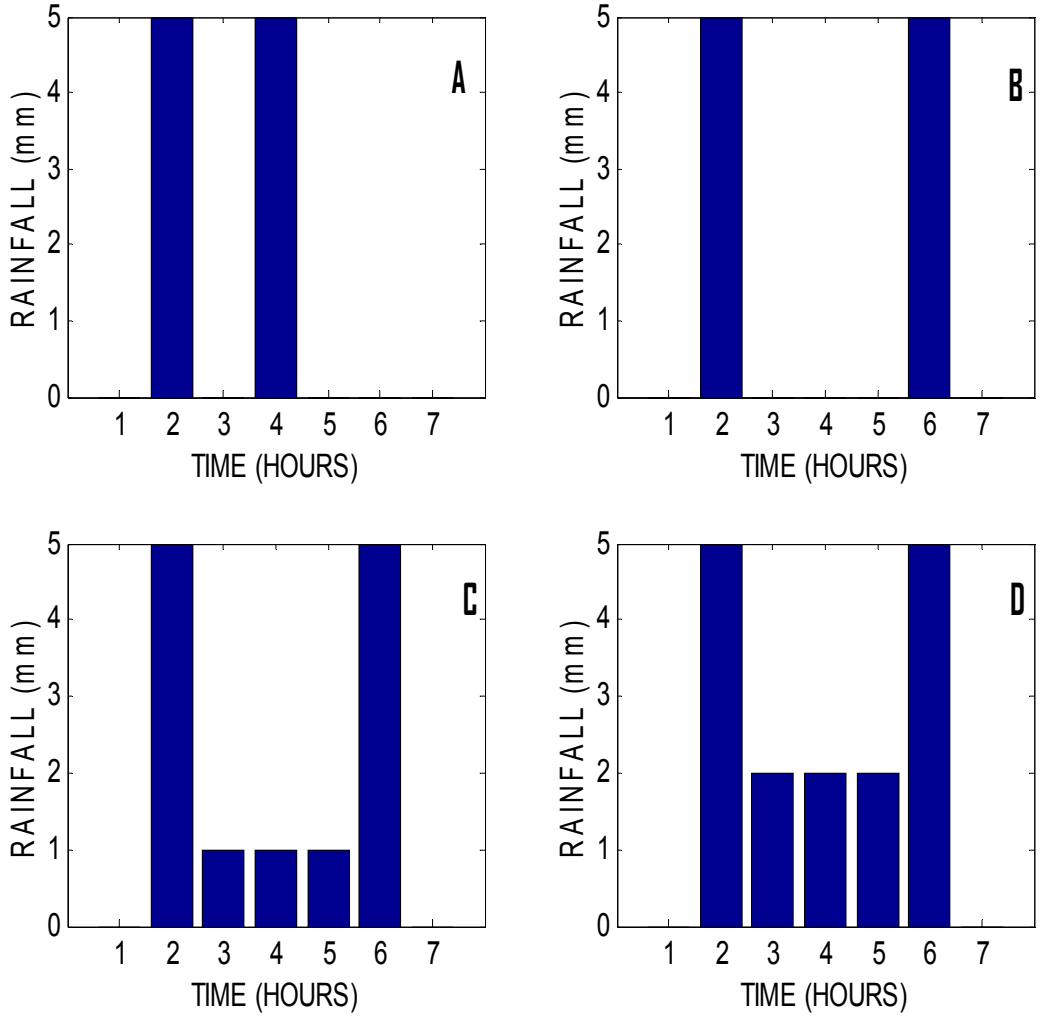

Fig.4.2*: Illustration of the continuity parameters. Choosing the values* Δh_o*=1.5 mm and* Δt_o*=2 hours, the precipitations displayed in Figure 4.2A and 4.2D correspond to a single shower. On the other hand, the precipitations displayed in Figure 4.2B and 4.2 C correspond to two distinct showers.*

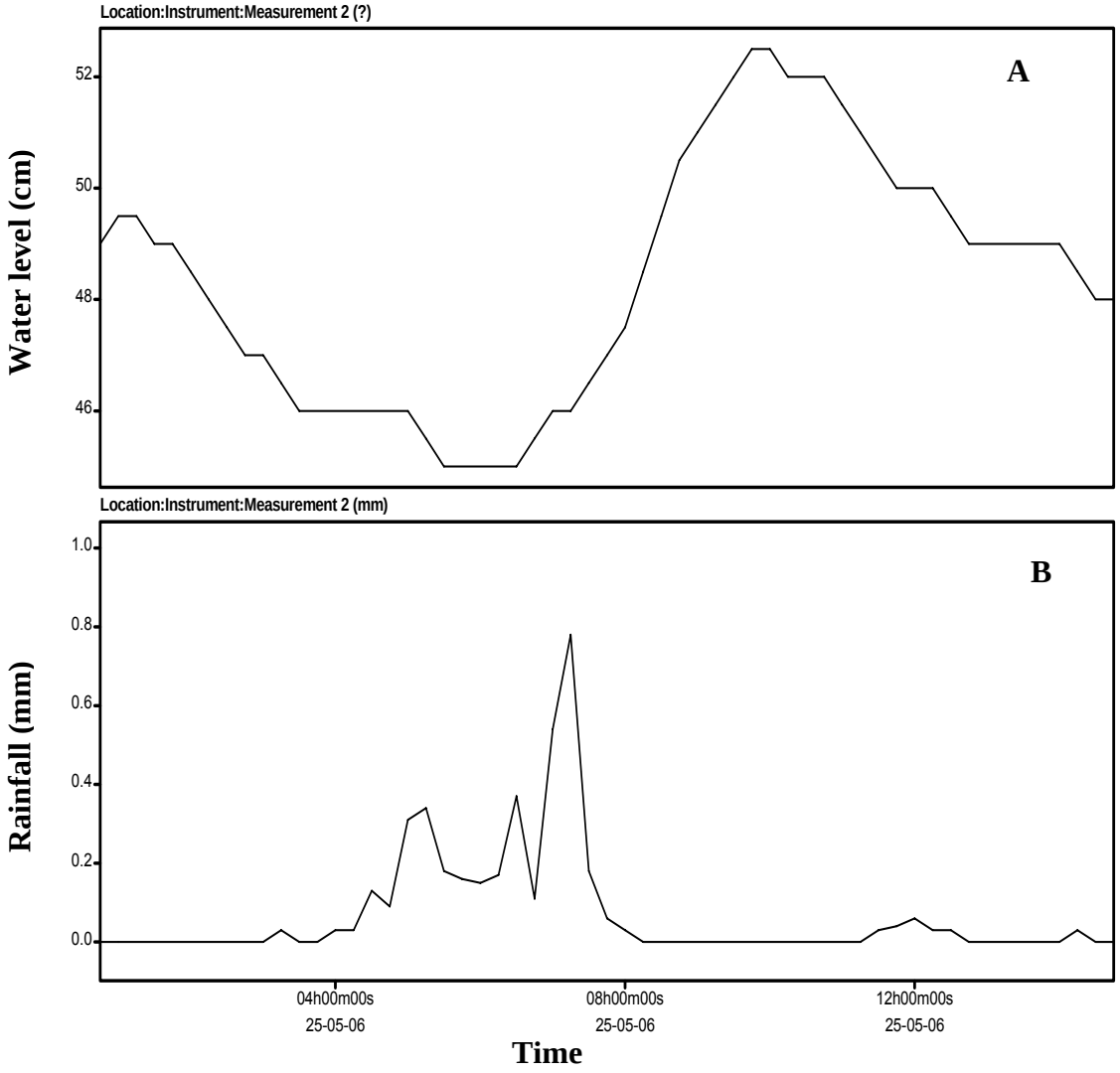

Fig 4.5*: Rainfall heights in mm (B) and water level in cm (A) for the ensemble of precipitation events occurring on 25-05-06. The precipitation events appear to be related to the same water increase phase. Therefore, it is reasonable to choose the continuity parameters in order to define a single shower.*

In addition to the continuity parameters, the principal quantitative parameters characterizing a shower are:

- The integrated water content of a shower, usually measured in terms of rainfall height (mm), represents the total amount of water precipitated throughout the shower duration
- The shower duration, representing the time elapsed between the beginning and the end of the shower, is a multiple of the reference sample time interval Δt.
- The shower average intensity, representing the ratio between the integrated content of a shower and the shower duration.

- The shower maximal intensity, representing the highest precipitation rate in the course of the shower.

Other parameters also affect the hydrological response. The structure of a shower (see Section 1.1) is defined as the temporal distribution of the precipitation heights during the shower.

If the maximal heights are found in the final part of the shower, the higher amount of precipitation falls on soil that is already saturated. In this case, the effects of the precipitation on both the amount and rate of river level change will be more relevant than if the maximal heights are situated in the initial part of the shower.

4.4 Time delay between gravity, rainfall and water level signal

In order to analyze the temporal relationships between the signals, it is more appropriate to work on the time derivatives of the gravity and river level time series. This choice allows us to filter part of the noise and of the medium and long period variations. Consequently, the gravity variations and water level variations driven by the shower events can be more clearly identified.

The Meteorological Station of Walferdange provides the Alzette water level data at 15 min intervals. Consequently, this time interval will be used as the reference for the numerical time derivatives of both the water level time series and the gravity time series.

Defining Δt as the reference time interval, the numerical time derivative of the Alzette water level time series is expressed as:

$$\dot{L}(t) = \frac{L(t+\Delta t) - L(t)}{\Delta t} \tag{4.1}$$

where *L(t)* represents the water level time series and $\dot{L}(t)$ represents the numerical time derivative of the water level time series.

The numerical time derivative of the hydrological gravity time series is can be defined in a similar way:

$$\Delta\dot{g}(t) = \frac{\Delta g(t+\Delta t) - \Delta g(t)}{\Delta t} \tag{4.2}$$

where Δg(t) represents the hydrological gravity time series and $\Delta\dot{g}(t)$ represents the numerical time derivative of the hydrological gravity time series.

Therefore, $\dot{L}(t)$ and $\Delta\dot{g}(t)$ represent the rates of change of the water level and of the hydrological gravity, respectively.The rainfall heights (mm), the numerical time derivatives of the water level time series (cm/sec) and the numerical time derivatives of the hydrological-gravity time series (nm s^{-3}) for the period January 2004 to April 2007 are displayed in Figure 4.6.

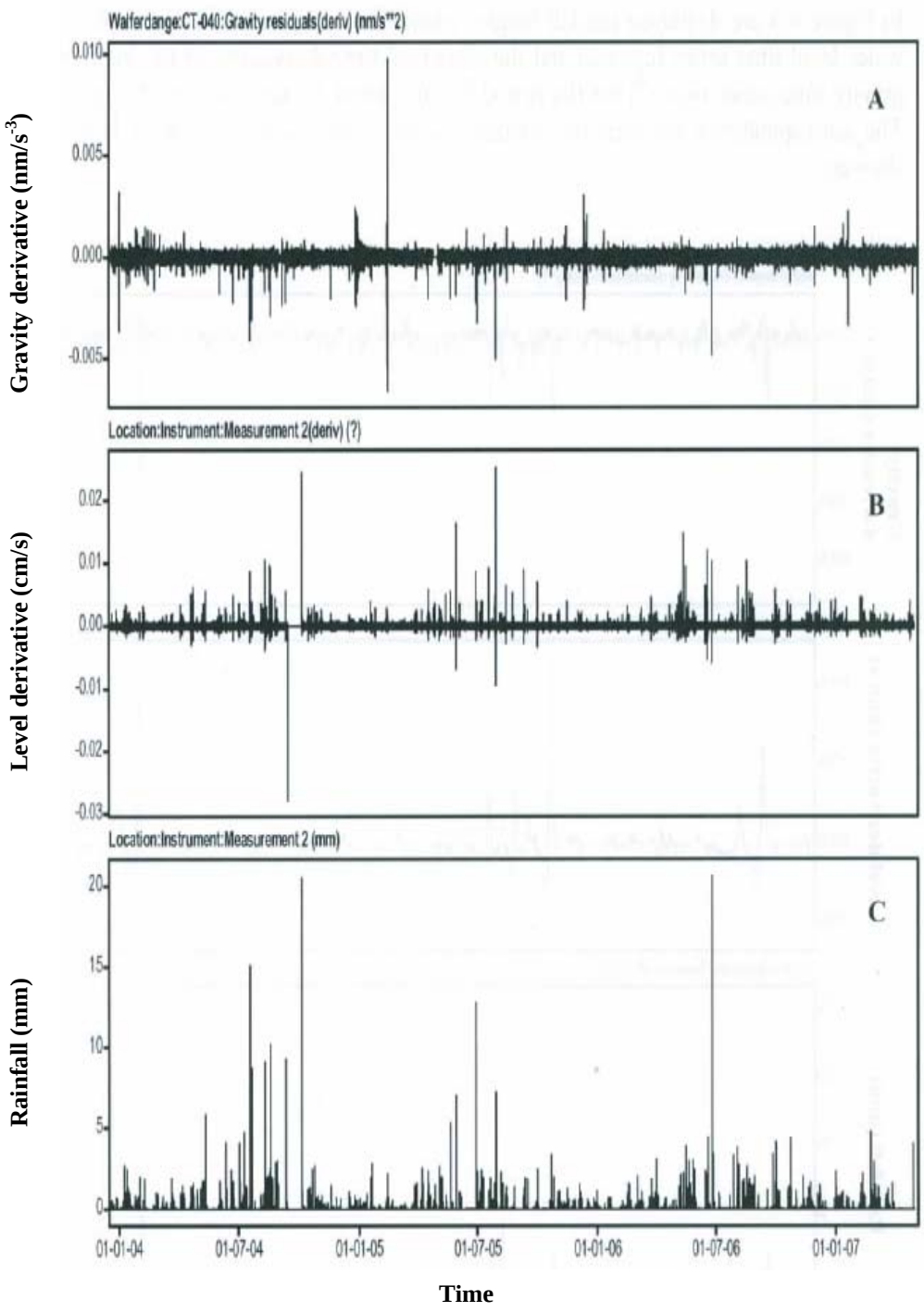

Fig 4.6: *Rainfall heights (C) in mm, level time derivative (B) in cm/sec and gravity time derivative (A) in nm s^{-3} for the period January 2004 to April 2007*

In Figure 4.7, we display the rainfall heights (mm), the numerical time derivatives of the water level time series (cm/sec) and the numerical time derivatives of the hydrological gravity time series (nm s^{-3}) for the period for the period 15 June 2006 to 26 June 2006. The correspondence between the signals can be clearly identified for at least three showers.

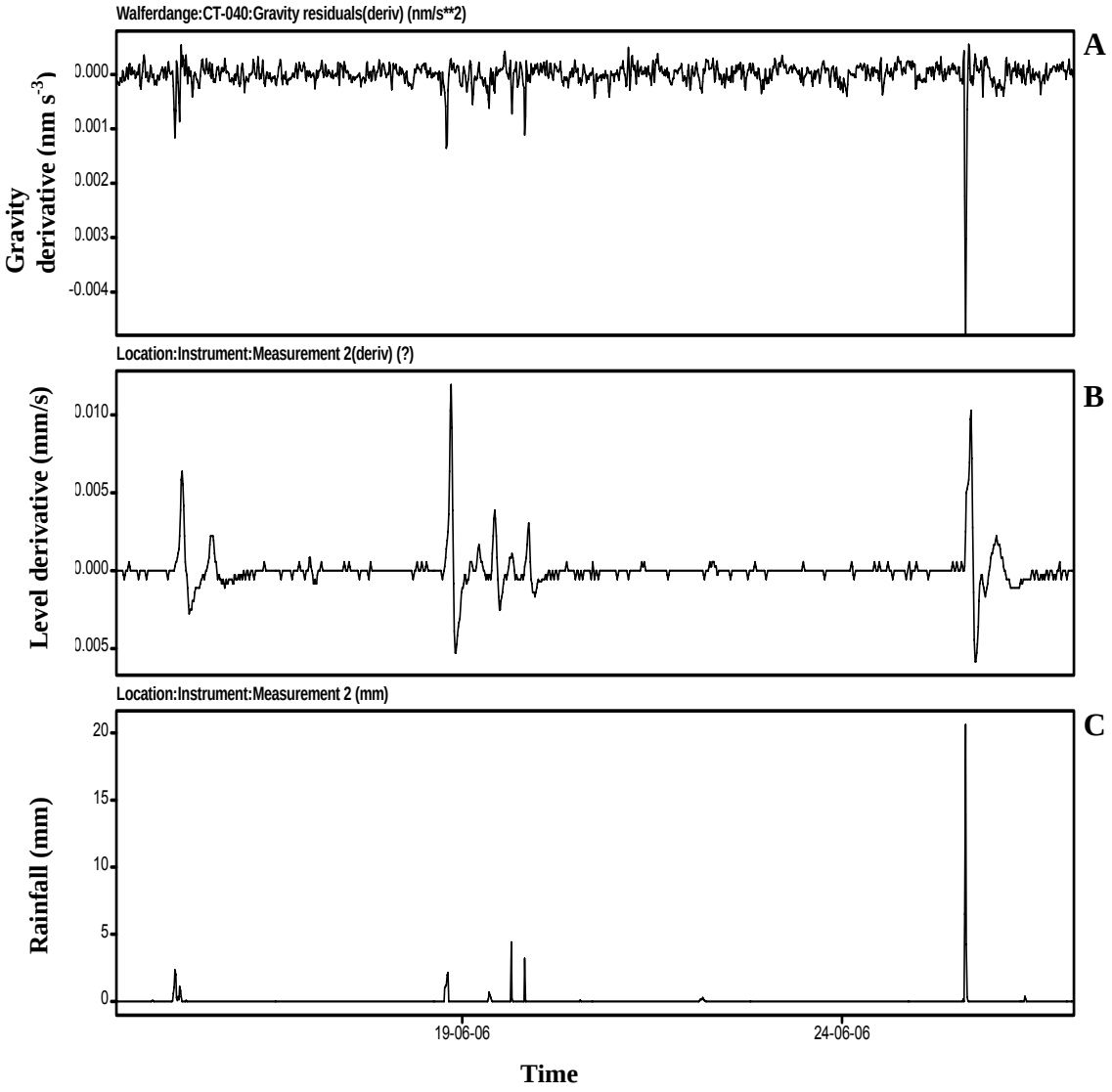

Fig 4.7: *Rainfall heights (C) in mm, level time derivative (B) in cm/sec and gravity time derivative (A) in nm/s^{-3} for the period15 June 2006 to 26 June 2006. The relationship between the signals can be clearly identified for at least three showers.*

We define two additional parameters: t_l is the time delay between the maximum values of the precipitation intensity and the gravity time derivative related to a shower, t_s is the time delay between the maximum values of water level and gravity time derivatives

related to a shower. Defining t_{Lmax} as the instant when the water level derivative is maximal during a shower, t_{gmax} the instant when the gravity derivative is maximal during a shower, and t_{Rmax} as the instant of maximum shower intensity, we have:

$t_l = t_{Rmax} - t_{gmax}$

$t_s = t_{Lmax} - t_{gmax}$

The definition of these parameters is clarified in Figure 4.8, where we display the rainfall height (mm), the gravity time derivative (here expressed in μGal hour^{-1}) and the water level time derivative (cm hour^{-1}) related to the shower, which occurred on the 25 June 2006.

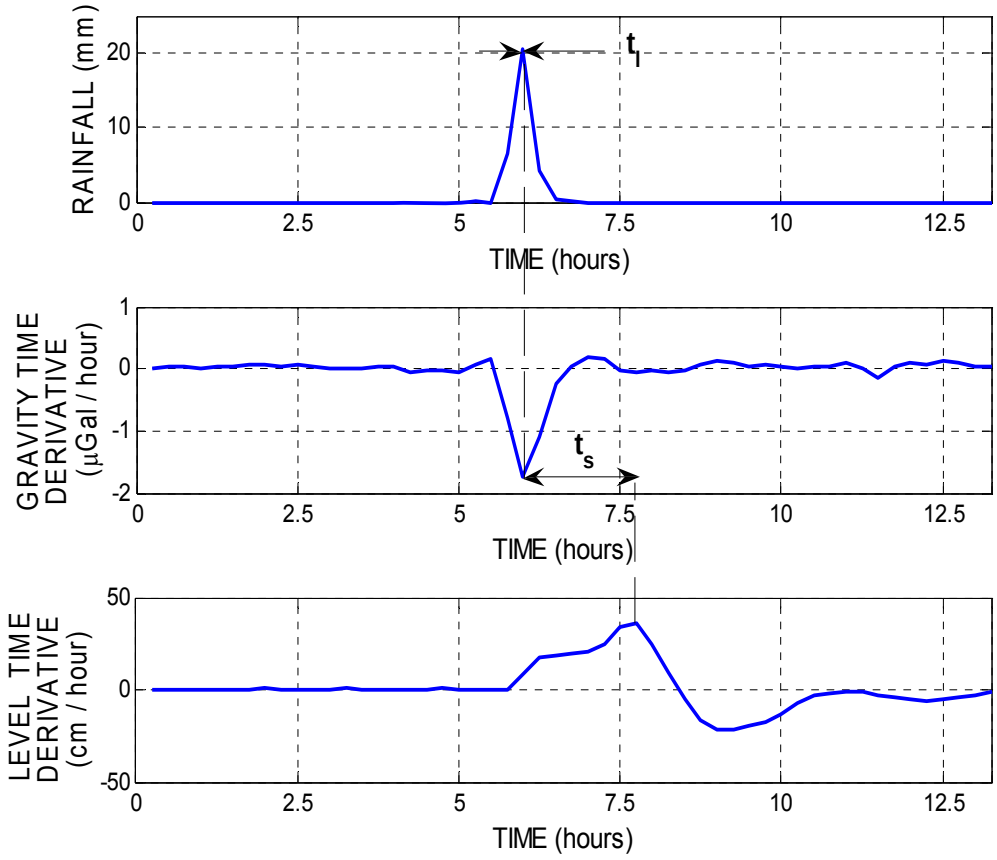

Fig. 4. 8*: Rainfall height (mm), gravity time derivative (μGal/hour) and water level time derivative (cm/hour) related to the shower that occurred on the 25 June 2006.*

The statistical analysis is carried out for 30 showers sampled between January 2005 and February 2007. In general, it is difficult to estimate the time delay between the signals as

the relationship can be clearly identified for only some types of showers: high intensity showers and medium intensity showers with their maximum intensity concentrated in the initial phase.

In order to detect an eventual seasonal variability of the time delays between the signals, the sample of 30 showers is subdivided into two subsets. In the first subset, we include the showers occurring in the months between April and September (the "warm months") and in the second subset are included the showers occurring in the months between October and March (the "cold months"). The statistical analysis is carried out on the entire sample and on the two subsets: the average values and the standard deviation of t_l and t_s are calculated for the aggregate sample, for the warm months and for the cold months.

The average value, calculated for the aggregate sample, of the time delay between the maximum shower intensity and the maximum gravity derivative is t_l =4+-9 min. The value obtained for the warm months subset is t_l =5+-9 min. The value obtained for the cold months subset is t_l =1+-9 min.

The time delay between the signals is globally inferior to 5 min and, as the uncertainties of the t_l values are even greater than the values themselves, the SG observations do not provide any additional or complementary information, that is not already provided by the pluviometer. The average values of t_l obtained for the warm months and the cold months show no substantial difference, but because of the qualitative and quantitative limitations of the sample, the results must be interpreted with caution. The calculated average values of t_l and their standard deviations are presented in Table 4.1.

	January 2005-February 2007	April-September 2005-2007	October-March 2005-2007
t_l	4±9 min	5 ±9min	1 ±9 min

Table 4.1*: Time delay t_l between the maximum values of shower intensity and gravity time derivative, for the showers sampled between January 2005 and February 2007.*

The average value of the time delay between the maximum water level derivative and the maximum gravity derivative, calculated for the aggregate sample, is t_s =88+-34 min. The value obtained for the warm months is t_l =85+-34 min. The value obtained for the cold months is t_l =93+-34 min. Also in this case the average values of t_s obtained for the warm months and the cold months show no substantial difference. Normally, we would expect the average level of soil saturation to be higher in the cold months than in the warm months. Consequently, we could expect that the time delay between the gravity signal and the water level signal may be shorter in the cold months than in the warm months. Our results offer no indications with respect to these expectations. The limitations of the sample size and the methodological simplicity of this investigation do not allow us to reach any definitive conclusions. The calculated average values of t_l and

their standard deviations for the aggregate sample and the two subsets are presented in Table 4.2.

	January 2005-February 2007	April-September 2005-2007	October-March 2005-2007
t_s	88 ±34 min	85±34 min	93 ±34 min

Table 4.2*: Time delay t_s between the maximum values of gravity and water level time derivatives, for the showers sampled between January 2005 and February 2007.*

4. 5 Correlations between the integrated water content of showers, entity of water level changes and entity of gravity changes

In this section, a statistical analysis is carried out on the correlation between the amount of gravity change associated to showers and the corresponding amount of Alzette River level change. A comparative analysis is done with the correlation between the total amount of precipitation of showers and the corresponding amount of Alzette River level change. As already indicated, our motivation for this analysis is to determine whether hydrological gravity shows a better correlation with river water levels than with precipitation levels. This is because both gravity and the river level changes are dependent on soil hydrological parameters, whereas rainfall is not.

The Meteorological Station of Walferdange provides the Alzette River water level time series (limnimetry) at 15 min intervals. We use this this time interval (indicated as Δt) as the reference interval for the gravity time series and the precipitation time series.

A preliminary observation is necessary. The showers taken into account for the investigation correspond to the local precipitation. But the Alzette River water level changes do not depend only on the local precipitation. The water levels also depend on rainfall occurring upstream. Consequently, local precipitation provides only partial information on the total water volume contributing to the water level increase.

Furthermore, gravity changes may occur in the absence of precipitation. Part of these effects may superimpose themselves onto the effects related to precipitation. Consequently, when showers occur, it is not possible to identify exactly which part of the gravity change is actually related to the amount of precipitation contained in the shower.

In Figure 4.9 we display the water level changes (A) in mm, the gravity changes (B) in nm s^{-2} and the precipitation heights (C) in mm for the period between the end of June 2006 to end July 2006. We notice a significant gravity decrease in absence of precipitation.

In Figure 4.10 we display the water level changes (A) in mm, the gravity changes (B) in nm s^{-2} and the precipitation heights (C) in mm for the entire sampling period extending from January 2004 to April 2007.

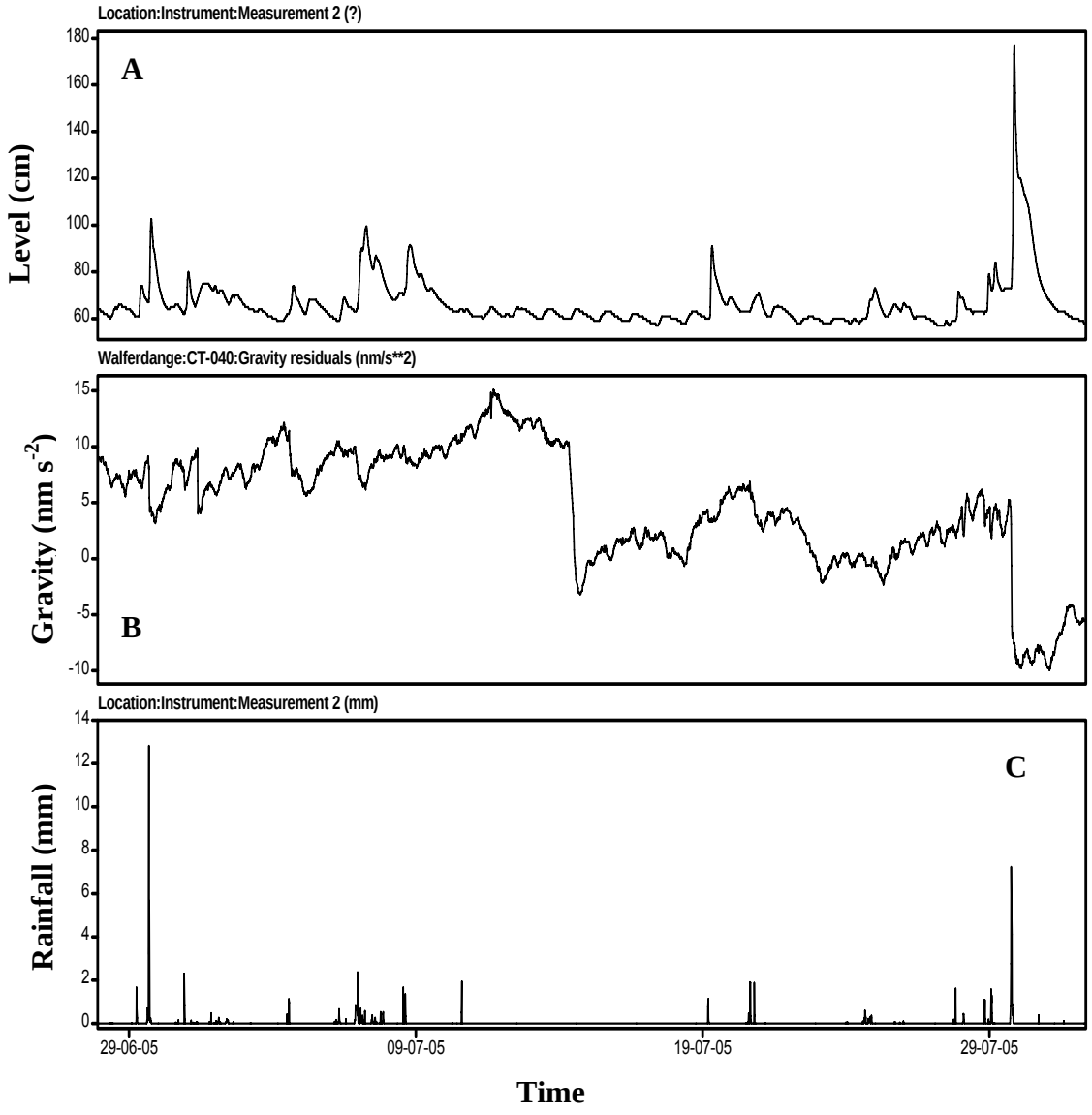

Fig. 4.9: *Water level changes (A) in mm, the gravity changes (B) in nm s^{-2} and the precipitation heights (C) in mm for the period between the end of June 2006 to the end of July 2006. We notice a significant gravity decrease in absence of precipitation.*

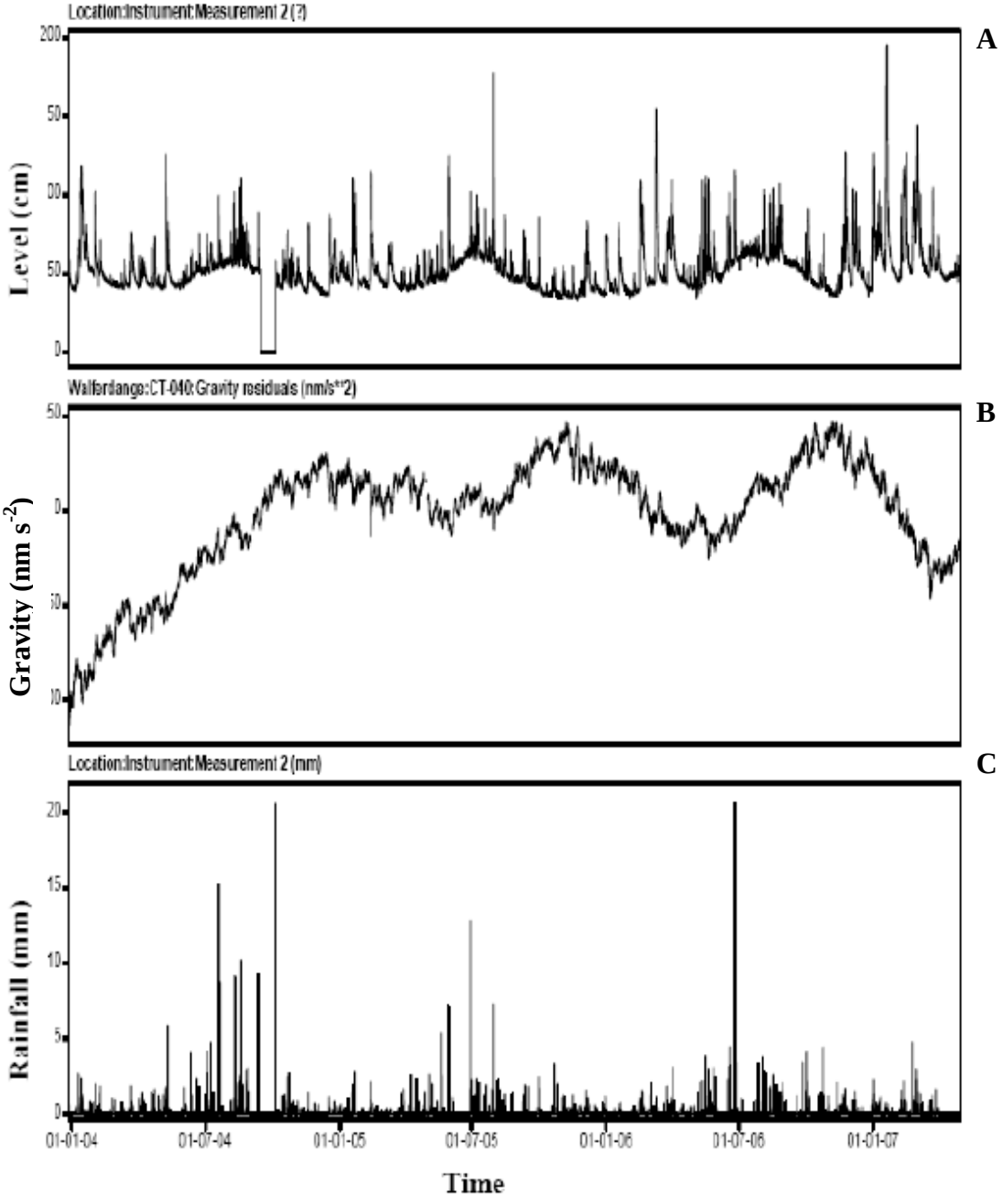

Fig 4.10: *Alzette River water level (A, cm), gravity changes (B, nm·s^{-2}) and precipitation heights at Walferdage for the period extending from January 2004 to April 2007.*

Nevertheless, it is relatively easy to identify the correlation between the precipitation height, the gravity variations and the Alzette River water level changes in the case of high intensity showers, where the precipitation is concentrated over a short time.

With reference to Figure 4.11, where we display the rainfall, gravity variations and the Alzette River water level changes for the shower, which occurred the 25th of June 2006, we define the following parameters:

- R_s is defined as the integrated water content of a shower. R_s represents the total amount of precipitation, expressed in mm, occurring throughout the duration of the shower.
- Δg_s is defined as the total gravity variation associated with a shower, representing the gravity difference between the commencement of the gravity decrease and the cessation of the gravity decrease.
- L_s is defined as the total Alzette River water level change associated with a shower, representing the water level difference between the commencement of the water level increase and the cessation of the water level increase

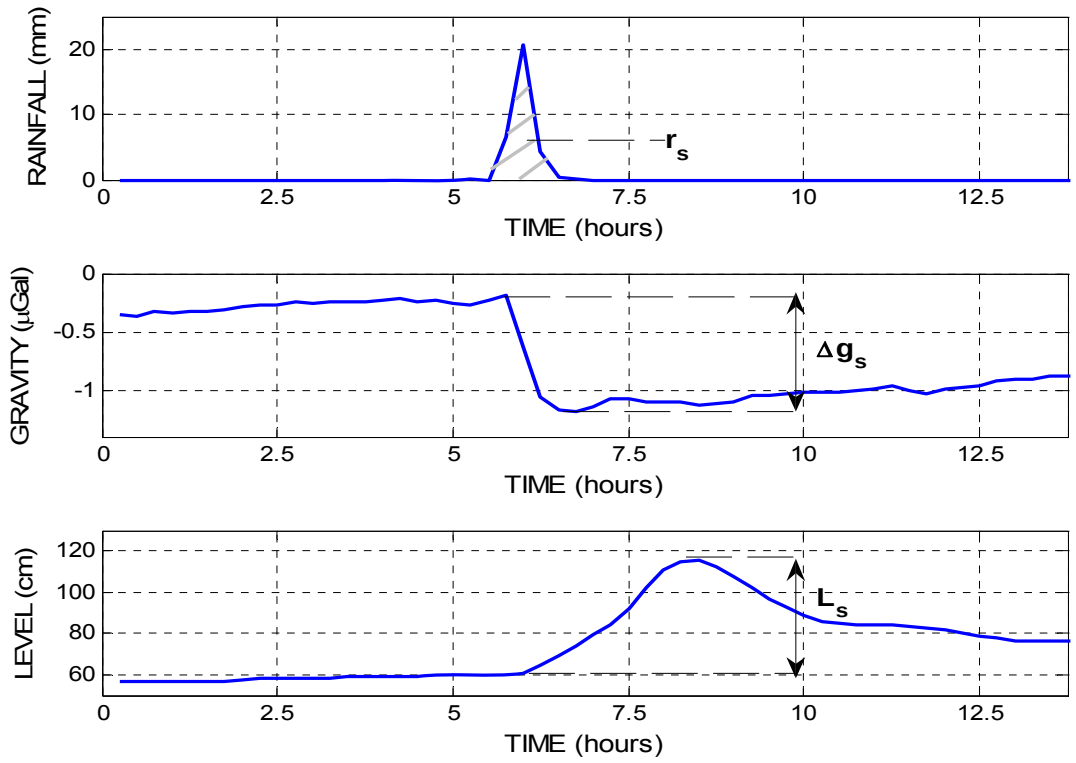

Fig. 4.11: *Time evolution of rainfall (mm), gravity (μGal) and Alzette River water level (cm) related to the shower that occurred on 25 June 2006.*

The statistical analysis is carried out on 45 showers sampled between January 2005 and April 2007. The sample description is provided in Table 4.3, where we report the values of the integrated amount of water for the shower R_s, the values of the gravity variations Δg_s, the values of the water level changes L_s and the values of the shower intensity for the sampled showers.

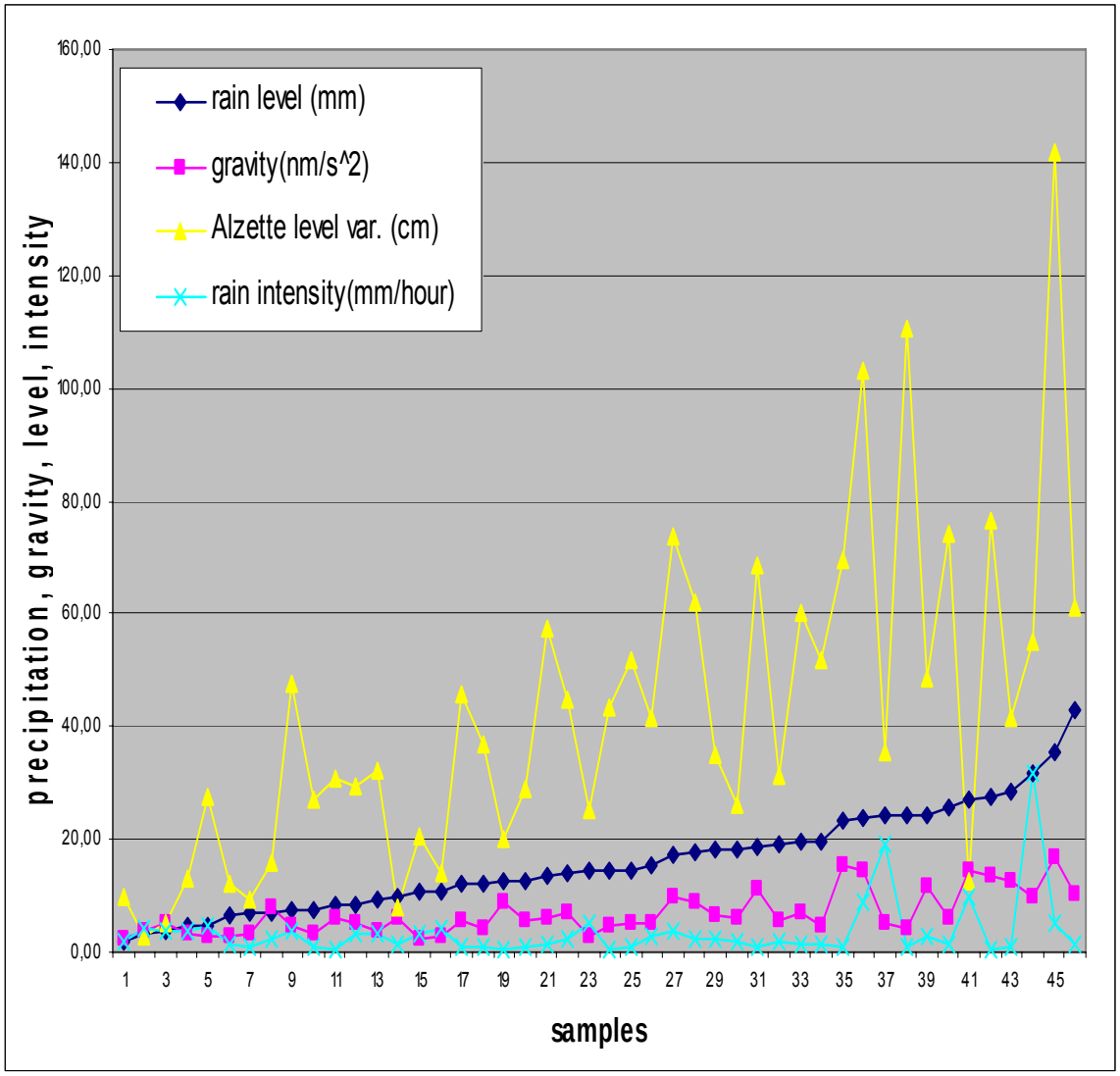

Fig 4.12: *Water amounts in mm (blue, in growing order), gravity variations in nm s^{-2} (pink), water level changes in cm (yellow) for the sampled showers.*

A graphical description of the sample is provided in Figure 4.12, where the integrated water amounts for each shower (mm) are displayed, in blue, following the order of growing amounts. The gravity variations are displayed in blue and expressed in nm s^{-2}. The Alzette River water level changes are displayed in yellow and expressed in cm. The mean intensities are displayed in green and expressed in mm/hour.

As examples, the precipitation amounts, gravity changes and water level changes as a function of time are displayed for some of the sampled showers in Figures 4.11 and 4.12.

The purpose of the analysis is to compare the level of correlation existing between Δg_s. and L_s with the level of correlation existing between L_s and R_s. As previously noted, in addition to the precipitation, which depends only on atmospheric parameters, both the gravity variations and the river water level changes also depend on soil hydro-geologic parameters such as the degree of soil saturation or the hydraulic conductivity. This may allow us to consider the hypothesis that the hydrologic gravity changes contain more information than only precipitation related changes so that we may infer information on the River level changes.

We refer to the Bravais Pearson index of linear correlation. For two given ensembles of n values $X(x_1 \ldots x_n)$ and $Y(y_1 \ldots y_n)$, the Bravais-Pearson index is expressed as:

$$r_{xy} = \frac{\sum_{i=1}^{n}(x_i - m_x)\cdot(y_i - m_y)}{\sqrt{\sum_{i=1}^{n}(x_i - x_m)^2}\cdot\sqrt{\sum_{i=1}^{n}(y_i - y_m)^2}} = \frac{\sigma_{xy}}{\sigma_x \cdot \sigma_y} \tag{4.3}$$

where r_{xy} represents the correlation between the series X and Y, and m_x and m_y are the means of the series X and X, respectively.

The term $\sigma_x = \sqrt{\sum_{i=1}^{n}(x_i - x_m)^2}$ is the standard deviation of X, the term $\sigma_y = \sqrt{\sum_{i=1}^{n}(y_i - y_m)^2}$ is the standard deviation of T and $\sigma_{xy} = \sum_{i=1}^{n}(x_i - m_x)\cdot(y_i - m_y)$ represents the covariance between X and Y.

The value of the correlation r_{gl} between gravity variations and Alzette River water level variations is determined to be 0.59. The admittance between L_s and Δg_s is calculated to 45±5 cm μGal^{-1}. The L_s values as a function of the Δg_s values are displayed in Figure 4.15.

The value of the correlation r_{rl} between the precipitation integrated amounts and Alzette River water level variations is calculated to be 0.59. The admittance between L_s and r_s is calculated to be 2.2±0.4 cm·mm^{-1}. The L_s values as a function of the R_s values are displayed in Figure 4.16.

Again, the slightly improved correlation between L_s and r_s shows that the SG observations (as compared to predictions based solely on the pluviometer) fail to provide a better insight into river levels. But because of the quantitative and qualitative sample limitations it is not possible to extract definitive conclusions from our results.

Tab 4.3: *Sample description*

	date						
	18/01/2005	21/01/2005	11/02/2005	29/03/2005	17/04/2005	14/05/2005	21/05/2005
rainfall (mm)	18,45	8,37	27,30	1,72	3,06	12,63	8,46
gravity (nm s-2)	11,29	6,04	13,39	2,10	3,82	9,03	5,27
level (cm)	68,53	30,66	76,28	9,97	3,00	19,94	29,37
intensity (mm/hour)	1,07	0,50	0,42	1,72	4,08	0,48	3,08

	date						
	30/05/2005	29/06/2005	29/07/2005	01/10/2005	22/10/2005	06/12/2005	31/12/2005
rainfall (mm)	17,14	24,10	23,95	12,25	6,80	18,06	12,31
gravity (nm s-2	9,92	4,98	14,30	5,48	3,26	6,55	4,23
level (cm)	73,58	35,54	103,01	45,52	9,16	35,18	36,89
intensity (mm/hour)	3,80	19,30	8,70	0,96	0,85	2,33	0,71

	date						
	17/01/2006	15/02/2006	08/03/2006	24/03/2006	01/04/2006	05/05/2006	17/05/2006
rainfall (mm)	14,48	23,55	24,22	19,09	3,90	10,68	17,65
gravity (nm s-2)	4,67	15,61	4,28	5,83	4,96	2,50	8,63
level (cm)	43,53	69,35	110,68	31,34	5,10	20,69	61,82
intensity (mm/hour)	0,65	1,05	1,09	1,66	3,90	3,28	2,37

	date						
	20/05/2006	26/05/2006	15/06/2006	18/06/2006	25/06/2006	28/07/2006	04/08/2006
rainfall (mm)	19,66	18,23	9,22	7,49	31,87	4,64	15,48
gravity (nm s-2)	7,03	6,02	3,86	4,47	9,87	3,33	5,18
level (cm)	60,35	26,34	32,04	47,44	54,86	13,12	41,55
intensity (mm/hour)	1,51	1,75	3,07	3,75	31,87	3,71	2,84

	date						
	11/08/2006	17/08/2006	21/08/2006	24/08/2006	28/08/2006	30/09/2006	03/10/2006
rainfall (mm)	10,80	14,14	14,44	24,35	12,67	4,75	28,65
gravity (nm s-2)	2,65	6,91	2,75	11,50	5,38	2,62	12,59
level (cm)	13,86	44,94	25,03	48,45	29,15	27,63	41,35
intensity (mm/hour)	4,32	2,26	5,25	2,78	0,96	4,75	0,96

	date						
	23/11/2006	03/12/2006	07/12/2006	08/12/2006	17/01/2007	08/02/2007	11/02/2007
rainfall (mm)	25,73	43,10	6,94	7,66	35,67	14,54	13,70
gravity (nm s-2)	5,95	10,18	7,92	3,04	16,99	5,15	6,02
level (cm)	74,09	61,08	16,09	27,14	142,03	51,59	57,59
intensity (mm/hour)	1,39	1,18	2,31	1,02	4,98	0,79	1,21

	date			
	23/02/2007	27/02/2007	22/03/2007	29/04/2007
rainfall (mm)	6,64	27,10	19,77	9,93
gravity (nm s-2)	2,80	14,28	4,84	6,27
level (cm)	11,93	12,45	51,77	8,04
intensity (mm/hour)	1,35	9,85	1,46	1,59

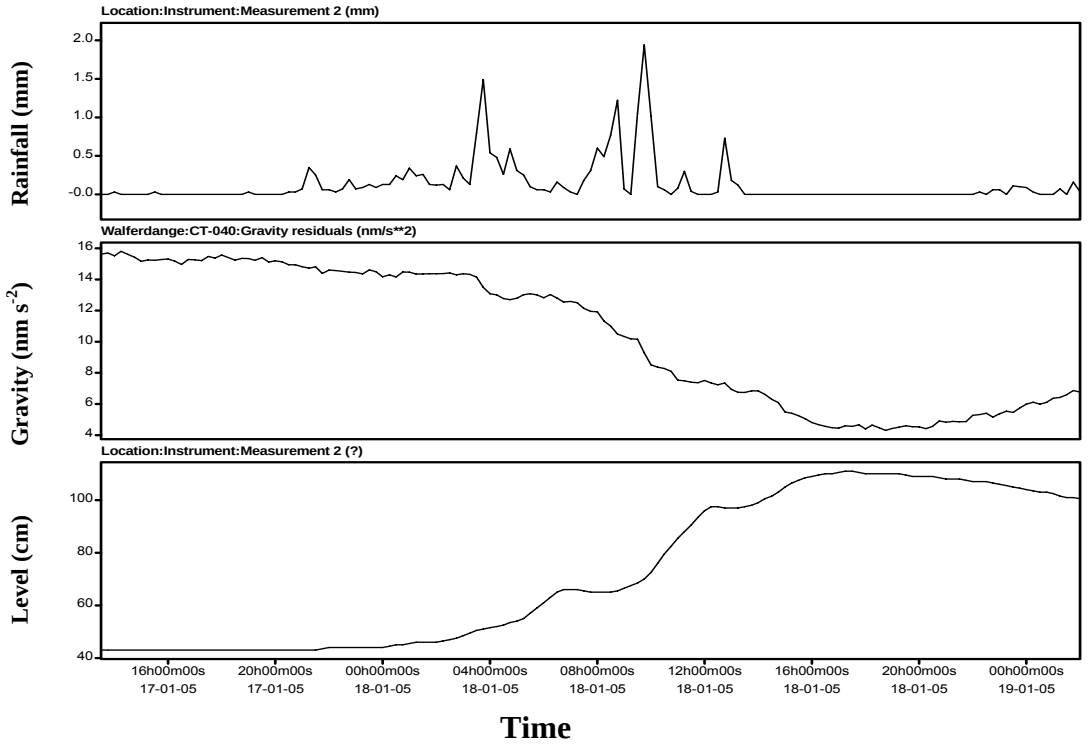

***Fig 4.13**: Rainfall (mm), Gravity change (nm s^{-2}), River water level change (cm) for the shower occurring the 18-01-2005.*

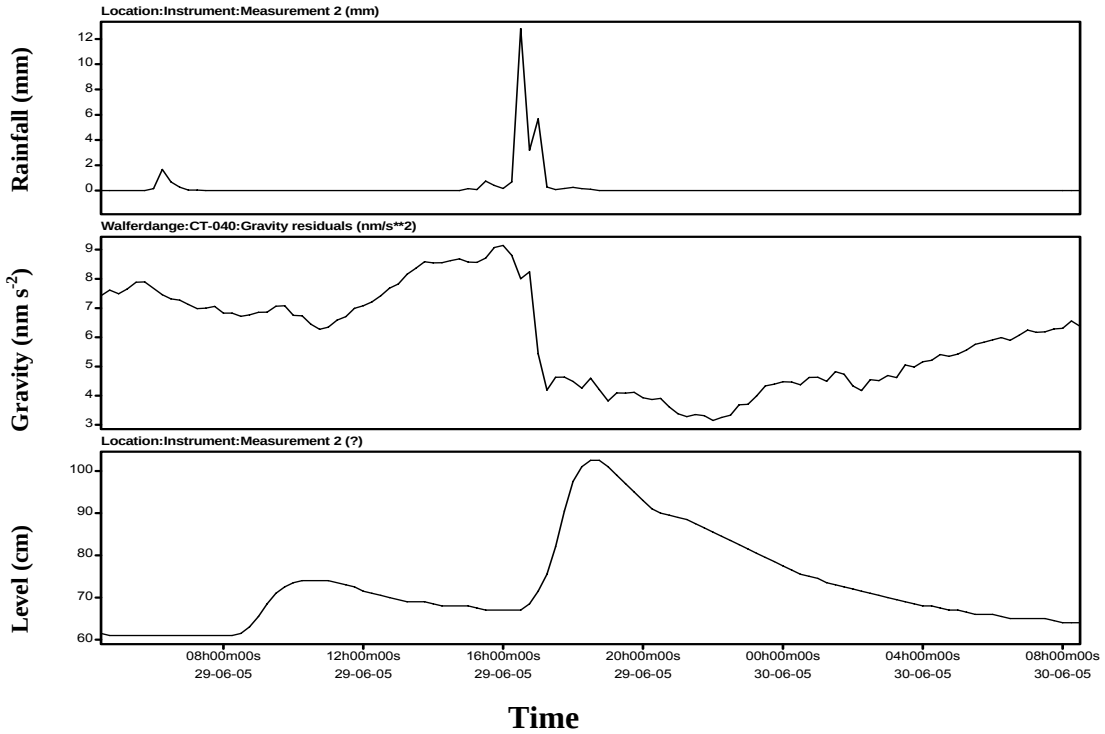

***Fig 4.14**: Rainfall (mm), Gravity change (nm s^{-2}), Level change (cm) for the shower occurred the 29-05-2005.*

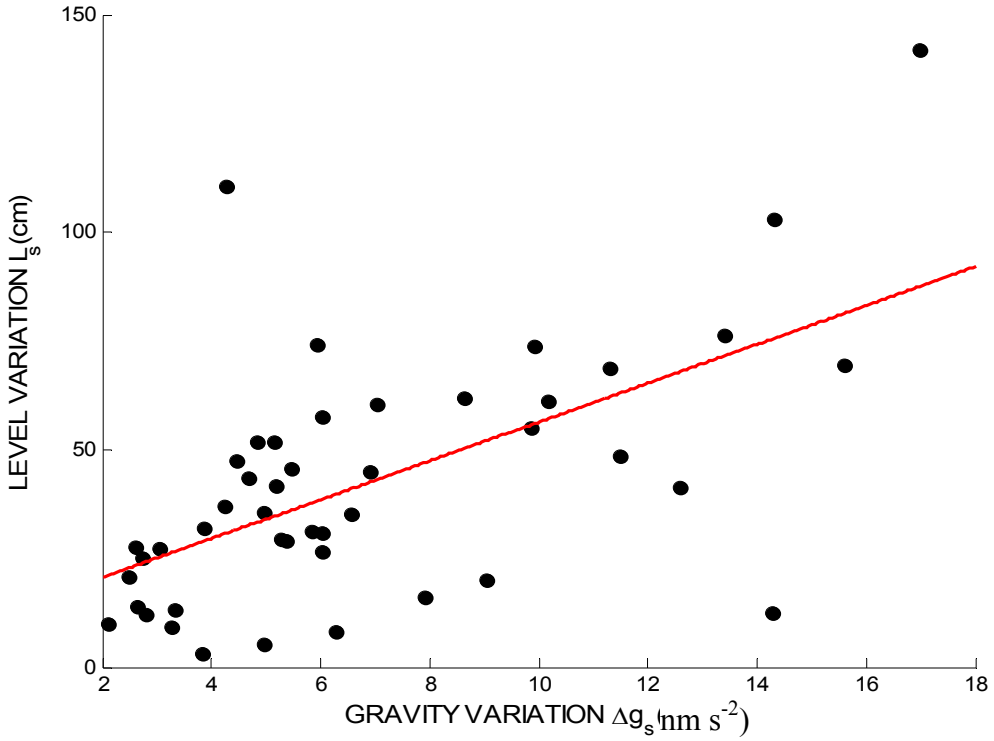

***Fig. 4.15**: Correlation between gravity and water level changes for the showers occurring between January 2004 and April 2007.*

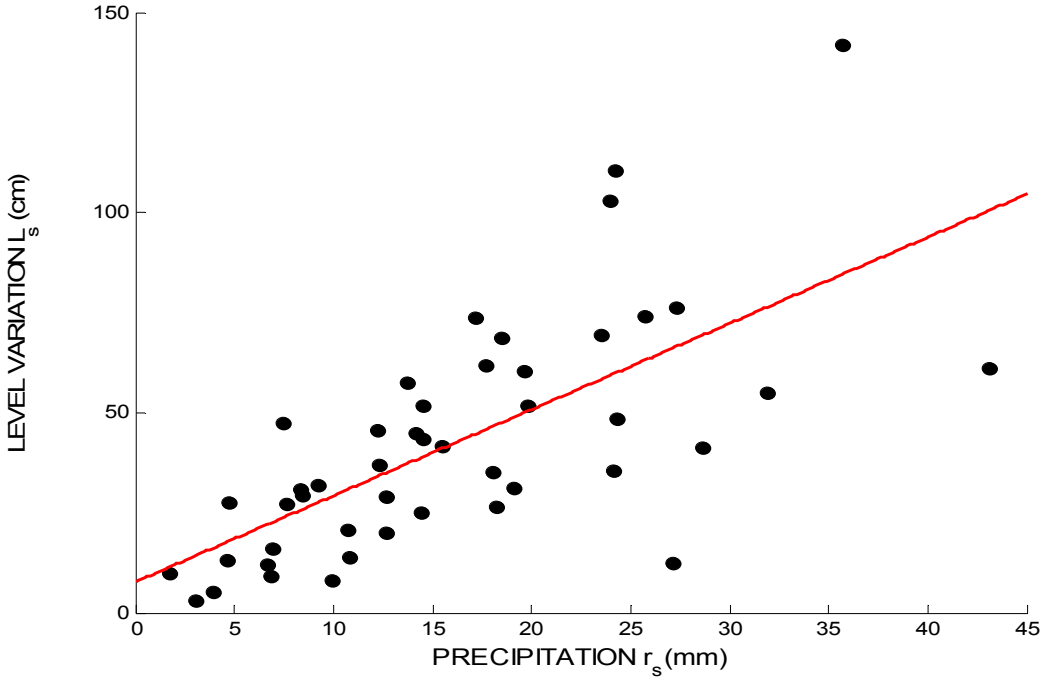

***Fig.4.16**: Correlation between precipitation heights and water level changes for the showers occurring between January 2004 and April 2007.*

4.6 Conclusion

We have carried out a purely statistical investigation to investigate the correlation between the hydrological gravity changes observed by the SG located in the WULG and the Alzette River water level changes observed by the WMS in a nearby location. The investigation was subdivided into two main parts.

First, we have estimated the time delays between gravity, Alzette River water level and precipitation signals for an ensemble of showers sampled, which occurred between 2004 and 2007. We have calculated an average time delay of 4+-9 min between the maximum gravity variation rate and the maximum precipitation intensity. We have calculated an average time delay of 88+-34 min between the maximum gravity variation rate and the maximum Alzette River water level variation rates. We could not detect significant seasonal differences. We conclude that the gravimeter provides no additional time information with respect to the pluviometer in order to anticipate the Alzette River water level variations.

Secondly, we have investigated the correlations between the gravity changes, Alzette River level changes and integrated amounts of precipitation for an ensemble of showers sampled between 2004 and 2007. The correlation between the gravity changes and the Alzette River level changes was calculated to 0.59. The correlation between the Alzette River level changes and the integrated amounts of precipitation was calculated to be 0.68. The improved correlation obtained for the precipitation amounts and water level changes as opposed to the correlation between the gravity changes and the water level changes indicates that the gravity data offer no additional information, with respect to the precipitation data, that would allow us to predict the amount of River level changes resulting from the showers.

The admittance between gravity and water level variations and between the precipitation amount and the water level variation was calculated to be 44.7±0. 5 cm $\cdot \mu Gal^{-1}$ and 2.15±0.4 cm $\cdot mm^{-1}$, respectively.

Conclusions

Conclusions

The present research can be subdivided in two parts, strictly related but methodologically independent.

In the first and main part of the research, comprised in chapters from one to three, two basic models have been modified and implemented in order to describe the gravity changes driven by hydrological causes at the station of Walferdange, in the Grand Duchy of Luxembourg:

- The Tank Model, based on the combination of a mass continuity equation and Darcy's law, which relates the flow of fluids through porous media to the hydraulic head. This model describes only the discharge process (corresponding the gravity recovery phase).
- The Double Exponential Model, which describes both the discharge process and the recharge process (corresponding in our specific situation to the gravity decrease phase after rainfall, because the gravimeter is underground located) with the use of two exponential functions.

Both the models, in absence of direct information on local hydro-geological parameters and on the level of the local water table, were empirically parameterized.

The two basic models have been modified by introducing the hypothesis of the seasonal variability of two important parameters: the gravity recovery rate for the Tank Model and the discharge time for the Double Exponential Model. We have shown that these two parameters are strictly correlated. We have also shown that when the hydraulic discharge duration is significantly greater than the hydraulic recharge duration, the two models offer a similar description of the gravity variations after a precipitation event.

Both the models have been implemented using solely the local precipitation time series as input. The models outputs, representing the modeled hydrological gravity time series, have been compared with the observed hydrological gravity time series, provided by the Observatory Superconducting Gravimeter CT040 located in the Walferdange Underground Laboratory for Geodynamics (WULG).

The survey of the observed gravity time series shows that the discharge time is actually relevantly greater than the recharge time. Consequently, the Tank Model, which requires a significantly shorter computing time with respect to the Exponential Model, is accurate enough to be adopted for the description of the hydrological gravity variations in Walferdange.

The percentage of signal scatter reduction obtained with the tank model is 73%. However, this result is achieved by introducing a 60% seasonal variation of the gravity recovery rate. Because the model is empirically parameterized, it is uneasy to analyze the actual physical signification of this hypothesis. First, it could be due to variability of the hydraulic conductivity K, which is related to the parameter γ. K can be expressed in the form $K=k\cdot\rho\cdot g\cdot\mu^{-1}$, where k (length^2) is the permeability of the solid matrix, which depends only on the characteristics of the porous medium. The term $\rho\cdot g\cdot\mu^{-1}$ depends only on the fluid characteristics, where ρ and μ represent the density and the viscosity of the

fluid, respectively. The viscosity depends on groundwater temperature. At mid-latitude locations such as Walferdange, groundwater temperature has a definite seasonal variability, even if it is less sensitive in the saturated zone. *Bartolino* (2003) investigated the annual groundwater temperature fluctuations as a function of depth below the surface beneath the Rio Grande in New Mexico. He estimated an annual groundwater temperature range varying from 22°C at 1 m depth below the surface to 4°C at 15 m depth below the surface.

A second seasonal effect could be due to the infiltration variability. The runoff coefficients, and consequently the fraction of precipitation infiltrating the soil, can have a significant seasonal variability, related to the degree of saturation of the root zone.

Thirdly, the improvement could be due to evapotranspiration variability. The process of evapotranspiration has a strong dependence on air and soil surface temperatures that are subjected to significant seasonal oscillations.

Finally, it could be due to regional effects. The model is based on local precipitation. However, the gravity recovery rate variability hypothesis may absorb longer wavelength seasonal effects as well [*van Dam et al., 2001*; *Crossley et al., 2005*].

Implementing the tank model with a constant value of γ, the seasonal variations are not absorbed and the maximum percentage of signal scatter reduction in Walferdange is only 25%.

Preliminarily to this first part of the research, the admittance between the gravity change and the precipitation height was computed with the use of a Digital Elevation Model (DEM) of the area above the gravimeter. The value of the admittance α=36 μGal $m^{-1}$is obtained. For reference, the value given by the Bouguer infinite plate model is 42 μGal m^{-1}. This value is generally adopted for almost flat surfaces. The significant height differences of the area above the WULG justify the calculation made on the actual topography.

In the second part of the research, comprised in Chapter four, we have carried out a purely statistical investigation on the correlation between the gravity changes observed by the Superconducting Gravimeter and the water level changes of the nearby Alzette level, registered by the Walferdange Meteorological Station, in correspondence of sets of sampled shower events. The time delay between the signals has also been evaluated.

Because of the distance between the gravimeter and the Alzette River, a direct effect of the river level changes on the gravity signal can be excluded. The motivation of the investigation is that the gravity data may provide more accurate information than the precipitation data in order to anticipate the water level changes, because both gravity and water level changes are dependent on soil hydro geological parameters, whereas precipitation is not. Therefore, it can be interesting to attempt a comparative analysis of the correlation between gravity and water level variation and precipitation amounts and water level variations.

The time delay between the maximum gravity and water level time derivatives and maximum precipitation intensity and gravity time derivative is 88±34 minutes and 4±9 minutes, respectively. The correlation between the gravity and water level variation and the precipitation amount and water level variation is calculated to 0.59 and 0.68, respectively. The admittance between water level and gravity variation and water level variation and precipitation amount is calculated to 45±5 cm μGal^{-1} and 2.2±0.4 cm mm^{-1}, respectively.

In conclusion, the gravity signal does not allow for a better prediction of the water level of the Alzette as compared to the prediction based solely on the pluviometer. Nevertheless, the correlation between gravity and water level variation increases with the shower mean intensity. But, because of the samples quantitative and qualitative limitations, the results of this part of the research must be evaluated with caution.

References

Ambroise B. (1998). La dynamique du cycle de l'eau dans un bassin versant. *Editions H.G.A. Bucarest*, *204 pp.*

Anderson M.P. (2007). Introducing groundwater physics. *Physics today, vol. 60, 42-47.*

Banerjee, B. , Das Gupta, S. P. (1977). Gravitational attraction of rectangular parallepiped, *Geophysics*, *42, 1053-1055*.

Bartolino, J.R. (2003). Heat as a tool for studying the movement of groundwater near streams, *U.S. Geological Survey circular n^o. 1260, 97 pp*.

Bear J. (1972). Dynamics of fluids in porous media. *American Elsevier Publ. Co., New York, 784 pp*.

Bertoni A., Campadelli P., Grossi G. (2003). Introduzione alla elaborazione dei segnali. *Università degli studi di Milano, 102 pp*.

Bois P. H. (2000). Hydrologie Générale. *Institut National Polytechnique de Grenoble*, *176 pp.*

Bois P.H., Obled C., Zin I. (2007). Introduction au traitement des données en hydrologie. *Institut National Polytechnique de Grenoble*, *265 pp*.

Bower D.N., Courtier N. (1998). Precipitation effects on gravity measurements at the Canadian Absolute Gravity Site, *Physics of the Earth and plan, int. 106, 353-369.*

Boy J., Hinderer J. (2006). Study of the of the seasonal gravity signal in superconducting gravimeter data , *J. Geodyn*. , *41, 227-233*.

Bredehoeft J.D., Cooley R.L. (1983). Comment on "A note on the meaning of the storage coefficient" by T.R. Narasimhan and B. y. Kanehiro. *Water Resources Research, vol. 19, n^{o}6, 1632-1634.*

Caquot A. (1941). Ecoulement des eaux pluviales. Comptes rendus de l'académie des sciences 20-10, Paris.

Cooper, H.H., Jr., (1966). The equation of groundwater flow in fixed and deforming coordinates. J*ournal of Geophysical research, vol.71, n^{o}20, 4785-4790.*

Crossley, D, J., Hinderer, J., Boy, J.-P., (2005). Time variation of the European gravity field from superconducting gravimeters, *Geophys. J. Int.,161*, *257-264.*

Crossley, D., Xu, S., (1998). Analysis of superconducting gravimeter data from Table Mountain, Colorado. *Geophys. J. Int.*, *135*, *835-844.*

Cuenod M. (1956). Contribution a l'étude des crues. Détermination de la relation dynamique entre les précipitations et le débit des cours d'eau au moyen du calcul a l'aide de suites. *La 'Houille Blanche' n°3-1956, Grenoble, 391-403.*

Damiata, B.N., Lee, T.C. (2006). Simulated gravitational response to hydraulic testing of unconfined aquifers. *Journal of Hydrology 318, 348–359.*

Darcy H. (1856). Les fontaines publiques de la ville de Dijon. *V. Dalmont, Paris.*

Davis, S.N., De Wiest R.J.M. (1966). Hydrogeology. *John Wiley & sons, Inc. New York-London-sydney, 464 pp*.

De Marsily G. (1981). Hydrogeologie quantitative. *Masson*, *464 pp.*

Delcourt-Honorez M. (1986). Earth tide response and barometric effect in three well aquifer systems. The effect on gravity of the three water level variations. *Proceedings of the 10th Int. Symp. On Earth Tides, Madrid, ed. R. Vieira, 843-854.*

Delcourt-Honorez M.(1989).Water level fluctuations in a borehole at the Royal Observatory of Belgium: effects on local gravity, Earth-tidal and barometric responses, *XIth international symposium on Earth tides, 389-411.*

Dessargues. A. (1995). Modèles mathématiques en Hydrogéologie. Editura didactică şi pedagogică, Bucarest, *132 pp*.

Domenico P.A.(1972). Concepts and models in groundwater hydrology. Mc Graw-Hill International series in the Earth and planetary sciences. Mc Graw Hill book company-new york, 416 pp.

Duband D. (1982). Hydrologie statistique approfondie. *Institut national polytechnique de Grenoble, 276 pp.*

Dufour J.P. (2001). Introduction à la géodésie. *Hermes Science, Paris, 332 pp.*

Dupuit J. (1863). Etudes théoriques et pratiques sur le mouvement des eaux dans les canaux découverts et a travers les terrains perméables. *Dunod, Paris, 304 pp.*

Falleiros M.C., Portezan O., Oliveira J.C.M., Bacchi O.O.S., Reichardt K. (1998). Spatial and temporal variability of soil hydraulic conductivity in relation to soil water distribution, using an exponential model. *Soil & Tillage research, vol. 45, n°3-4, pp. 279-285.*

Fetter, C. W., (2001). Applied hydrogeology, 4th ed. *Prentice-Hall. Upper Saddle River, N. J., 598 pp.*

Forchheimer P. (1940). Hydraulik. *B.G. Teubner, Leipzig.*

Freeze A. (1971). Three-dimensional, transient, saturated-unsaturated flow in a groundwater basin. *Water resources research, vol. 7, n°2, 347-366.*

Gerstenecker C. (1978). The influence of air pressure changes in precise gravity measurements. *Beiträge zur Astronomische Geodäsie und Geodynamic, Inst.f.Phys.Geodäsie der Techn. Hochschule Darmstadt, 101-110.*

Goodkind, J. M. (1999). The superconducting gravimeter. *Review of scientific insruments Volume 70, Number 11, 4131-4152.*

Goodkind, J.M. (1986). Continuous measurement of nontidal variations in gravity. Journal of Geophysical research, vol..91, n°B9, 9125-9134.

Harnisch, M., Harnisch, G. (2002). Seasonal variations of hydrological influences on gravity measurements at Wettzell. *Bull. Inf. Marees Terrestres (BIM) 137, 10849–10861.*

Hecimovic Z., Basic . T. (2005). Terrain effect on gravity field parameters using different Terrain models. *Newton's bulletin n°3, pp. 92-102.*

Hinderer J., Lemoine F., Crossley D., Boy J. (2006). Time changes of the European gravity field from GRACE: a comparison with ground measurements from superconducting gravimeters and with hydrology model predictions, *Geophysical Journal International, Vol. 61 issue 2, 257-264.*

Hokkanen T., Virtanen H., Pirttivaara M. (2005). Hydrogeological noise in superconducting gravimeter data, *Near Surf. Geophys, 5: 125–132.*

Hubbert M.K. (1940). The theory of ground-water motion. *J.Geol., vol. 48, 785-944.*

Hupet F., Vanclooster M. (2005). Micro-variability of hydrological processes at the maize row scale: implications for soil water content measurements and evapotranspiration estimates, *Journal of Hydrology, Volume 303, Issues 1-4, 247-270.*

Iffly J.- F., Drogue G., El Idrissi A., Hoffman L., Matgen P., Talliez C., Pfister L. (2004). Empirical relationship between rainfall, groundwater level and basin humidity as a tool for predicting peak discharge, *Geoph.Res.Abs., Vol 6, 04489. SRef-ID: 1607-7962/gra/EGU04-A-04489.*

Imanishi Y., Sato T., Higashi T., Sun W., Okubo S. (2004). Submicrogal coseismic gravity changes detected by a network of superconducting gravimeters, *Science, Vol 306, No 5695, 476-478.*

Jacob C.E. (1950). Flow of groundwater. *Engineering Hydraulics (Ed. Hunter Rouse), John Wiley and sons, New York.*

Kroner C., (2001). Hydrological effects on gravity data of the geodynamic observatory Moxa, *J. Geod. Soc. Jpn., 47(1), 353-358.*

Kroner C., Jahr T. (2006). Hydrological experiments at Moxa observatory, *J. Geodyn., 41(1-3), 268-275.*

Laborde J.P. (2000). Eléments d'hydrologie de surface. *Universités de Nice-Sophia Antipolis, 192 pp.*

Lambert A., Beaumont C. (1977). Nano variations in gravity due to seasonal groundwater movements: Implications for the gravitational detection of tectonic movements. *Journal of Geophysical Research, vol. 82, 297-306.*

Landau L., Lifchitz E. (1971). Mécanique des fluides. *Editions Mir, Moscou.*

Ledoux E. (2003). Modèles Mathématiques en Hydrogéologie. *Ecole Nationale Supérieure des Mines de Paris, 132 pp.*

Lefebvre R. (2006). Ecoulement multi phase en milieu poreux. *Université du Québec, Institut National de la Recherche scientifique, 23 pp.*

Leirão S., He. X., Christiansen L., Andersen O.B., Bauer-Gottwein P. (2008). Calculation of the temporal gravity variation from spatially variable water storage change in soils and aquifers. *Journal of Hydrology 365 (2009), 302-309.*

Lindquist E. (1935). The flow of water through porous soil. *Premier Congrès des Grands Barrages , stockolm, 81-101.*

Llubes M., Florsch N., Hinderer J., Longuevergne L. & Amalvict M., (2004). Local hydrology, the Global Geodynamics Project and CHAMP/GRACE perspective: some case studies., *Journal of Geodynamics, 38 :355-374.*

Manabe S., (1969). Climate and ocean circulation. I. The atmospheric circulation and the hydrology of the Earth's surface. *Mon. Wea. Rev.*, 97, 739-774.

Melchior P.J. (1971). Physique et dynamique planétaires, *vol. 2, Vander-Leuven-Bruxelles.*

Melchior P.J. (1972). Physique et dynamique planétaires, *vol 3, Vander-Leuven-Bruxelles.*

Meurers B. (2007). Long and short term hydrological effects on gravity in Vienna. *www.astro. oma.be.*

Meurers B., Van Camp M., Petermaans T. (2007). Correcting superconducting time-series using rainfall modeling at the Vienna and Membach stations and application to Earth tide analysis, *J. Geod 81:703-712.*

Milly P.C.D., Shmakin A.B. (2002). Global Modeling of land water and energy balances, part1: the Land Dynamics (LaD) Model. *Journal of Hydrometeorology, vol. 3, 301-310.*

Morland L.W. (1978). A theory of slow fluid flow through a porous thermoelastic matrix. *Geophys. J.R. Astr. Soc., n°55, 393-410.*

Musy A., Higy C. (2003). Hydrologie, *Presses Polytechniques et Universitaires Romandes, 314 pp.*

Narashiman T.N., Kanehiro B.Y. (1980). A note on the meaning of storage coefficient. *Water resources research, vol.16, n°2, 423-429.*

Naujoks M., Weise A., Kroner C., Jahr T.(2007). Detection of small hydrological variations in gravity by repeated observations with relative gravimeters, *J. Geod DOI 10.1007 / s00190-007-0202-9, vol. 82[9],543-553.*

Neuman, S.P. (1972). Theory of flow in unconfined aquifers considering delayed response of water table. *Water Resources Research 8 (4), 1031–1045.*

Newman T.P., Witherspon P.A. (1970). Variational principles of confined and unconfined flow of groundwater. Water resources research, vol.6, n°5, 1376-1382.

Peter G., Klopping F.J., Berstis K.A. (1995). Observing and modeling gravity changes caused by soil moisture and groundwater table variations with superconducting gravimeters in Richmond, Florida, USA, *Cahiers du Centre Européen de Géodynamique et de Séismogie, Vol 11, 147-159.*

Polubarinova-Kochina P. Y. (1962). Theory of groundwater movement. *Princeton University Press, Princeton, New York, 636 pp.*

Quarteroni A. (2003). Modellistica numerica per problemi differenziali. *Sprinter-Verlag Italia, Milano, 332 pp.*

Quarteroni A.,Sacco R., Saleri F. (2008). Matematica numerica. *Springer- Verlag Italia, Milano, 510 pp.*

Reynolds W.D, Elrick D.E. (1991). Determination of hydraulic conductivity using a tension interferometer. Soil Sci. Soc. Am.J., 633-639.

Richter B. (1987). Der supraleitende Gravimeter. *Verlag des Instituts für Angewandte Geodäsie, Frankfurt am Main, 126 pp.*

Roche M. (1963). Hydrologie de surface, *Gauthier-Villars Orstom, Paris, 431 pp.*

Rosenshein J., Bennet G. D. (1984). Groundwater hydraulics. *Water resources monograph series 9. American Geophysical Union, Washington D.C.*

Rosenthal W.D., Harlan J.C., Blanchard B.J. (1982). Case study: estimating antecedent precipitation index from Heat Capacity Mapping Mission day thermal infrared data. *Hydr. SC. Journal, vol. 7, no 4, déc. 1982, pp. 415-426.*

Scheidegger A. E. (1974). The physics of flow through porous media, 3th ed. *University of Toronto Press, 353 pp.*

Takemoto, S., Fukuda, Y., Higashi, T., Ogasawara, S., Abe, M., Dwipa, S., Kusuma, D.S., Andan, A. (2002). Effect of groundwater changes on SG observations in Kyoto and Bandung. *Bull. Inf. Marees Terrestres (BIM) 136, 10839–10848.*

Talwani, M.(1973) Computer usage in the computation of gravity anomalies. *Methods in computational physics. Volume 13 - Geophysics. (A74-40792 20-13) New York, Academic Press, Inc., Academic Press, 343-389.*

Telford W.M., Geldart L.P.,Sheriff R.E.(1990). Applied Geophysics. *Cambridge University Press, 792 pp.*

Theis C.V. (1935). The relation between the lowering of a the piezometric surface and the rate and duration of discharge of a well using groundwater storage. *BOS Trans. AGU, vol.16, 519-524.*

Todd D.K. (2008). Groundwater hydrology, 3th ed. *John Wiley & sons, New York, 656 pp.*

Trescott P.C., larson S.P. (1977). Comparison of iterative methods of solving two-dimensional groundwater flow equations.*Water resources Research, vol.13, n°1, 125-136.*

Van Camp M, Wenzel H. G., Schott P, Vauterin P., Francis O. (2000). Accurate transfer function for superconducting gravimeters. *Geohysical Research Letters, vol 20, N.1, 37-40.*

Van Camp M. (1998). Qualification d'un gravimètre cryogénique pour les périodes supérieures a 100 secondes. *Thèse de Doctorat. Université Catholique de Louvain, 208 pp..*

Van Camp M., Francis O. (2006). Is the instrumental drift of superconducting gravimeters a linear or exponential function of time?, *J. Geod. 81, 337-334.*

Van Camp M., Vanclooster M., Crommen O., Petermans T.,Verbeek K., Meurers B., van Dam T.,Dassargues A. (2006). Hydrological investigations at the Membach station, Belgium, and applications to correct long periodic gravity variations, *J.Geoph. Res. Vol.111, BI0403, 1-13.*

van Dam, T., Wahr, J., Milly, C., and Francis, O., (2001). Gravity Changes due to Continental Water Storage , *J. Geod. Soc. Japan Vol. 47, N. 1, 249-254.*

Van Genuchten, M.T. (1980). A closed-form equation for predicting the hydraulic conductivity of unsaturated soils. *Soil Sci. Soc. Am. J. 44, 892–898.*

Wooding R.A. (1968). Steady infiltration from a shallow circular pond. *Water Resour. Res., 1259-1273.*

Zerbini S., Raicich F., Richter B., Gorini V., Errico M. (2010). Hydrological signal in height and gravity in northeastern Italy inferred from principal component analysis. *Journal of Geodynamics 49, 190-204.*